UNIVERSIDADE DE LISBOA
FACULDADE DE CIÊNCIAS

Planetary atmospheres – From Solar System to exoplanets: atmospheric characterization and search for chemical disequilibrium compounds

“ Documento Definitivo”

Doutoramento em Astronomia e Astrofísica

Ruben Henrique Machado Gonçalves

Tese orientada por:
Dr. Pedro Machado, Dr. Pedro Figueira e Dr. Thomas Widemann

Documento especialmente elaborado para a obtenção do grau de doutor

2020

UNIVERSIDADE DE LISBOA
FACULDADE DE CIÊNCIAS

Planetary atmospheres – From Solar System to exoplanets: atmospheric characterization and search for chemical disequilibrium compounds

Doutoramento em Astronomia e Astrofísica

Ruben Henrique Machado Gonçalves

Tese orientada por:
Dr. Pedro Machado, Dr. Pedro Figueira e Dr. Thomas Widemann

Júri:

Presidente:

- José Manuel de Nunes Vicente Rebordão, Investigador Coordenador e Presidente do Departamento de Física, da Faculdade de Ciências da Universidade de Lisboa

Vogais:

- Doutora Therese Encrenaz, Emeritus Scientist, Laboratoire d'Etudes Spatiales et d'Instrumentation en Astrophysique – LESIA, do Observatoire de Paris, França;
- Doutor Alejandro Cardesin Moinelo, Aerospace Engineer, European Space Astronomy Centre (ESA), Espanha;
- Doutor Ricardo Hueso Alonso, Titular de Universidad, Escuela de Ingeniería de Bilbao da Universidad del País Vasco/Euskal Herriko Unibertsitatea, Espanha;
- Doutor João Manuel de Morais Barros Fernandes, Professor Auxiliar com Agregação, Departamento de Matemática da Universidade de Coimbra;
- Doutor Pedro Miguel Borges do Canto Mota Machado, Professor Auxiliar Convidado, Faculdade de Ciências da Universidade de Lisboa, Orientador.

Documento especialmente elaborado para a obtenção do grau de doutor

Colaboração com o Instituto de Astrofísica e Ciências do Espaço, financiada por Fundação para a Ciência e a Tecnologia (PD/BD/128019/2016)

2020

"...To look at the stars always makes me dream, as simply as I dream over the black dots of a map representing towns and villages. Why, I ask myself, should the shining dots of the sky not be as accessible as the black dots on the map of France?"

Vincent Van Gogh

Nota prévia

A presente tese, redigida em Inglês, apresenta artigos científicos já publicados ou submetidos para publicação científica. Uma vez que parte destes trabalhos foram realizados em colaboração, o candidato esclarece que participou activamente na concepção dos trabalhos, obtenção e redução de dados, produção, análise e discussão de resultados, bem como na redacção dos respectivos manuscritos.

Aknowledgements

This thesis is not finish without expressing my gratitude towards those who support me and made possible this PhD degree.

I must start with my supervisor, my guide, my teacher, my academic godfather, my friend, Pedro Mota Machado. I could not imagine to have someone, at this early stage of my career, that was more helpful, more generous, more "door opener" and a better friend, then he was. He created and gave me so many great opportunities and experiences. He trusted in my capability and competence, gave me an opportunity to start as full-time researcher, taught me how to be a scientist, how to overcome obstacles, how to trust myself, how to improve my weak points. He did all this supervisor work while also understanding me in a personal level like few friends do. We was great teacher in the good moments and a great friend in the bad ones. I hope our partnership endures for many, productive, years. I know the friendship will. Thank you so much.

I am also very thankful to my co-supervisors Pedro Figueira and Thomas Widemann. Although their supervision was more intermitent, as planned, it was an honour and a privilege to have such world class experts giving me valuable feedback and insights, very complementary to Pedro Machado's guidance. I wish I could had more time and opportunities to absorb their knowledge and teachings.They both created unique and incredible opportunities that truly marked and boosted the beginning of my astronomer's career, such as visiting and working at ESO's facilities in Santiago,Chile, and observing in Mauna Kea, Hawaii. I have the impression they don't realize how much this unforgetable experiences meant for me, at a personal level. Thank you.

I need to thank my loving parents, Maria Teresa Machado and Henrique Gonçalves. They always supported my decisions, even when they disagreed with them, even when they truly believed that some decisions were not in my best interest, they let me learn with my own mistakes. And they will keep doing it. They did everything they could to help me achieve my goals, such as this goal, and they will keep doing it. That's why I'll always love them. I wouldn't be the person I am without

their love and values, each in his/her own way. I cannot thank them enough.

There was a quite a long phase in my life that the idea of becoming an astrophysicist was just an impossible dream. But there was someone that understood my love for astrophysics, understood that I was about to go on with my life without giving myself a chance because I was not believing in myself. Joana Ramos Pereira was responsible for making me realize that it was not impossible, that this was really my dream, that I did had the capability, that there was still time, that I could create my own opportunity and could actually achieve it, that I would regret not trying. She knew I could do it before I did. She was everything for me at that time: a support, a believer, a therapist, a lover, a friend. I'll always feel nothing but love and gratitute for having her in my life.

I want to thank my brothers, Daniel Gonçalves and Sérgio Gonçalves, for being way more than my brothers. They are an essential part of me, far beyond blood and DNA. I'm deeply thankful for their huge contribution to my education, to my values, to my achievements, for helping me to know myself in ways that neither nobody nor myself alone could do it. They guide me in self-awareness, as so I guide them, in a perfect complementarity, holy triangle.

Thank you all. I truly couldn't have done without your support and love.

This research his supported by the Portuguese Fundação Para a Ciência e a Tecnologia fellowship (ref. PD/BD/128019/2016 and ref. PTDC/FIS-AST/29942/2017) through national funds and by FEDER through COMPETE 2020 (ref. POCI-509 01-0145 FEDER-007672).

I thank the VIRTIS and Venus Express team, the European Space Agency, and the Project EuroVenus. I thank the Akatsuki team for the data and support. I also aknowledge the support of Faculdade de Ciências da Universidade de Lisboa (FCUL), the Fundação da Faculdade de Ciências de Universidade de Lisboa (FFCUL), and the Instituto de Astrofísica e Ciências do Espaço (IA).

Abstract

This thesis is based on an ambitious challenge: to provide useful tools in the study and characterization of planetary atmospheres, from the Solar System to exoplanets. There are four steps in the field of planetary atmospheres. Studying Earth' atmosphere is the first step. The second is the study of Venus' atmosphere, essential in our understanding of the origin and mechanisms that drive the super-rotational atmosphere, the differences between Venus and Earth's atmosphere and their evolution and what differentiates an Earth-like from a Venus-like exoplanets and how to model and characterize them.

The Venus' cloud-top (70 km) wind results presented in this thesis were retrieved using two techniques: 1) ground-based Doppler Velocimetry (DV), using visible high-resolution spectroscopy (CFHT/ESPaDOnS and TNG/HARPS-N observations) 2) space-based Cloud-Tracking (CT) using UV and visible imaging (VenusExpress/VIRTIS and Akatsuki/UVI observations). The most complete and precise meridional wind profile ever retrieved was based on HARPS-N observations from Gonçalves et al. (2020).

Our team has also retrieved zonal wind velocities from Venus' lower cloud deck (48 km), night-side, using CT on ground-based observations at the TNG/NICS, yielding results consistent with the data provided by space observations.

The third and fourth steps of planetary atmospheres study would be the Solar System's and exoplanet's atmospheres, respectively.

Our team is currently adapting the DV method to measure horizontal winds from Mars, Jupiter and Saturn's atmospheres. We are also leading ESA's space mission ARIEL scientific working group "Synergies with Solar System". Our expertise on SS atmospheres is highly valuable in the context of building a bridge between SS and exoplanets. We are developing a tool that provides an average spectra (point source) using comprehensive coverage data of different SS planets (Venus, Jupiter and Saturn) yielding a proxy of how we would see if those were exoplanets at a chosen distance from Earth.

Keywords: Venus, Atmosphere, Doppler Velocimetry, Cloud-Tracking, Spectroscopy.

Resumo

O derradeiro desafio da exploração espacial será, discutivelmente, a descoberta de uma "nova Terra". A existência de água líquida e de uma atmosfera compatível estão no topo da lista de factores a procurar numa possível Terra que possa vir a ser habitada por humanos ou que seja potencialmente habitada por vida inteligente. A evolução e composição da atmosfera não é independente da vida que sustenta, estão ambas interligadas num equilibrado e sensível ciclo de água, oxigénio e dióxido de carbono. A procura por uma "Terra" ou por possível vida inteligente passa, necessariamente, pela procura de uma atmosfera com características específicas.

O objectivo desta tese era o de desenvolver técnicas de characterização de atmosferas planetárias, do Sistema Solar aos exoplanetas. O primeiro passo no estudo da atmosferas planetárias começa, naturalmente, com o estudo da atmosfera terrestre. Apesar de milhares de anos de história humana e décadas de exploração espacial, aparentemente ainda não compreendemos por completo o quão complexa e sensível é a nossa atmosfera e em que medida a nossa actual existência e decisões (ou ausêcia delas) a pode afectar. O segundo passo será o estudo da atmosfera de Vénus, o planeta mais próximo da Terra (em média). Apesar de ser visto como o planeta "gémeo", a sua atmosfera é altamente complexa apresentando um efeito de estufa descontrolado e uma superrotação atmosférica cujos mecanismos estão ainda pouco estudados. O terceiro passo no estudo de atmosferas planetárias passa pelo estudo de outras atmosferas do Sistema Solar, tais como Marte, Titã (lua de Saturno) ou mesmo Júpiter e Saturno. Por fim, o último e mais desafiante passo será o estudo e caracterização de atmosferas de exoplanetas (planetas que orbitam outras estrelas).

Embora à primeira vista Vénus e Terra sejam planetas muito semelhantes (dimensão, densidade, massa, composição química), as condições atmosféricas e à superficie são bastante distintas. Na superfície de Vénus a temperatura média é de $\sim$470°C e a pressão atmosférica de $\sim$90 bar. O efeito de estufa descontrolado, originado pelo CO_2 presente na atmosfera (cerca de 96%), é o grande responsável pela elevada temperatura superficial. Este fenómeno constitui um notável caso de estudo para o aquecimento global e as subsequentes alterações climáticas terrestres. A climatologia comparativa entre Vénus e Terra é essencial para

a compreensão da evolução de atmosferas planetárias, e também de exoplanetas, podendo contribuir para a distinção entre os chamados exoplanetas tipo-Terra e tipo-Vénus. A atmosfera venusiana está num estado de superrotação, tendo um período de rotação (4,4 dias terrestres) muito inferior ao do corpo sólido do planeta (243 dias terrestres). A circulação de vento zonal dá-se na direcção paralela ao equador, sentido este-oeste (rotação retrógrada) equanto a circulação de vento meridional é responsável pelo transporte de momento e energia entre o equador e os polos, numa estrutura do tipo célula de Hadley, uma por hemisfério. A caracterização da circulação atmosférica, nomeadamente no topo das nuvens a cerca de 68-70 km de altitude, é crucial para a compreensão dos mecanismos que criam e a mantêm a superrotação. A densa camada de nuvens, formadas por gotículas de ácido sulfúrico e de um composto ainda não identificado que absorve a radiação ultravioleta, recobrem por completo o planeta impondo-lhe um elevado albedo. O contraste das nuvens faz com que sejam marcadores quase ideais do movimento atmosférico, o que possibilita, através do seguimento dos seus movimentos, calcular a velocidade média dos ventos, através da técnica conhecida como "cloud-tracking" (seguimento de nuvens). Os aerossóis altamente reflectores em suspensão ao nível da camada de nuvens são transportadas pelo vento carregando consigo informação relativa à dinâmica atmosférica. Os gases e aerossóis interagem com a radiação solar permitindo realizar medições da velocidade do vento com base no estudo das riscas espectrais de absorção e de emissão. A técnica denominada de velocimetria de Doppler (DV) baseia-se na dispersão de radiação solar visível pela camada superior das nuvens na direcção da Terra.

O método de DV utilizado neste trabalho foi inicialmente desenvolvido por Widemann et al. (2008) e posteriormente afinado e melhorado por Machado et al. (2012, 2014). O método consiste, sumariamente, na análise da luz solar que é reflectida, na nossa direcção, pelas moléculas presentes no topo da atmosfera de Vénus. Os resultados apresentados neste projecto de investigação, utilizando DV, basearam-se em observações efectuadas em Abril de 2014 (Machado et al., 2017) e Março de 2015 (Gonçalves et al., 2020b submitted) com o espectrógrafo ESPaDOnS do CFHT em Mauna Kea no Hawaii, e em Janeiro de 2017 com o espectrógrafo HARPS-N do TNG em San Miguel de La Palma, Espanha (Gonçalves et al., 2020). As observações de Abril de 2014 e Janeiro de 2017 foram coordenadas com observações espaciais levadas a cabo pela VenusExpres (missão da agência espacial europeia ESA) e Akatsuki (missão da agência espacial japonesa JAXA), respectivamente. Os resultados demonstram um perfil latitudinal de vento zonal simétrico, com velocidades de 110-120 ms^{-1} a baixas latitudes (<30°), e decréscimo acentuado de velocidade a partir dos 50°. O vento zonal não apresenta variaçãos inequívocas a curto (dias) ou médio prazo (2012-2015). A longo da longitude ou hora local de Vénus, todos os resultados apresentam um aumento de velocidade zonal de até 15 ms^{-1} em pontos junto ao terminador da manhã (6:00

hora local) ou tarde (18:00 hora local), conforme a geometria das observações. Esta variação junto ao terminador também se verifica nos resultados das observações espaciais usando a técnica de CT.

As observações de Janeiro de 2017 (Gonçalves et al., 2020) resultaram na obtenção do mais completo e preciso perfil de vento meridional alguma vez obtido. Os resultados DV apresentam velocidades meridionais nulas a baixas latitudes (<10°), com velocidades máximas de até 25 ms^{-1} por volta dos 35°, em anos os hemisférios, e um descréscimo acentuado de velocidade a partir de latitudes acima de 50° N e S. Estas observações foram pioneiras no uso do espectrógrafo de alta resolução HARPS-N para o estudo de atmosferas do sistema Solar, abrindo-se assim uma importante janela de oportunidade para novas observações de planetas do sistema Solar com este ou outros espectrógrafos inicialmente pensados para o estudo de exoplanetas.

Os resultados obtidos através da técnica de CT basearam-se em observações espaciais da VenusExpress, com o instrumento VIRTIS-M, feitas em Abril de 2014 (Machado et al., 2017) e em observações da Akatsuki com o instrumento UVI, feitas em Janeiro de 2017 (Gonçalves et al., 2020). O vento zonal obtido nestas observações apresenta um perfil latitudinal consistente entre observações utilizando a mesma técnica (CT) e semelhante ao obtido pelos resultados com DV. No entanto, as velocidades zonais obtidas por CT são, em média, inferiores às velocidades zonais obtidas por DV, em cerca de 10-15 ms^{-1}. Esta diferença nas velocidades sugere que as técnicas estarão a sondar altitudes diferentes no topo das nuvens de Vénus. Alguns modelos sugerem que uma diferença de 2-3 km entre as altitudes observadas poderá ser suficiente para se medir velocidades 10-15 ms^{-1} superiores na camada mais elevada.

Usando a técnica de CT a partir de observações terrestres, com a camera NICS do TNG em Julho de 2012, medimos velocidades de ventos zonais da camada inferior das nuvens de Vénus, a cerca de 48 km de altitude, do lado nocturno do planeta. Estes resultados são, não só consistentes, como apresentam uma precisão semelhante á dos resultados obtidos pelas observações espaciais, abrindo perspectivas promissoras de futuras medições de ventos da camada inferior das nuvens de Vénus a partir de telescópios terrestres.

Relativamente a outros alvos do sistema Solar, a nossa equipa está a trabalhar em dados de observações de Marte, Júpiter e Saturno, com o intuito de adaptar a técnica de DV e obter velocidades zonal e meridional das atmosferas destes planetas. As observações de Júpiter (levadas a cabo pessoalmente *in situ*), foram efectuadas em Julho de 2019 no VLT utilizando o espectrógrafo de alta resolução ESPRESSO.

Por fim, e tendo como mote a colaboração com a missão espacial ARIEL da ESA, e a liderança da nossa equipa do grupo de trabalho “sinergias com o Sistema Solar”, propomos a utilização dos espectros de Júpiter (numa primeira fase),

Vénus e Saturno, já obtidos em observações anteriores, como espectros-modelo de possíveis exoplanetas. Poderemos simular e modelizar como seria observar estes planetas se fossem exoplanetas, estando a anos-luz de distância a ser observadores pela ARIEL ou por outros telescópios com condições e geometrias de observação semelhantes às de observação de exoplanetas. O nosso conhecimento e experiência na observação e estudo de atmosferas do Sistema Solar é reconhecido e altamente valorizado pela liderança científica da missão, sendo uma contribuição essencial para a actual e futura caracterização e modelização de atmosferas de exoplanetas.

Palavras-chave Vénus, Atmofera, Velocimetria de Doppler, Seguimento de nuvens, Espectroscopia.

List of acronyms and abbreviations

CAHA	Centro Astronḿico Hispano-Alemán
CARMENES	Calar Alto high-Resolution search for M dwarfs with Exoearths with Near-infrared and optical Échelle Spectrographs
CFHT	Canada France Hawaii Telescope
CT	Cloud Tracking
DV	Doppler Velocimetry
ELT	Extremely Large Telescope
ESA	European Spatial Agency
ESO	European Southern Observatory
ESPaDOnS	Echelle SpectroPolarimetric Device for the Observation of Stars
ESPRESSO	Echelle SPectrograph for Rocky Exoplanets and Stable Spectroscopic Observations
FOV	Field Of View
HARPS-N	High Accuracy Radial-velocity Planetary Searcher - North
JAXA	Japanese Aerospace eXploration Agency
NICS	Near Infrared Camera Spectrometer
SS	Solar System
TNG	Telescopio Nazionale Galileo
UTC	Universal Time Coordinated
UVES	Ultraviolet and Visual Echelle Spectrograph
UVI	Ultra Violet Imager
VEx	Venus Express
VIRTIS-M	Visible and Infrared Thermal Imaging Spectrometer
VLT	Very Large Telescope

List of Figures

List of Tables

Contents

Chapter 1

Thesis overview

1.1 Scientific context

We, humans, are conscious 'intelligent' life. We have evolved and we live on the surface of this planet, under and within its atmosphere. Earth's atmosphere provides us the oxygen we so dearly need and protect us from harmful UV and cosmic radiation. But the evolution and composition of the atmosphere is not independent from the life it supports, they are intertwined. The oxygen cycle on Earth's atmosphere is deeply connected with the flora present at the surface. As so the ozone layer can be damaged by our global actions (or inactions). The carbon cycle on our atmosphere is interconnected with the dynamics of the tectonics and volcanism phenomena. The atmospheres of all terrestrial planets/moons are deeply connected and interdependent with its surface dynamics and, if existent, lifeforms.

As the search for life outside planet Earth progresses, so does our understanding of the essential role that an atmosphere plays in the existence of life, even if only remotely similar to our. We will not find complex life, as we know it, or find a extraterrestrial planet (or moon) potentially habitable by humans without finding a suitable atmosphere. It doesn't mean it has to be exactly like our atmosphere, but it definitely cannot be any atmosphere. So, our search for complex life and for a 'second Earth is, in its essence, a search for a suitable atmosphere.

The closest atmosphere to us, as so is the closest planet, it's Venus. While the study of Earth's atmosphere is the first step in the field of planetary atmospheres, the second step is naturally the study of Venus' atmosphere. Venus should be the Earth-like planet most similar to Earth we know: both have almost the same size (5% difference), mass and density, they were formed at the same time, with similar ingredients, at almost the same location in the solar system. Yet, Venus has ended up with an extreme climate. By comparing surface conditions, one can

realize that each planet followed a distinctive path at some point of evolution. The dense Venus' atmosphere (about 90 times the mass of Earth's atmosphere, yielding a surface pressure higher then Earth's one by the same factor) is dominated by CO_2, which is responsible for a runaway greenhouse effect and consequently high surface temperatures (reaching about 470°C).

By its proximity and paradoxical similarities/differences, Venus poses as a key subject in our understanding of planetary evolution. Failing to understand why two almost twin planets had such different destiny means we will neither fully understand the conditions in which life appeared on Earth, nor apprehend the long-term evolution of our own climate, nor distinguish if an exo-planet is more Earth-like or Venus-like. Thus, the major key aspects in studying Venus' atmosphere are the follow:

- The comparative study of Venus and Earth atmospheric physics and dynamics may help us to understand the enormous differences that led planetary evolution in both planets and also constrain the prevision of Venus and Earth long-term atmospheric transformations.
- The study of Venus' runaway greenhouse effect should improve our understanding of the present climate change process taking place on Earth.
- Understanding the climate of Venus should be a prime task for planetary science as well as for the exoplanet community. Comparative climatology between Venus and Earth will also contribute to constrain the concept of Habitable Zone (HZ) and its application to Earth-like exo-planets.

1.2 Initial Goals

The goal of this PhD was to develop a set of skills and techniques in the characterization of planetary atmospheres to be primarily used in Solar System (SS) atmospheres while also envisioning a potential usefulness in a subsequent study of exoplanets atmospheres. For the main goal, Venus was be the perfect starting point in the study of planetary dynamics for both SS and exoplanets: a slow rotator earth-like planet with a superrotation atmosphere dominated by a runaway greenhouse effect. The study of the dynamics of a superrotaion atmosphere is essential to further understand why and how is Venus so different form Earth. However, Venus can also be used as a 'field' laboratory to study, compare and develop models for Venus-like exoplanets, further contributing to distinguish Earth-like from Venus-like planets.

As the project developed, our team had several opportunities to observe with world class spectrographs while also using data from space missions in coordi-

nated observations yielding promising and relevant results. Additionally, preparing and conducting Venus observations require very specific skills and experience, also requiring the *in situ* presence of the researchers, not comparable with more straightforward observations from other fields in astrophysics and cosmology. Therefore, the main focus of the PhD was naturally kept on Venus' dynamics atmosphere due to (i) its scientific interest, (ii) the gathered experience of the team on the DV and CT techniques and observations, (iii) and the ongoing collaborations which provided data and observations opportunities. Regarding the search for chemical disequilibrium compounds, as mentioned in the tittle, despite not being presented in this thesis, there are ongoing collaborations on the detection of chemical tracers on Titan's atmosphere. The required data was already collected, thus the project should be concluded in the next year.

1.3 Achievements

The project naturally evolved to the development and adaptation of two techniques used in the study of Venus' atmospheric dynamics: DV and CT. The previous work on DV, coupled with previous and new collaborations with VenusExpress and Akatsuki teams, respectively, using CT, paved the way to further study the dynamics of Venus' atmosphere using these techniques.

DV was initially developed and fine tuned by Widemann et al. (2008); Machado et al. (2012, 2014). Subsequent results were obtained, with my direct contribution, through coordinated ground and space observations in Machado et al. (2017); Gonçalves et al. (2020), the later providing the adaptation of the method to a new telecope/instrument while also yielding the first study of a SS atmosphere using HARPS-N. New results presented in this work, from March 2015 observations are from Gonçalves et al. (2020b submitted).

As for CT, it's a technique successfully used by VenusExpress and Akatsuki to retrieve horizontal winds from Venus atmosphere (Sánchez-Lavega et al., 2008; Hueso et al., 2012, 2015; Peralta et al., 2018; Horinouchi et al., 2018). There are different methods to use this technique that differ in some aspects, such as fully automatic or manual, different criteria to track and match cloud features in images, among other factors (Hueso et al., 2012; Peralta et al., 2018; Horinouchi et al., 2018). For the VEx/VIRTIS we used a manual method based on a software developed by Hueso et al. (2010), while for Akatsuki images we used a cloud-tracking technique based on a phase correlation method between images developed by Peralta et al. (2018). However, CT was also used in ground-based observations using TNG/NICS, which provided horizontal wind at lower cloud deck ($\sim$48 km) on Venus nightside (see section 6).

Regarding other SS planets, section 7.1 details the ongoing projects and ob-

servations on adapting the DV technique to retrieve wind on Mars, Jupiter and Saturn. Our team is leading the ARIEL working group "Synergies with Solar System" with the main goal of fostering the collaboration and share expertise between the scientific community working in the SS planet atmosphere and the new growing community working for the ARIEL Science team. ARIEL is a mission dedicated to measuring the chemical composition and thermal structures of hundreds of transiting exoplanets.

The results presented in this thesis are summarized as follow:

1. Venus
    - Venus cloud top (∼70 km) horizontal wind measurements from April 2014: coordinated ground and space observations using DV and CT with CFHT/ESPaDOnS and VEx/VIRTIS-M respectively (Machado et al., 2017)
    - Venus cloud top (∼70 km) horizontal wind measurements from January 2017: coordinated ground and space observations using DV and CT with TNG/HARPS-N and Akatsuki/UVI respectively citepGoncalves2020.
    - Venus cloud top (∼70 km) horizontal wind measurements from March 2015: DV observations with CFHT/ESPaDOnS (Gonçalves et al., 2020b submitted).
    - Venus lower cloud (∼48 km) horizontal wind measurements from July 2012: night-side CT observations with TNG/NICS (Machado et al., 2020a submitted)
2. Solar System
    - Mars horizontal wind measurements during global dust storm from June 2018: DV observations with VLT/ESPRESSO.
    - Jupiter horizontal wind measurements from July 2019: DV observations with VLT/ESPRESSO.
    - Saturn horizontal wind measurements from June 2017: DV observations with CAHA/CARMENES.
3. Exoplanet
    - ARIEL collaboration: leading the "Synergies with Solar System" working group.
    - Jupiter as an exoplanet: using spectra obtained with VLT/UVES (July 2019 observations) to produce a proxy of how we would observe Jupiter if it was an exoplanet being observed by ARIEL

- Solar System planets as exoplanets: using a tool developed by our team to obtain spectra of Solar System planets as if they were exoplanets, at a resolution and distance as if they were being observed by ground or space observations, such as ARIEL.

The results presented in this thesis are from the published works of Machado et al. (2017); Gonçalves et al. (2020), submitted works of Gonçalves et al. (2020b submitted); Machado et al. (2020a submitted) and the in preparation work of Machado et al. (2020b in preparation).

1.4 Thesis structure

1. The introduction (Chapter 2) will provide the reader with the state of the art regarding Venus and its atmosphere, particularly on the cloud dynamics driven by the superrotation.

2. Chapter 3 and 4 will focus on the zonal and meridional wind velocities retrieved from Venus' cloud-top atmosphere (at around 70 km altitude) using DV and CT respectively. Chapter 3 will focus on the DV results as follows: method, telescopes/instruments description, CFHT/ESPaDONs April 2014 data (observations, results and discussion), TNG/HARPS-N January 2017 data (observations, results and discussion) CFHT/ESPaDONs March 2015 data (observations, results and discussion). The DV results presented were obtained from 3 observation runs:

   - April 2014 observations using ESPaDOnS at the CFHT. These were coordinated ground and space observations with VenusExpress/VIRTIS using CT technique. The respective results were published in Machado et al. (2017).
   - January 2017 observations using HARPS-N at the TNG. These were also coordinated ground and space observations with Akatsuki/UVI using CT technique. The respective results were published in Gonçalves et al. (2020).
   - March 2015 observations using ESPaDOnS at the CFHT. The respective results were submitted as Gonçalves et al. (2020b submitted)

   The alignment will follow the chronological order in which the results and respective articles were produced, and not in the chronological order of the actual observations. This will simplify the structure allowing to follow the line of investigation as it was conducted.

3. Chapter 4 has a similar structure as the previous one, but is focused on CT: method, space missions and instruments description, VenusExpress/VIRTIS April 2014 data (observations, results and discussion), Akatsuki/UVI January 2017 data (observations, results and discussion). The CT results presented were obtained from 2 observation runs

    - April 2014 observations using VIRTIS on VenusExpress. These were coordinated ground and space observations with CFHT/ESPaDOnS using DV technique. The respective results were published in Machado et al. (2017).
    - January 2017 observations using UVI on Akatsuki. These were also coordinated ground and space observations, with TNG/HARPS-N using DV technique. The respective results were published in Gonçalves et al. (2020).

4. Chapter 5 presents an in-depth comparison between DV and CT results for cloud-top wind velocities. This includes long-term wind variability from both techniques, as well as comparisons with Venus' General Circulation Models (GCM). The goal is to question and understand exactly what which technique is actual measuring and what altitudes are being probed. The chapter uses information and figures to be published as Machado et al. (2020b in preparation)

5. On Chapter 6 we move from cloud-top ($\sim$70 km) dayside to the lower cloud deck, located at around 48 km, on the night hemisphere of Venus. The results presented were obtained through CT technique from ground observations, using the NICS camera at the TNG. The chapter's structure is similar to the ones find in Chapter 3 and 4: Method, Observations, Results and Discussion. However, The description of the instrument used, NICS, was included in Chapter 3.

6. Chapter 7 is dedicated to other SS planets and the link with exoplanets. The first section will focus on our completed observations of SS planets: Mars, Jupiter and Saturn. The second section will introduce the collaboration of our team with the ARIEL mission, as we are leading the "Synergies with Solar System" working group. This section will also present our projects to develop a new tool to produce spectra of SS targets as if they were exoplanets, with the resolution and distance as if being observed by ARIEL or other telescopes and space missions.

7. Finally, Chapter 8 will present the discussion and conclusions of the thesis, including remarks of ongoing and subsequent work and collaborations.

1.5 Personal contribution

In this section I will discuss my personal contribution for each of the projects presented in this thesis.

I'm the PI (principal investigator) of the project and results presented in (Gonçalves et al., 2020) and Gonçalves et al. (2020b submitted). For both projects, although the observations were not conducted by myself, I led the processes of observation proposal and preparation, data reduction, retrieval of the results (DV and CT), analysis and discussion of the results and writing of the manuscript.

As for the the work presented in Machado et al. (2017), while supervised by the PI, I was the main contributor in the processes of observation proposal and preparation, data reduction, retrieval of the results (DV and CT), analysis and discussion of the results and writing of the manuscript.

In the project by Machado et al. (2020a submitted), while supervised by the PI, I substantially contributed to the processes of data reduction, retrieval of the results (CT) and analysis of the results.

As for the work to be presented as Machado et al. (2020b in preparation), I contributed with the results previously presented in Gonçalves et al. (2020) (CT using UVI 365 nm filter) as well as contributed to the process of retrieval of horizontal winds (CT using UVI 283 nm filter), analysis and discussion of the results.

Additionally, I substantially contributed to the observation proposal of Mars 2018 observations, as well as to the preparation of the observation run (VLT/ESPRESSO) and subsequent data reduction.

I co-authored the observation proposal and co-conducted Jupiter's *in situ* observations on July 2019, using ESPRESSO at the VLT. I also led the entire data reduction process. The retreieval of horizontal winds from Jupiter's atmosphere using DV will lead to the co-authorship of one manuscript. Regarding the use of Jupiter spectra as a proxy to exoplanets, apart from the observations, I contributed to the process of averaging the spectra retrieved, which led to the development of a tool (see section 7.2.2) to be used to retrieved other median spectra, such as Venus and Saturn. This will lead to the co-authorship of a manuscript regarding the analysis of Jupiter's spectra as if an exoplanet.

As for Saturn's observations, my major contribution was in the data reduction process, as described in section 7.4.

Chapter 2

Introduction - Venus

2.1 Venus: Earth's false twin

Venus is the closest planet to Earth, usually referred to as Earth's sister or twin planet, since both appear to be very similar planets. Venus and Earth were formed at roughly the same time, evolved from the same proto-solar nebula, have endured the same bombardments in the early stages (as icy planetesimals, cometary-like bodies or rocky asteroids), have similar densities, size, mass and bulk chemical composition (table 2.1). However, despite similar initial conditions, both plants evolved in radically different ways (Grinspoon, 1997).

The surface conditions are dramatically distinct in both planets. The average temperature in Venus's surface is about 470°C (this is higher than the melting temperature of lead) and the pressure is about 90 times the atmospheric pressure on Earth's surface (the equivalent pressure found at a depth of 1 km in Earth's oceans). Thermodynamically speaking, the pressure and temperature at surface led the atmospheric properties to be closer to the liquid phase than the gaseous one. This is the case of its major compound, CO_2, which has its critical point at a temperature of 304°K (51°C) and a pressure of 73 bars, so at the first scale height of Venus atmosphere (at about 16 km altitude) the carbon dioxide is a supercritical fluid (Kastings, 1988).

Venus is also the slowest rotating planet. This can be seen by the absence of pole flattening on Venus, whereas every other planet in the Solar System has experienced flattening at their poles due to the speed of their spin. One Venusian day is about 243 Earth days. Considering its retrograde motion as well, Venus has a solar day of about 117 Earth days (Grinspoon, 1997), i.e., it takes about 117 Earth days for an observer (stationary) at Venus surface to see two consecutives Sun rises. So, at any location along the equator it will be day time for about 59 Earth days, and the same period for night time. Although this could indicate a

	Earth	Venus
Radius (km)	6378	6051
Density (g/cm^3)	5.5	5.3
Distance to Sun (UA)	1	0.72
Sidereal Year (days)	365	226 (0.62year)
Rotacional Period (days)	1	243 (ret)
Obliquity (°)	23.5	177
Solar Constant	1380	2620
Albedo	0.3	0.75
Equilibrium Temperature (°C)	-15	15
Surface Temperature (°C)	15	460
Surface Pressure (atm)	1	92
Atmospheric Composition	78.1% N_2 20.9% O_2 0.034% CO_2	96% CO_2 3% N_2
Atmospheric Condensables	H_2O	H_2SO_4

Table 2.1: Earth and Venus physical and atmospheric characteristics. (left: Earth; right: Venus). Data: https://sci.esa.int/web/venus-express/-/34067-venus-vs-earth.

high temperature gradient from the day side to the night side, the temperature is quite homogeneous at the entire surface. Venus is the only planet with retrograde rotation in the solar system, with an obliquity of 177°. Due to the low inclination of the rotational axis relatively to the ecliptic (about 3° considering the retrograde rotation), and an almost circular orbit, the two hemispheres receive approximately the same amount of radiation over the year, thus, there are no season as we have on Earth (Bougher et al., 1997).

2.1.1 Why is Venus so hot?

Due to distance to the Sun, Venus receives about twice as much solar energy as Earth does. However, Venus' albedo (Bond albedo of about 0.75) is much bigger than Earth's albedo (0.3). Thus, from the total radiation that Venus receive from the Sun, about 90% is reflected. If we would consider Venus as a black body while also taking into account its albedo, the surface temperature value would be of about -90°C (this would exclude any greenhouse atmospheric effects) - Venus would be cooler than Earth. So, the major contribution for the high surface temperature in Venus is its atmosphere. The dense atmosphere, high concentration of CO_2 and the consequent strong greenhouse effect causes the planet infrared radiation to be trapped and reabsorbed (fig2.1). These facts make Venus the prime case study for comparison with Earth.

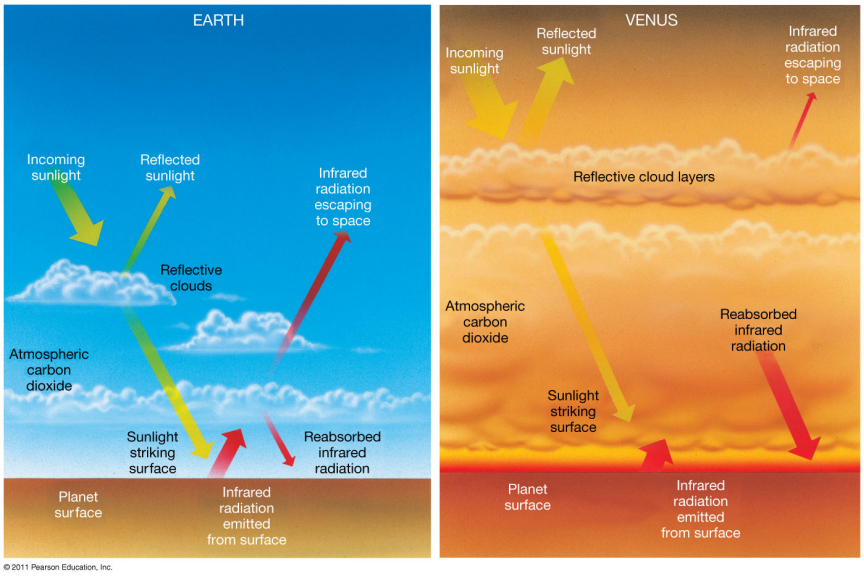

Figure 2.1: Illustrative schematics of the greenhouse effect on Earth (left) and Venus (right). Credits: Pearson Education

2.1.2 Plate tectonics

Venus doesn't have plaque tectonics like Earth has. Since Venus has lost its water, it has become a more rigid, low viscosity body, and so, the plaque dynamics are more standstill - it is a single-plated planet (Bengtsson and Grinspoon, 2013). There are some evidence that Venus' core might be comparatively more solid and much colder than the Earth's core (Lewis, 2004). There are major periodic volcanic events in Venus surface, but they happen at a planetary scale. On Earth, the plate tectonics process is part of the carbon dioxide cycle, being responsible for the subduction of large amounts of CO_2, contributing to the stabilization of atmospheric CO_2 (Holland, 1978). Such process would not occur in the single plate Venus' crust.

2.1.3 Magnetosphere

Planets that generate magnetic fields in their interiors, such as Earth, Mercury, Jupiter and Saturn, are surrounded by invisible magnetospheres. Their magnetic fields deflect the charged particles of the solar wind (electrons and protons) as they stream away from the Sun. This deflection creates a magnetosphere - a protective "bubble" around the planet - which ends in an elongated magnetotail on the lee side of the magnetosphere. Venus does not internally generate a magnetic field. As on Earth, solar ultraviolet radiation removes electrons from the atoms and molecules in the upper atmosphere, creating a region of electrically charged gas known as the ionosphere. Since Venus has no intrinsic magnetic field to act as a shield against incoming charged particles, the solar wind sometimes interacts directly with the upper atmosphere. The evidence of a weak magnetic field around the planet, suggested the hypothesis of a magnetosphere generated, not by a dynamo effect, as on Earth, but rather by the interaction of solar wind with the charged particles of the ionosphere (Goody et al., 1975) - an induced magnetic field (figure 2.2). Venus' magnetosphere is weaker than Earth's and closer to the planet.

2.1.4 Summary

To understand planetary evolution, particularly in our solar system, it's essential to understand why is Venus, a planet so close and similar (at first glance) to our Earth and yet so different and apparently hostile to our specie. After describing the dynamics and characteristics of Venus and its atmosphere, we can now summarize the major differences between Venus and Earth.

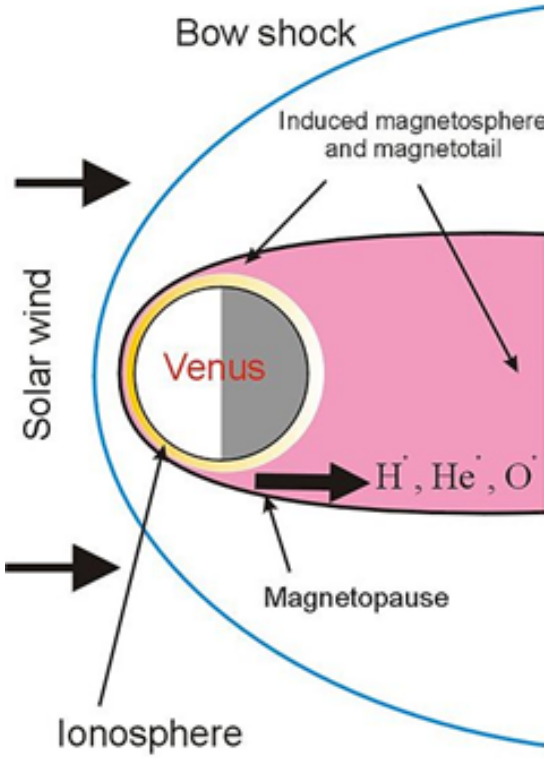

Figure 2.2: Bowshock of the interaction between the plasma particles of solar wind and the induced Venus' magnetosphere. Credits: https://commons.wikimedia.org/w/index.php?curid=6435191

- Obliquity - 23°obliquity for Earth's axis, while Venus has the axis reversed and almost normal to the ecliptic (3°), resulting in non-existing seasons.
- Natural satellites - also noteworthy is the rotation stabilising influence of a terrestrial satellite (the Moon) while there is none on Venus.
- Rotation rate - Earth's rotation rate is much faster than Venus (243 terrestrial days), plus a retrograde Venusian motion.
- Solar constant - Venus solar constant is almost the double relatively to the Earth's one.
- Surface temperature - a runaway greenhouse effect on Venus (due to a CO_2 dominated atmosphere) and a much lower one on Earth, contribute to an average surface temperature of about 460° C and 15° C, respectively.
- Surface pressure - the much denser atmosphere of Venus causes a surface pressure of 92 times the atmospheric pressure at Earth's surface.
- Water presence - water vapor and oceans on Earth, in contrast with the almost absence of water on Venus.
- Plaque tectonics - the terrestrial volcanism and the plate tectonics, by opposition of the single-plated Venus and its specific volcanism (described in section 2.1.2), also related with the absence of water.
- Magnetic field - Earth has an internal magnetic field and a correlated "protective" magnetosphere on Earth, whereas on Venus there's just a weak induced magnetic field (see section 2.1.3).
- Atmosphere composition and consensable - Earth's atmosphere is mainly composed by N_2 (78%) and O_2 (20%) with water vapor as condensable, contrasting with the CO_2 (96%) dominated Venus' atmosphere with sulphuric acid H_2SO_4 as condensable.
- Atmospheric equilibrium - the rotation rate is directly related to the atmospheric geostrophic balance for the fast rotating planets (Earth and Mars) and cyclostrophic equilibrium in the slower ones (Venus and Titan).
- Atmospheric dynamics - while on Earth there is a triple cell mechanism for the meridional wind circulation, on Venus, there is a single Hadley cell in each hemisphere extending from the equatorial region to the polar region (see section 2.2.3)

2.2 Venus amtosphere

2.2.1 Composition

After formation, Venus, Earth and Mars had presumably similar atmospheres, both in primordial composition and in relative abundances of its constituents. While on Earth part of the CO_2 is absorbed or renewed by the ocean and surface, on Venus, the CO_2 stays within the atmosphere (figure 2.3) originating a runaway greenhouse effect. This should be studied as comparative climatology to better understand if it's possible and how far is Earth atmosphere from reaching a critical concentration that could lead to dramatical climate changes.

Despite Venus being a "CO_2 dominated" planet, its atmospheric balance is fine-tuned by the SO_2 concentration (among other minor components) at this evolution stage of present atmospheric conditions (Bullock and Grinspoon, 2001). Both SO_2 and CO, also present in the upper atmosphere due to the photolysis of CO_2, tend to sink in the clouds toward the surface. The presence of H_2O was also found in the upper atmosphere, despite only in trace quantities (Beatty et al., 1999). Considering the loss of Venus' atmospheric CO_2 and H_2O by photolysis, and SO_2 in the reactive process of sulphuric acid formation, a source of these molecules is needed to maintain the overall chemical composition. Large-scale volcanism episodes are considered the the main source, injecting large quantities of these molecules into the atmosphere.

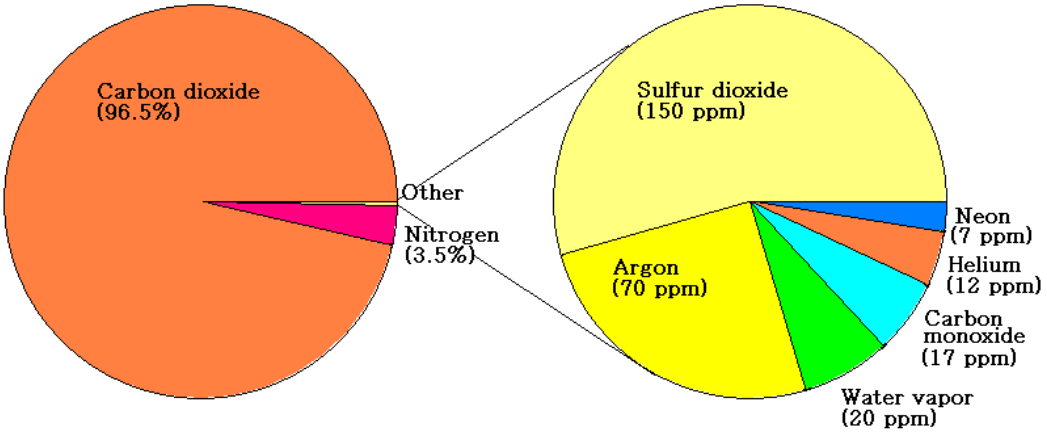

Figure 2.3: Venus atmosphere relative composition (left). On the right, the relative abundances of minor chemical elements (other than CO2). (figure: NASA website).

2.2.2 Cloud deck

The clouds on Venus cover the entire planet, causing an albedo of about 0.7-0.9. The atmosphere consists mainly of carbon dioxide, with clouds of sulphuric acid droplets and an yet unknown composition (responsible for the UV abortion), covering the entire planet.

The cloud layer extends in the atmosphere from 48 km to 70 km (about 22 km thick), with tenuous hazes above (reaching 90 km) and below the main cloud deck (from roughly 30 km) (Esposito et al., 1983). The clouds are not homogenous regarding the average size of their aerosol particles. The cloud deck can be divided into three layers (Knollenberg and Hunten, 1980):

- **Upper layer** - Altitude between 57-68 km with an averaged particle radius of 0.3 μm, and a total optical depth of 7 at 0.63 μm;
- **Middle layer** - From 51 till 56 km altitude, with a predominance of 1-1.4 μm particle sizes, with an optical depth of about 9, at same wavelength (0.63 μm);
- **Lower layer** - The lower cloud extends from the cloud base at 48 km till 50 km, optical depth of nearly 10 (at 0.63 μm), due essentially to 3.65 μm size particles.

2.2.3 Dynamics and structure

The atmosphere of Venus is extremely dense. The total mass of the atmosphere on Venus represents approximately 92 times the mass of Earth's atmosphere, despite the planets size similarity. Thus, the atmospheric pressure on the surface of Venus is about 92 bar.

The retrograde zonal winds at the cloud tops circles the planet in about 4 days (at around 70 km altitude), $\sim$60 times faster than the solid globe (243 days), thus, the atmosphere is said to super rotate the planet (Schubert et al., 1980; Gierasch et al., 1997). While on Earth the total surface coverage by clouds is only, on average, 40%, on Venus, it reaches 100%. Venus atmospheric dynamics is essentially driven by thermal heating and by its low rotation rate. As a consequence from its low rotational velocity, the Venus' atmospheric dynamics major mechanisms are quite different from Earth. We define the components of the wind to be a zonal wind u (along the isolatitude lines), a meridional wind v (along the meridians), and a vertical wind w (upwards). There are three major atmospheric global circulation processes that characterize the Venus atmospheric dynamics:

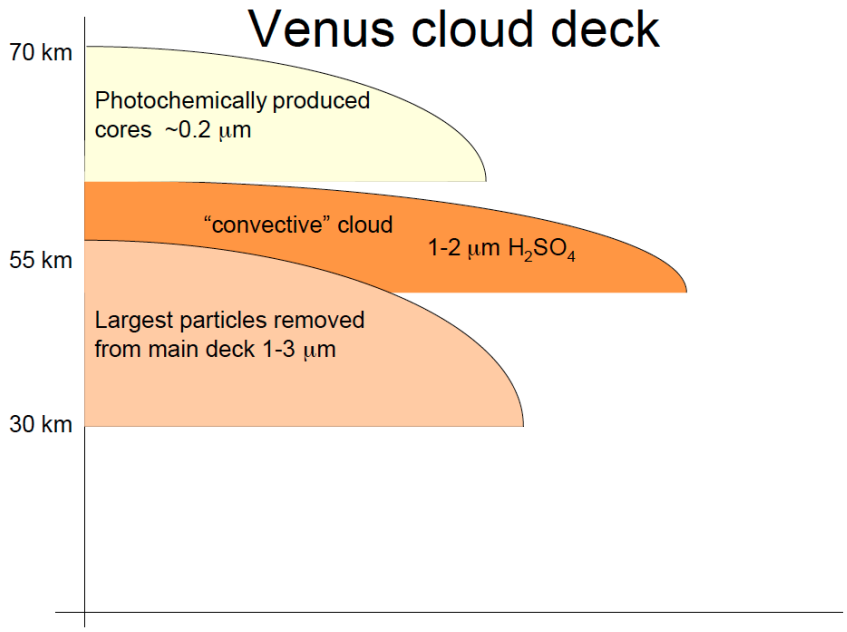

Figure 2.4: Venus' sulphuric acid cloud deck and hazes extension in altitude. Regarding the averaged aerosol particles size, the cloud deck can be divided in the three layers shown in this scheme. Figure: Titov, D., private communication.

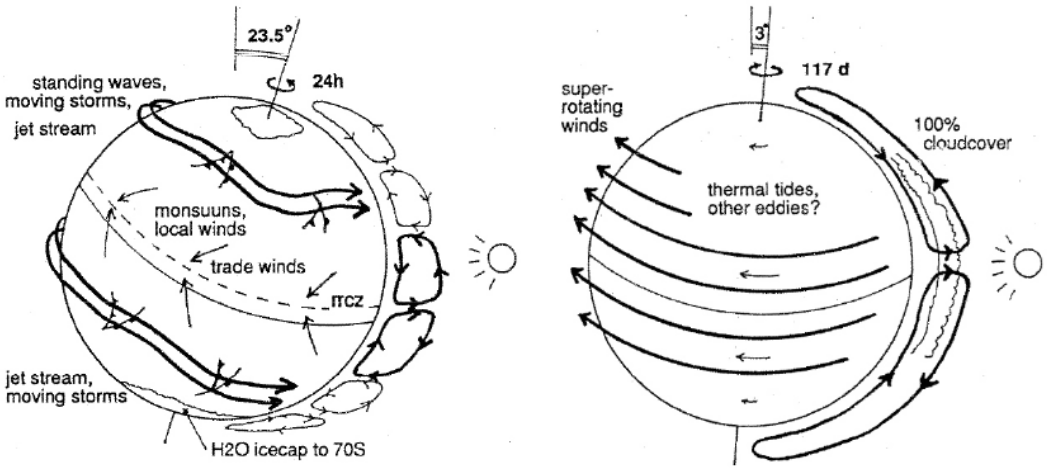

Figure 2.5: Large-scale motion of planetary atmospheres are dominated by various types of circulation patterns according to latitude, altitude and local time (left: Earth; right: Venus).

- **Super-rotational retrograde zonal wind (RZW)** - flowing in quasi-laminar bands parallel to equator, between the altitudes of 60-100 km and stretching between mid-latitudes. The wind starts to build up at 10 km and amplifies with altitude, reaching a maximum at cloud tops ($\sim$ 70 km). The RZW is accompanied by a Hadley-type meridional circulation from the equator to poles and both converge to an unique polar vortex circulation. On the superrotating zonal retrograde circulation, two main large scale, non-axisymmetric features are superimposed: (i) a four-day planetary wave at low and mid-latitudes and (ii) a polar vortex in the polar regions.

- **Sub-solar to anti-solar circulation (SS-AS)** - transporting the overheated air from high insolation regions towards the nightside radiation deficit area, above 120 km altitude (thermosphere). This air motion can be inferred through the density and temperature's contrast between day and night hemispheres. Above the cloud layer, Venus' mesosphere (70-120 km) is a highly variable transition region between the zonal retrograde circulation of the lower atmosphere (up to 70 km) and the subsolar to antisolar (SS-AS) flow of the upper thermosphere (above 120 km).

- **Meridional circulation** - characterized by one cell (Hadley) in each hemisphere, responsible for the transport of the heat excess from low latitudes, poleward to cooler high latitudes regions. The Hadley circulation consists on average of two equator-to-pole cells, with rising air at low latitudes and subsiding air at the poles, and both converge to an unique polar vortex circulation (Suomi and Limaye, 1978). The net upward transport of angular momentum by the Hadley cells is able to maintain an excess of angular momentum in the upper atmosphere, balanced by equatorward transport by planetary waves (Gierash, 1975; Rossow, 1979). However, this Hadley circulation has not been clearly characterized observationally (Sánchez-Lavega et al., 2008; Hueso et al., 2012), which is of most importance to support the therotical circulation presented in Venus' GMC models (Takagi et al., 2018; Gilli et al., 2017). The results presented in this work could help to constrain the meridional wind velocities, presenting the most complete and precise meridional profile ever retrieved (Gonçalves et al., 2020).

Polar Vortex

At the both poles, there's a vortex type structure that surpasses in size the terrestrial major hurricanes by a factor of four (see figure 2.7 for a comparison). This three dimensional feature is highly variable, and has been seen as dipole-like shape (Pioneer Venus observations, north pole) although it can change rapidly.

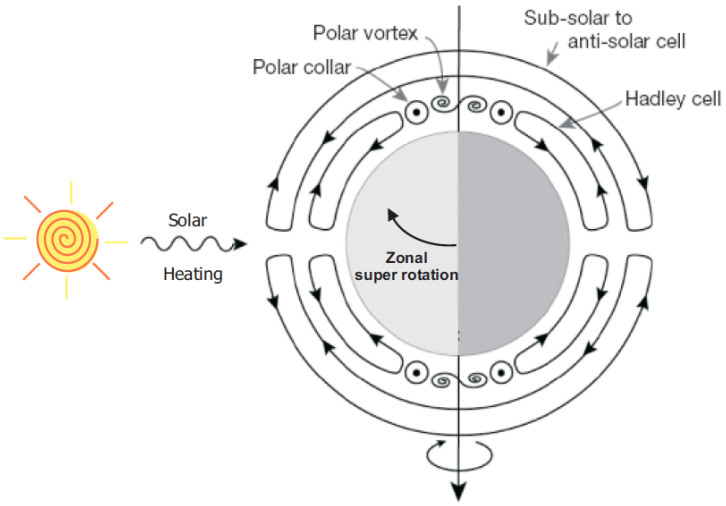

Figure 2.6: Venus atmosphere's global circulation. Figure: Taylor and Grinspoon (2009).

The vortex eye rotates around the polar axis even faster than the super-rotating zonal winds of the mid latitudes range. The south pole vortex was observed (Luz et al., 2011; Garate-Lopez et al., 2013) showing a period of about 2.7 terrestrial days (twice the angular velocity of the zonal wind). The inner and outer part of the vortex evidenced a differential rotation rate (Luz et al., 2011). It had also been observed with the shape of a dipole, triple and monopole (Taylor and Grinspoon, 2009; Luz et al., 2011; Garate-Lopez et al., 2013). The vortex structure on Venus has been observed for over three decades and it is thought to be a feature connected with the superrotation state.

There's also the presence of an atmospheric circumpolar circulation called the cold collar (Piccioni et al., 2007). The "cold collar" (or "polar collar") structure appears to be a permanent structure (as is the vortex) all around the vortex, located between 60°and 70°latitude (both hemispheres).

Jets

The previous measurements by Pioneer Venus, reanalyzed in Limaye et al. (2007), showed the presence of high latitude zonal jets close to 50°latitude in both hemispheres, with a slight asymmetry between the northern and southern ones. However, long temporal averages of cloud-tracked winds by the Galileo SSI instrument (Peralta et al., 2007), and by the Venus Express VMC and VIRTIS instruments (Sánchez-Lavega et al., 2008; Moissl et al., 2009) do not display

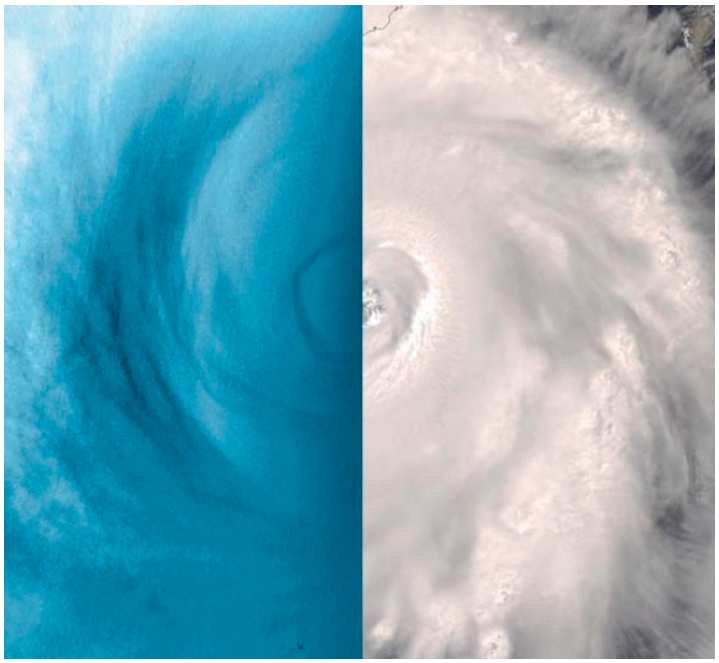

Figure 2.7: Venus' south pole vortex (left) and comparison with a terrestrial hurricane (right). Figure: Limaye et al. (2009).

any clear evidence for high latitude jets at cloud tops, although shorter time scale averages of VMC measurements in Moissl et al. (2009) indicate that jets may occur but are short-lived. The latitudinal wind profile retrieved by Doppler velocimetry (Machado et al., 2012) and from cloud tracking methods (Moissl et al., 2009; Sánchez-Lavega et al., 2008) coincide in the presence of a jet with an increased velocity of the order of 20 m/s at the latitudes of 50-60 °. Different wind measurements have provided important insight into the variability inherent to the circulation of Venus. In this work (Machado et al., 2017; Gonçalves et al., 2020,b) direct measurements of instantaneous zonal winds brings additional evidence for the occasional presence of jets and, in general, for spatial and temporal variability.

Planetary waves

Venus atmosphere presents a complex dynamic of, powered by a superrotational state. In such complexity, several planetary waves have been detected at and above the clouds. Atmospheric waves, such as gravity waves or Rossby-Kelvin waves, are thought to be indispensable factors, along with solar tide, in the transport of momentum that drives the super-rotation (Sánchez-Lavega et al., 2017).

At the cloud top, around 65-70 km, a distinctive large-scale Y-shaped wave

(tilted 90°) was discovered in 1961 by Boyer and Carmichel (1961). This four-day period planetary wave has been identified in ultraviolet images from many space missions (Rossow, 1979; Peralta et al., 2007; Titov et al., 2012). The Y feature has been interpreted as the combination of a Kelvin and Rossby modes at equatorial and mid-latitude regions respectively (Del Genio and Rossow, 1990; Gierasch et al., 1997; Imamura et al., 2006; Kouyama et al., 2015). Using images from JAXA's Akatsuki mission, Fukuhara et al. (2017) detected an stationary bow-shaped wave (10000 km across) at the cloud-top level. The author suggested that the structure is the result of an atmospheric gravity wave generated in the lower atmosphere by mountain topography that then propagated upwards. Peralta et al. (2017) also reported the detection of stationary waves and slowly moving features in the night upper clouds of Venus.

Despite several planetary-scale waves or stationary patterns have been detected on cloud-top level, the middle and lower clouds do no present any of this waves or features. However, in the lower clouds, at around 47.5-56.5 km, a sharp cloud discontinuity at equatorial latitudes with long-term coherence has been recently found by Peralta et al. (2020).

Vertical temperature profile

In an atmosphere in equilibrium, the weight of the atmosphere at each layer is balanced by the pressure of the air. The *hydrostatic equilibrium* is given by ($\frac{\partial p}{\partial z} = -\rho \times g$). The equilibrium leads to a vertical stratification of the atmosphere, where the pressure and the density decreases exponentially with height ($p = p_o \times e^{-z/H}$, H is the scale height).

The variation of temperature with altitude divides Venus' atmosphere into three distinct layers:

- *troposphere* (0-65 km) Extends to the top of the cloud and where the temperature decreases with altitude with the thermal gradient ratio of about $9K \cdot km^{-1}$ (close to the adiabatic lapse rate: $\Gamma_d = \frac{g}{C_p} = 7.39K \cdot km^{-1}$, which shows that convection is not significant at this atmosphere region).

- *mesosphere* (65-110 km) It is characterized by a less pronounced vertical thermal gradient ($\Gamma = \frac{\partial T}{\partial z}$) (Ahrens, 2003), being noteworthy the relevant horizontal variability with latitude, increasing from the equator to the poles, which is consistent with the existence of a Hadley circulation cell (Taylor et al., 1980).

- *thermosphere* (110-200 km) The balance between the incident UV radiation and the thermal conductivity of the present molecules prevails. Here, there is an asymmetry between the day and night hemispheres, as the daytime

temperature tends to increase with altitude between 100 and 140 km, while at night it tends to decrease along the same altitudes range, higher than 140 km the temperatures, at both hemispheres, remain stable, see figure 2.8.

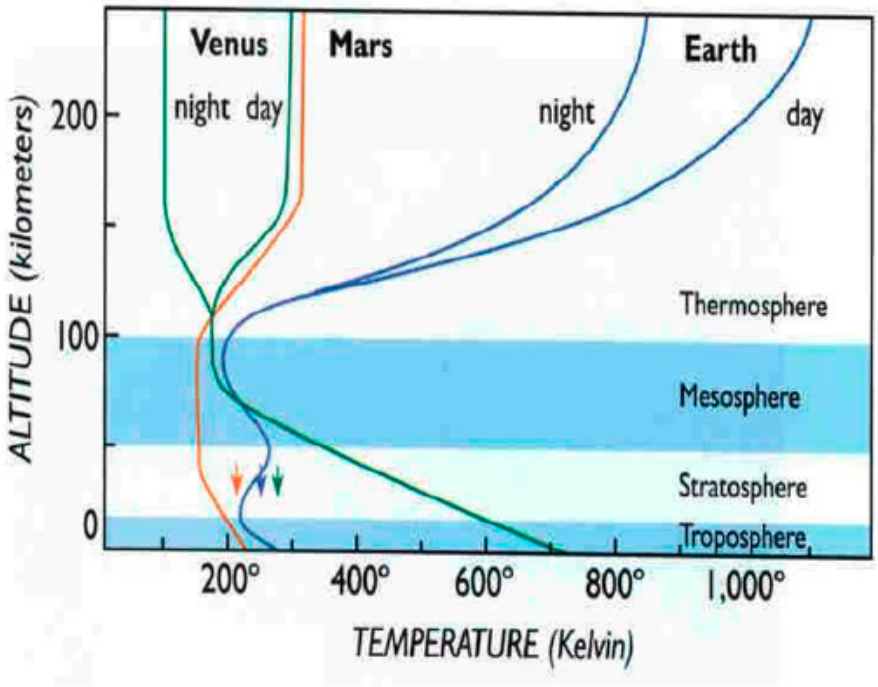

Figure 2.8: Vertical temperature profile of Venus' atmopshere (green lines), compared with Mars' (red line) and Earth's (blue lines) thermal profiles. Venus' and Earth's profiles are represented for both day and night. (image from B. Jakovsky).

The unidentified UV absorber, at the cloud layer, is responsible for about half of the total absorbed energy from solar irradiation. The so called "cold collar", at the heights of about 65 km, presents a temperature decrease from equator to about 65° latitude, of around 25 K (Taylor et al., 1983; Piccioni et al., 2007).

2.2.4 Comparative climatology

Coriolis effect on Earth

Coriolis effect (named after Gaspard de Coriolis, 1792-1843) is a consequence of the principle of conservation of angular momentum. The Coriolis or geostrophic

force is an apparent or hypothetical force that only acts when air is moving. A particle of air (or water), on either hemispheres, rotates from west to east with the Earth's surface at a certain speed. If that particle of air starts to move towards the equator, the conservation principle requires that the particle continue to rotate eastward at the same speed. However, the rotational speed of the Earth' surface at the equator is higher than at the poles. Thus, air moving towards the equator is deflected westward relative to the Earth's surface, while air moving from low latitudes to high latitudes (away from the equator) is deflected eastward. The *Coriolis effect* is stronger at the poles (high latitudes) and is negligible near the equator.

Cyclostrophic or geostrophic balance

The measurements of the Venus' wind velocity profile show a structure approximate to the cyclostrophic equilibrium, which postulates the balance between the pressure gradient force and the centrifugal force at a certain atmospheric layer (at fixed height). In slowly rotating bodies (such as Venus or Titan, the largest Saturn's moon), the Coriolis term will be negligible. This leads to the appearance of a wind's zonal flow, parallel to equator. In contrast to this case, we have the geostrophic balance, the one established on Earth, where the Coriolis force has an essential role in the genesis of the well known cyclonic and anticyclonic structures and their macro structures of the prevailing winds, such as the trade winds or the westerlies. In the Earth's case (and Mars), the Coriolis force overlaps the centrifugal effect due to the higher Earth's rotational velocity.

Habitable Venus

In exoplanetary science, 'habitable zone' (HZ) is a term used to define the area around a star in which a planet would have conditions to sustain liquid water at its surface and, therefore, life. Water is a good solvent in which, given enough time and suitable conditions, life could be created from simple molecules. Therefore, a planet/moon with liquid water, given enough time and conditions, will likely have the presence of some kind of life. However, the limits of the habitable zone can vary depending on the which factors are considered (such as atmospheric CO2 percentage, star type, period and tidal lock) . As the field of astrobiology develops, it is becoming clearer that multiple factors, characteristics and processes, can impact whether a planet is able to acquire and maintain liquid water on its surface and therefore changing the our initial perception of a fixed HZ. (Meadows and Barnes , 2018; Kopparapu et al., 2019). The current 'accepted' model of HZ does not include Venus, as seen in fig. 2.9. However, several studies strongly suggest Venus have had an ocean of liquid water at its surface (Grinspoon and Bullock, 2007; Way et al., 2016; Way and Del Genio, 2020). This would mean life could

have existed on the surface on Venus.

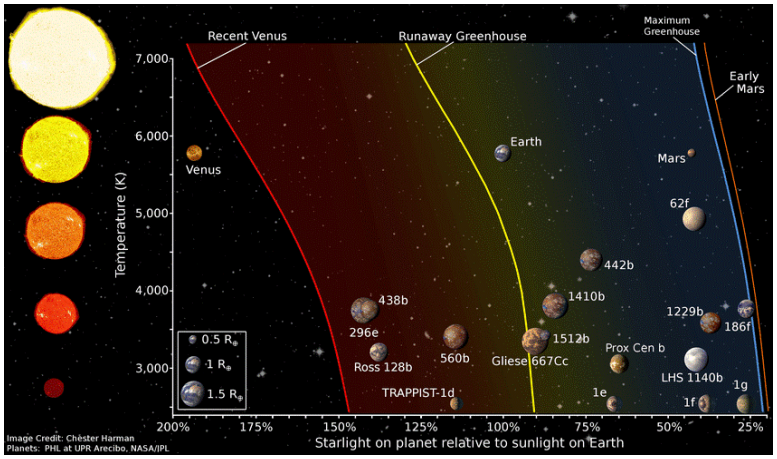

Figure 2.9: HZ limits for an Earth-like planet around stars with different stellar temperatures (vertical axis) in terms of incident stellar flux (horizontal axis) on the planet. The 'conservative HZ' is the region between the runaway greenhouse and maximum greenhouse limits. The 'optimistic HZ' is the region between recent Venus and early Mars limits. Currently confirmed terrestrial exoplanets, along with the Solar system ones, are also shown. (Figure: Chester Harman, NASA/JPL)

Back to the present, while life on the surface of Venus is very unlikely, not to say impossible, the clouds of Venus present a plausible scenario for the existence of life. The existence of life on Venus clouds has been proposed for decades (Grinspoon and Bullock, 2007; Dartnell et al., 2015; Limaye et al., 2018), a theory that was probably initiated by the iconic Carl Sagan in Morowitz H. and Sagan (1967). The proposed possible forms of live on Venus clouds vary in an array of different chemical and environment conditions, from lower deck to cloud-top (48-70 km). The eventual existence of lifeforms could even be correlated with the unknown UV absorber (Limaye et al., 2018). Recently, the hypothesis of life on Venus' clouds gained a new *'life'* with the possible detection of phosphine on Venus atmosphere (Greaves et al., 2020). The presence of PH3 would be unexplained on Venus' atmosphere. No currently known abiotic production routes in Venus's atmosphere, clouds, surface and subsurface, or from lightning, volcanic or meteoritic delivery could explain the presence of phosphine in Venus' clouds. PH3 could originate from unknown photochemistry or geochemistry, or, by analogy with biological production of PH3 on Earth, from the presence of life. Further studies are required on this subject, a) to confirm the presence of PH3 and b) to either suggest or refute explanations for the presence of phosphine; only then, the eventual presence of biological activity could be considered a likely.

However, Trompet et al. (2021), using multiple ocultations with the SPICAV/SOIR experiment aboard Venus Express, presented a negative detection of phosphine, retrieving upper limits between 0.2 and 20 ppbv of phosphine between 2006 and 2010, providind the lowest known upper limits for PH 3 in the atmosphere of Venus.

Nevertheless, this unconfirmed detection of phosphine on Venus, and the eventual link to life, has brought new light to the importance of studying Venus. Both the general public as the scientific community are now more aware of how Venus is a Earth-like planet with much yet to be studied. Hopefully, new space missions will gain momentum and visibility to further explore Venus.

2.3 Venus exploration

2.3.1 Past Missions

There's a long history of Venus space exploration since the beginning of robotic space exploration. The first attempts to launch robotic probes to Venus were made in February 1961, by the USSR (Union of Soviet Socialist Republics) missions *Sputnik 7* and *Venera 1*, but they resulted in failures. The first successful flyby was carried out by *Mariner 2* (NASA) in December 1962. The images sent by the probe were a disappointment because it revealed only an opaque atmosphere that shrouded entirely the planet, like a veil that hid the planet's surface. Several missions were launched to study Venus, some with more success than others, as summarized in the following.

- Venera missions (1961-1984)
- Mariner program (1962-1973)
- Pioneer mission (1978-1992)
- Vega mission (1984-1985)
- Magellan (1989-1994)

The Venera program collected the first images from the surface (figure 2.10), gathering information about and surface physical and chemical conditions. Venera missions (4 to 7) confirmed the existence of an atmospheric super-rotation (Dollfus et al., 1975b).

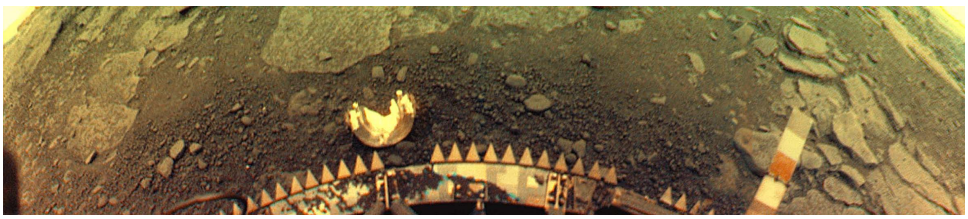

Figure 2.10: Surface photograph from the Soviet *Venera 13* spacecraft (lander touched down on 3 March 1982). The first of the Venera missions to include a color TV camera (image:: Soviet Planetary Exploration Program).

Several missions were also successful in performing Venus' fly-bys, taking advantage of the planet's gravity to gain velocity and continue the voyage to their final destinations:

- Galileo (1989-2003)
- Cassini (1997-2017)
- Messenger (2004-2015)
- Bepi-Colombo (2018-...)

BepiColombo is a joint European and Japanese (ESA and JAXA, respectively) space mission designed to study Mercury, launched on 19 October 2018. Its instruments will be used from Mercury's orbit to study its surface, interior, atmosphere and magnetosphere. This spacecraft has planned two Venus fly-bys on its way to Mercury, the first one was in 15 October 2020 and the second is due to 10 August 2021.

2.3.2 Recent exploration

Venus Express (ESA)

After a long pause, of about a quarter of a century, in spacecraft exploration of Venus, the first European Space Agency (ESA) Venus exploration mission was launched on November 9, 2005, arriving at Venus orbit in April 2006. The mission objectives were to conduct studies under the general circulation of the atmosphere, the chemistry of clouds and the atmospheric escape processes of several different volatiles, as well as the interactions between the surface and the atmosphere, with emphasis on the Venusian volcanism.

The orbit was elliptical, highly eccentric, with a planetary close pericentre of 250 km and an apocentre of 66 000 km, with a period of 24 hours. This orbit configuration provided optimal coverage of planetary latitudes and solar local time. The highly elliptic orbit allowed global large scale investigations, as high spatial resolution detailed studies of localized phenomena, at pericentric close approach.

After eight years in orbit and with propellant for its propulsion system running low, Venus Express was tasked in mid-2014 with a daring aerobraking campaign, during which it dipped progressively lower into the atmosphere on its closest approaches to the planet. This unique adventure was aimed at reducing the altitude and allowing an exploration of previously uncharted regions of the atmosphere. The lowest point of the orbit was gradually reduced to about 130-135 km altitude. The campaign also provided important experience for future missions - aerobraking can be used to enter orbit around planets with atmospheres without having to carry quite so much propellant. During an orbit maneuver to raise the spacecraft's altitude in the hopes of extending the mission's lifetime, the spacecraft's remaining fuel was exhausted and the contact with the spacecraft was lost on November

28, 2014. The mission was officially declared over by ESA on December 16, 2014.

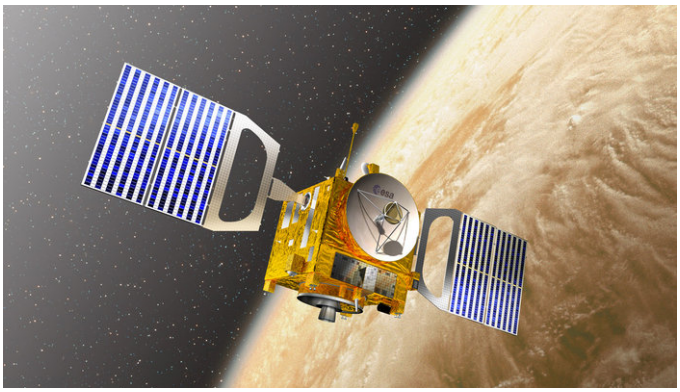

Figure 2.11: Artist's view of Venus Express probe in orbit around Venus (image: ESA's Venus Express mission website).

Akatsuki (JAXA)

The AKATSUKI spacecraft was launched in May 2010. After its smooth flight, JAXA attempted to insert the orbiter into the orbit circling around Venus on Dec. 7, 2010, but it failed as the main engine for orbit control was broken. JAXA established an investigation team to find the cause of the failure while studying a feasible plan for a second attempt. The spacecraft - whose name means "Dawn" in Japanese - had been circling the sun for five years, waiting for another shot at Venus. On Dec. 7, 2015, JAXA successfully inserted the orbiter into the Venus orbit by emitting thrust from the control engine.

Akatsuki's current path takes it as close as 400 km to Venus, and as far away as 440 000 km. This orbit is much more elliptical than the one Akatsuki was supposed to achieve in 2010, which featured a period of 30 hours and an apoapsis (most distant point from Venus) of about 80 000 km.

Akatsuki is the second interplanetary mission in Japan's history. The country's first, the Nozomi Mars probe, failed to arrive as planned at Mars in 2003. In 2007, Japan's Kaguya orbiter successfully launched to the moon to study the lunar surface from orbit. Kaguya's mission ended in 2009 and it ultimately crashed into the moon's surface.

Coordinated observations between ground-based and Akatsuki probe were made in January 2017, in order to study and measure wind velocity at could top of Venus' atmosphere, using both could-tracking (Akatsuki) and Dopppler velocimetry (TNG/HARPS-N) as in Gonçalves et al. (2020).

2.3.3 Future exploration: EnVision

ESA's M5 call for Medium-size missions for its Science Programme, submitted in October 2016 and to be launched in 2029, had a proposal for a Venus mission - the EnVision Venus orbiter.

EnVision is a medium class mission to determine the nature and current state of geological activity on Venus, and its relationship with the atmosphere, to understand how Earth and Venus could have evolved so differently, and to provide lessons for global environmental security on Earth (Ghail et al., 2017). EnVision is scaled for a Soyuz-Fregat/Ariane 6 launch, nominally in March 2028 or October 2029. Its payload will consist in (i) VenSar phased, an array synthetic aperture radar, (ii) VEM, Venus Emission Mapper, an infrared mapper and spectrometer and (iii) SRS, a subsurface radar. The nominal science mission is predicted to last for at least 5 years.

The approval of this mission, while taking advantage of Europe's world-leading position in both Venus research and in interferometric radar, would represent a major opportunity to study some of the questions that remain unanswered on Earth's sister planet, about the evolution and habitability of terrestrial planets.

Chapter 3

Doppler Velocimetry

3.1 Method: Doppler Velocimetry

The Doppler velocimetry technique presented in this study was developed to provide direct and instantaneous wind velocity measurements of Venus' atmosphere, using visible Fraunhofer lines scattered by cloud particles. The sunlight is absorbed by the particles in Venus' top clouds and re-emitted in Earth's direction (in a single back-scatter approximation). The solar Fraunhofer spectrum results from absorption of continuum radiation emitted from warmer, deeper layers by atoms and molecules of the solar atmosphere (such as H, S, Si, Fe, Ba, Mg, CN).

The major problem of ground observations of planetary winds reside in the difficulty of maintaining a stable velocity reference during the course of acquisition. The techniques developed in planetary wind measurements in the visible range using high-resolution spectroscopy from the ground (Civeit et al., 2005; Luz et al., 2005, 2006; Widemann et al., 2007, 2008; Machado et al., 2012, 2014, 2017; Gonçalves et al., 2020) all address the fundamental problem. There are systematic errors involved in trying to measure absolute wavelengths or Doppler shifts (or RV, Radial Velocities) with grating spectrographs, simply because the dispersion law and instrumental uncertainties, for simple line shifts, could not achieve an absolute accuracy better than about 100 ms^{-1} with older spectrographs, as pointed by Young et al. (1979). However, more recent high-resolution spectrographs such as ESPRESSO or HARPS, can achieve radial velocities with precision as low as 10 ms^{-1}. In measuring the global wind circulation at cloud tops, we are addressing wind amplitude variations or wind latitudinal gradients on Venus of the order of 5-10 ms^{-1} projected on the line-of-sight. To further improve the precision, the Doppler measurement is based on an optimal weighting of the Doppler shifts of all the lines present in the spectrum, with relation to a reference spectrum (in this case, a Th-Ar spectrum, obtained through a exposure lamp).

The Doppler velocimetry method used throughout this work was initially developed by Dr. Thomas Widemann (Widemann et al., 2008) and further evolved by Dr. Pedro Machado for both long slit and fibre-fed spectrographs, using UVES/VLT and ESPaDOnS/CFHT respectively (Machado et al., 2012, 2014).

3.1.1 Method Summary

In order to derive the wind radial velocity w_i at each point (along the line-of-sight) in the planetocentric frame (P), i.e. in Venus' frame, the following steps are required:

1. Spectral wavelength calibration performed at beginning and end of the acquisition session, using a Th-Ar exposure lamp.

2. Since Earth's atmosphere also scatter solar radiation, the pipeline identifies two peaks in the spectrum with a relative shift - the solar radiation is scattered by both Venus' and Earth's atmospheres, though some lines are absorbed by Earth's atmosphere.

3. The Venus-scattered velocity h (in barycentric frame - B) is extracted by applying a least-squares deconvolution fit to the correlation function between Fraunhofer lines scattered at Venus and Earth's atmospheres.

4. Correction from Earth's spin and orbital motion ($berv$) and Venus' orbital motion (V_{topo}).

5. Correction of the Young effect (the influence of an unbalanced illumination from the two limbs of the rotating Sun).

6. Correction of the instrumental spectral drift (an on-target monitoring of the instrumental spectral drift to a specific location on Venus' disk - reference point)

Since the obtained values are the line-of-sight components of the wind velocities, it's necessary to perform a de-projection of the radial velocities to obtain the final zonal (parallel to the equator) and meridional (along the meridians) wind velocities.

Table 3.1 details the nomenclature used for the deprojected and modeled horizontal winds.

3.1.2 Projected Radial Velocities

The Doppler shift measured in solar scattered light on Venus' day side is the result of two instantaneous motions: (1) an instantaneous motion between the Sun and Venus' upper cloud particles; this Doppler velocity is minimal near Venus sub-solar point and maximum at the sub-terrestrial point; (2) a motion between the observer and Venus clouds, resulting from the topocentric velocity of Venus cloud particles in the observer's frame; this effect is minimal near Venus' sub-terrestrial point and maximum at sub-solar point. These combined instantaneous motions add-up and the combined Doppler shift vary spatially as a function of the planetocentric longitude and latitude on Venus. Considering that Φ is the phase angle between the Sun and Earth, centered on the target (Venus), at $\Phi/2$ the sum of both Doppler components (the sunlight that reaches Venus, with redshift, and the light re-emitted from Venus to Earth, with blueshift) is zero (see figure 3.1).

Task	Measurement/calculation	output
	line of sight/horizontal velocities :	
w_i	$h-(berv+v_{topo})$	Line-of-sight velocity in (P)
v_i	$w_{i,c}-w_{i,c,ref}$	Line-of-sight velocity, Young / ref. corr.
v'_i	$v_i-v_{i,trend}$	Line-of-sight velocity, detrended w/pt-10 exp.
$\overline{v}'_i$		Horizontal velocity at point i, day averaged
$v_{z,i}$		Zonal wind component at point i, instantaneous
$\overline{v}_z$	1-wind, v_{eq} zonal fit to $\overline{v}'_i$	Zonal wind fit, all latitudes, day averaged
$\overline{v}_m$	1-wind, v_{45° meridional fit to $\overline{v}'_i$	Meridional wind fit, HPA meridian, 2-day averaged
$\overline{v}_{z,lat}$		Zonal wind fit, latitude band lat, day averaged
$v_{z,lat}$		Zonal wind fit, latitude band lat, one sequence

Table 3.1: Velocity symbols used for deprojected and modeled horizontal winds in visible Doppler velocimetry using CFHT/ESPaDOnS data and VEx/VIRTIS cloud tracking data (two last entries). All data and fit units are m s^{-1} in Figures and Tables unless specified otherwise. Results are expressed in planetocentric frame (P).

In other words, the particles velocities relatively to the radiation source and relatively to the observer cancel each other out, resulting in an apparent null-Doppler meridian, in the case of a pure zonal wind field.

Half-Phase Angle (HPA) local meridian

As stated before, the measured Doppler shift is the combined effect of two instantaneous motions (a motion between the Sun and Venus upper clouds particles and a motion between the observer and Venus clouds). At half-phase angle (HPA), at planetocentric longitude the two effects cancel out for the zonal component of the wind field, as the relative velocities of particles toward the source of incoming radiation and towards the observer cancel each other out (fig. 3.6, thick solid red line). Along all points lying along this meridian we assume that the retrieved Doppler velocities cannot be attributed to a zonal component, thus, a non-zonal wind regime, such as meridional wind flow, should explain the Doppler shifts observed along the HPA meridian.

We therefore assumed that the Doppler shift residue retrieved along this meridian can be used to investigate the meridional wind flow. A χ^2 analysis yields a consistent result for a meridional flow pattern, with a marginal significance of the zonal component at the 2-σ level (as in Machado et al. (2017); Gonçalves et al. (2020)).

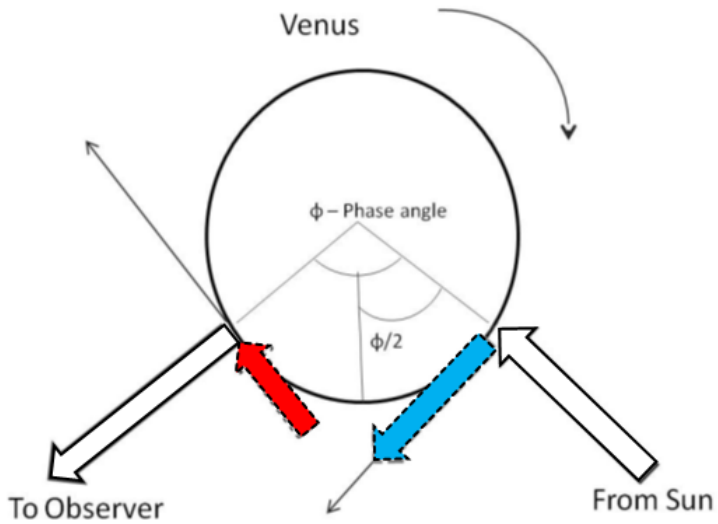

Figure 3.1: Schematics of the Doppler effect, considering a single scattering approximation. The direction of the Venus' rotations is shown by the curved arrow on the top. The solid white arrows represent radiation being absorbed (right hand side) and emitted (left hand side) without Doppler effect. Dashed arrows represent radiation being absorbed (red) or emitted (blue) with the respective Doppler effect. Φ is the phase angle between the Sun and Earth, centered on Venus.

3.1.3 Fraunhofer absorption lines at Venus and Earth

Solar radiation is scattered from both Venus' and Earth's atmospheres, although some of the Fraunhofer lines are absorbed by Earth's atmosphere. The instrument registers both spectra and a least-squares deconvolution is applied to the pattern of Fraunhofer lines, using a G2 type star mask (Sun's stellar type), providing the radial velocity (along the line-of-sight) in the solar system barycentric frame (B). The Venus-scattered velocity h is extracted by applying a double-Gaussian fit to the correlation function between Fraunhofer lines at Venus and Earth ones.

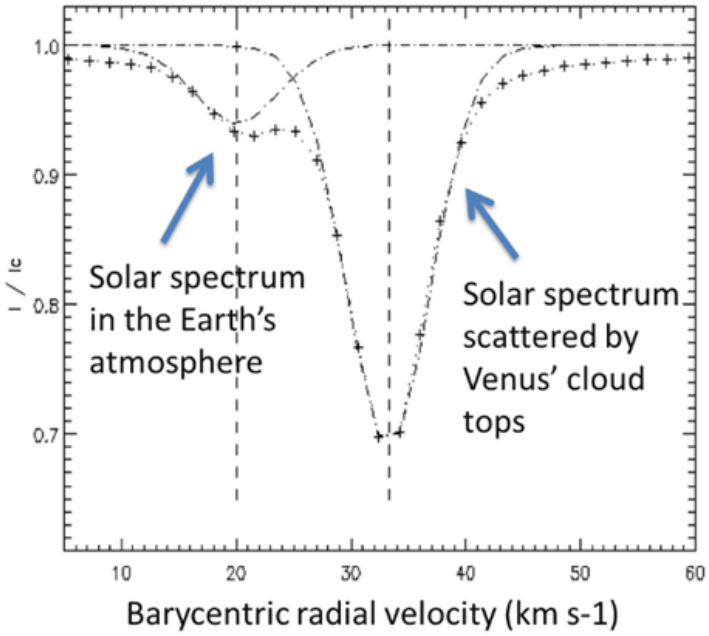

Figure 3.2: Correlation function of Fraunhofer lines scattered from Venus' and Earth's atmospheres.

3.1.4 Wind radial velocity

We derive the instantaneous Doppler shift for the motion of the cloud top aerosol particles in the planetocentric frame:

$$w_i = h - (berv + v_{topo}) \tag{3.1}$$

Where w_i is the radial component of the instantaneous velocity of Venus' top clouds in the observer's direction expressed in the Venus center rest frame (P,

planetocentric), h is the absolute velocity of solar lines scattered off Venus clouds expressed in the barycentric frame (B), *berv* is the correction from Earth's spin and orbital motion, i.e. observer's motion in the barycentric frame (B) (provided directly by the instrument pipeline), and V_{topo} is the instantaneous velocity of Venus' center of mass in the topocentric frame (T) (which is determined with *Horizons* ephemeris provided by the Jet Propulsion Laboratory - NASA-JPL).

3.1.5 Young effect

Due to the large, 0.5°, angular size of the Sun and its fast rotation (∼2 km/s), a differential elevation of the finite solar disk near terminator will result in unbalance between the contribution of the approaching solar limb (blue shifted radiation) and the receding solar limb (red shifted radiation). In such geometry, the excess of one or the other will affect the apparent line Doppler shifts measured along the Venus atmosphere. This is called the "Young effect". It can be shown that this effect is of the order of the Sun's equatorial velocity (2 km/s), multiplied by the ratio of its apparent radius as seen from Venus, to the angular distance from the target point to the terminator, and can be empirically approximated by:

$$Y \sim \frac{V_{\odot} D_{\odot}}{\sin\theta} \tag{3.2}$$

where $V_{\odot}$ is the solar equatorial velocity (2 km/s), $D_{\odot}$ is the solar angular diameter and θ the angular distance between the point being observed and the terminator. This equation is equivalent to the empirical relation proposed by Young (1975):

$$Y = 3.2\tan(SZA) \tag{3.3}$$

where SZA is the solar zenith angle (Young, 1975). The Young effect becomes significant near the terminator (which was near the central meridian in our observations), where it increases substantially. To correct the measured Doppler shift from the Young effect, we proceeded as follows:

$$w_{i,c} = w_i + Y(\phi, \psi) \tag{3.4}$$

where $w_{i,c}$ is the projected wind velocity along the line-of-sight, w_i is the measured Doppler shift (equation 3.1, section 3.1.4) Y is the corrective term due to the Young effect, function of ϕ and ψ, the planetocentric latitude and longitude of the observed point upon the disk. The equation 3.4 was therefore used in Machado et al. (2014, 2017) and Gonçalves et al. (2020).

Gaulme et al. (2018), in its extensive study on Doppler velocimetry on Venus and how to address limb darkening, suggested the use of the following equation.

$$\Delta V_Y(\varphi,\theta) = Y(\Lambda)\sin(\theta)\cos(\varphi) \tag{3.5}$$

Where φ is the SZA (angle of solar incidence), θ is the inclination of the solar rotation axis with respect to the local horizon and $Y(\Lambda)$ is a coefficient dependent on the wavelength. These improvements in the calculus of the Young effect were implemented after Gonçalves et al. (2020), which means, on the work based on March 2015 CFHT/ESPaDOnS observations (section 3.5.2). We used Y for a wavelenght of 550 nm, which corresponds to Y = 2.88 (see Gaulme et al. (2018) and Allen (1973)). While the previous equation (3.4) was valid only for the equator, this new approach to the Young effect actually extends its validity to the entire planet's disk and effectively reduces the associated error, therefore, we applied this equation on this work. However, the introduction of this new calculus only impacted the Young effect on the meridian closer to the evening terminator, $[\phi - \phi_E] = 20^\circ$ and by a factor of $\sim 1\%$.

3.1.6 Instrumental spectral drift

After the instantaneous velocity of Venus center of mass v_{topo} has been subtracted, the spectral wavelength calibration is performed at beginning and end of the acquisition session by means of a Th-Ar lamp exposure. Earth's atmosphere absorption lines superimposed to Venus' spectra are used as additional on-sky velocity calibration.

In measuring the global wind circulation at cloud tops, we are addressing wind amplitude variations or wind latitudinal gradients on Venus of the order of 5-10 m/s projected on the line-of-sight. It is therefore necessary to measure relative Doppler shifts between two sets of absorption lines. We proceed with relative Doppler velocities by choosing arbitrarily the first spectrum of each series of sequential acquisitions $w_{i,c,ref}$ as a velocity reference, so that

$$v_i = w_{i,c} - w_{i,c,ref} \tag{3.6}$$

Figure 3.3 shows line-of-sight velocities v_i with their error bars σ_i. They are plotted as a function of time, with target point numbers superimposed. Immediately apparent is a slow drift of the point 4 velocities. This drift occurs, presumably, due to still imperfectly corrected instrumental effects and measurement of solar absorption lines with respect to telluric lines (Young et al., 1979; Widemann et al., 2007).

On a fibre-fed spectrograph, such as ESPaDOnS or HARPS-N, Doppler velocimetry technique relies on a sequential spectral acquisition on Venus disk. This allows us to monitor a reference point on Venus disk during observations, in order to correct the Doppler velocities retrieved from the instrumental spectral drift

and/or spectral calibration variability with time. The reference point (point 22 as in fig. 3.6) is chosen as to be located along the equator and along the HPA meridian, so that both meridional and zonal components (respectively) of the wind retrieved from Doppler velocity should be zero. This makes the reference point an ideal tracker of the spectral drift, as long as it is observed frequently during the observation run.

Any variation along time measured on the Doppler shift of the reference point will be assume to be caused by the spectral drift of the instrument. We fit all the reference point velocities to a series of linear segments $v_{trend(t)}$ (dotted line on figure 3.3 bottom plot), assuming the initial velocity of point as the zero offset. Using this interpolated trend line, we can derive the offset caused by the spectrograph drift at any point in time, and therefore, correct this drifted offset to all the points observed, so that:

$$v'_i = v_i - v_{i,trend} \tag{3.7}$$

where each Doppler measurement v_i is subtracted by the value of the trend $v_{i,trend}$ at the time v_i was observed, obtaining a spectral drift corrected velocity v'_i.

This corrections requires an observation of a reference point before and after each sequence of points are observed. This way, we can measure the drift observed in the reference point and subtract it from all the measures of all the other points.

3.1.7 Error estimate

Absolute error on a given absolute velocity measurement $w_{i,c}$ results from the combination of a number of uncertainties: (i) the Th-Ar dispersion lamp spectrum uncertainty; (ii) the least-square deconvolution of Fraunhofer lines uncertainty; (iii) the additional fit to telluric line shift uncertainty; (iv) the errors due to additional weather conditions such as passing cirrus clouds, temperature variations or spectrograph mechanical flexure; (v) the uncertainly resulting from guiding and pointing errors during acquisition. Note that the reference trend polynomial $v_{i,trend}$ is also affected by these combined uncertainties.

Rather than trying to calculate an upper limit to the combination of the various error terms (i)-(v), we take advantage of repetition of short-time exposures at each point, to test the internal consistency of the retrieved radial velocity h. To estimate the individual error on each velocity measurement we repeated three times the short-time (3 sec) exposures at each target point and calculated the respective standard deviation (σ_i). The variability from successive exposures at each observational point indicates a high consistency, with an upper limit of 5 to 6 m/s between the mid latitudes range, but growing to twice this value at low SNR and/or higher latitudes or high SZA near terminator. Individual target point's velocities

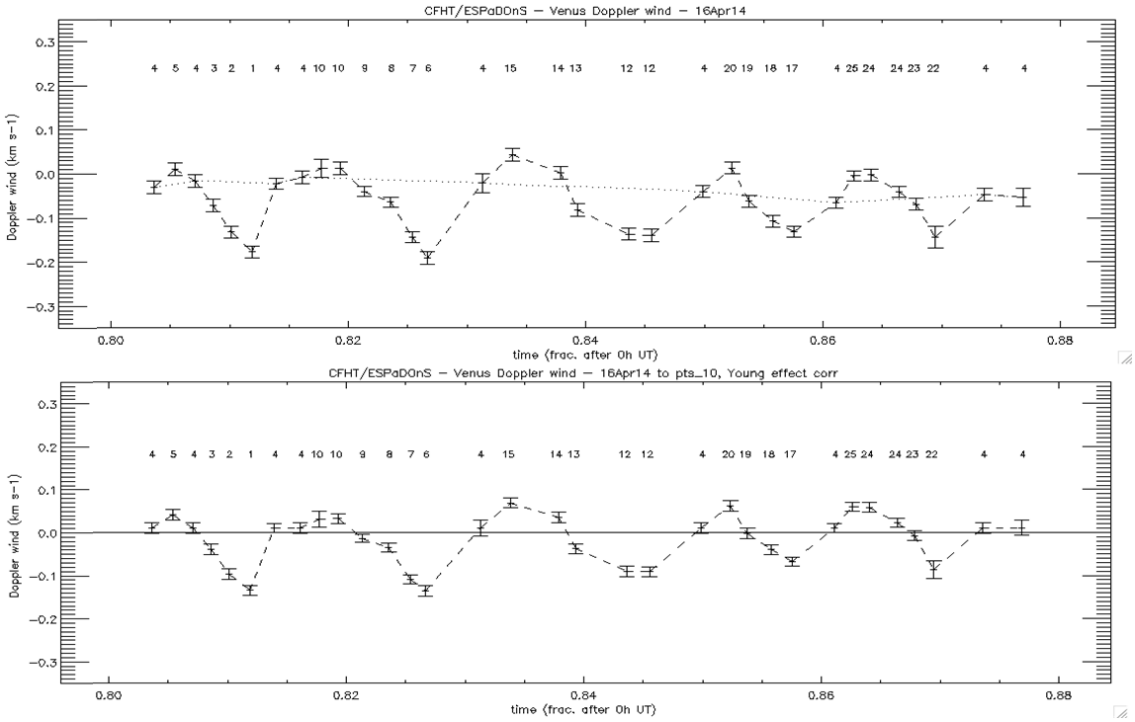

Figure 3.3: Doppler winds v_i and v'_i on April 16, as an example on the spectral drift correction technique. Point acquisition numbers are indicated in reference to Table 4.2 and Fig.4.13. X-axis is fraction of day after 0h UT. (a) top: relative velocity $v_i = w_{i,c} - w_{i,c,ref}$. Dotted line: vtrend(t) ; (b) bottom: kinematical fit to Apr. 16 differential wind field $v' = v_i - v_{i,trend}$ corrected for Young effect, to a pure zonal circulation with v = (117.4). The trend line (top plot) signalizes the spectral drift occurring in the observational run. By fitting the trend line of the reference point values (point 4) we can correct the drift effect that affects all the other measures (bottom plot).

were obtained by weight-averaging the retrieved values from the consecutive exposures taken at each Venus target pointing. Considering that σ_i is the error on the reference point velocity relative to the measurement v_i, therefore the statistical combined error at each point is given by

$$\sigma_i' = \sqrt{\sigma_{trend,i}^2 + \sigma_i^2} \tag{3.8}$$

To determine $\sigma_{trend,i}^2$ on the trend fitting function $v_{i,trend}$ at each point i, we linearly interpolated the error bar along the segment between two reference point exposures, which have been determined by taking advantage of repetition of short-time exposures. The associated error of each Doppler measurement, for both components of the wind, was in the order of 10-15 ms^{-1} for observations with ESPaDOnS and about 5-10 ms^{-1} for HARPS-N.

3.1.8 Pointing accuracy

The error associated with the fibre's FOV drift during an exposure, along Venus' disk, is bigger than the sum of all of the remaining uncertainties, since it will be propagated through the de-projection of line-of-sight shifts into horizontal zonal and meridional velocities. The observation run is thoroughly supervised, in situ and real time, by one of the researchers. If, during the 3 seconds exposure, the FOV of the fibre drifts away from the targeted point by more than a half of the fibre angular diameter, that exposure is discarded and repeated, until a total of 3 acceptable exposures is reached. This ensures a substantial containment of the errors caused from guiding and pointing drifts. The remaining error is further statistically reduced by observing the same point 3 times sequentially, for each time the point is being observed (see table 3.7 for a detailed line-up of the observation strategy).

The estimated combined pointing and tracking error is less than 0.4 arcsec, of the order of seeing conditions and within the ESPaDOnS FOV projected diameter of 1.6 arcsec on Venus. Note that this upper limit is equal for all points as the quality of guiding is independent of the solar zenith angle on Venus.

3.1.9 Kinematical wind models

The final velocities, relative to disk center, and corrected for the various effects discussed above, were then modeled using a kinematical model for the circulation in Venus' mesosphere. Line-of-sight Doppler velocities and horizontal zonal and/or meridional wind components are related by a matrix of projection coefficients for the velocity vector in heliocentric and topocentric reference frames. We calculated these coefficients for the zonal, sub-solar to anti-solar (SSAS), and

meridional components of the wind, with the help of a geometrical model (Lellouch et al., 1994). Explicit expressions for these calculations can be found in Goldstein (1989) and were also described in Widemann et al. (2007). Because the instrumental aperture covers a significant fraction of Venus' disk, the projection coefficients for each particular wind regime are calculated over a fine grid of points and then averaged over the aperture on Venus (0.6 arcsec). In order to first interpret the main global wind field at cloud top level we tested two different models:

1. A uniform velocity model between -60°and +60°

   $v_z(\lambda) = -v_{eq}$

2. A solid body model, where λ is the planetocentric latitude

   $v_z(\lambda) = -v_{eq} \times \cos(\lambda)$

Then the χ^2 best-fit has been performed between the measured velocities and the two described models. From the weighted average of all velocity measurements $\bar{v}'_i$ for each day, we fit to a one-parameter zonal circulation. At each individual point, a residue function $\bar{v}'_i - v_{mod,i}$ is retrieved. The parameter v_{eq} (the zonal wind equatorial velocity), minimizes the χ^2 best fit so that:

$$\chi^2_{vel} = \frac{1}{N_{df}} \sum_i \frac{(\bar{v}'_i - v_{mod,i})^2}{\bar{\sigma}'^2_i} \tag{3.9}$$

Where N_{df} is the number of degrees of freedom, $\bar{v}'_i$ is the day-averaged line-of-sight velocity at point i, and $v_{mod,i}$ is the line-of-sight model wind at point i. The fit quality is determined using the reduced χ^2, or $S_{min} = \sqrt{\chi^2_{vel}}$.

Zonal wind

To estimate the zonal wind, we used a 1-wind pure zonal model, as in Machado et al. (2017)). From the weighted average of all the velocity measurements (where the ponderation coefficients used were the inverse of each point variance), obtained on each observations night, we obtain the mean zonal velocity $\bar{v}_z$ in the planetocentric frame:

$$\bar{v}_z = \frac{\sum[c_{z,i} \cdot v'_{k,i}]/[\sigma^2_{k,i}]}{\sum[c^2_{z,i}/\sigma^2_{k,i}]} \tag{3.10}$$

where $c_{z,i}$ is the projection coefficient for point i, $v'_{k,i}$ is the measure k of velocity on the line of sight at point i and $\sigma_{k,i}$ its associated standard deviation. Both

uniform velocity and a solid body zonal wind models, yielded similar results in terms of v_{eq}, i.e. we could not distinguish the latitude dependence of the zonal flow between -50°and +50°.

Meridional wind

To estimate the meridional wind, we used a 1-wind pure meridional model, as in Machado et al. (2014)). The subsolar meridian was close to regions of maximum redshift while maximum blueshift was near sub-Earth. At half-phase angle (HPA) the two effects cancel out for the zonal component of the wind field (since the zonal wind is parallel to equator). Along all point lying along the meridian at $[\phi - \phi_E] = 36°$, we therefore assumed that the retrieved Doppler velocities, at those points, cannot be attributed to a zonal component. Hence, the contribution from other wind regimes such as a meridional flow was investigated in our analysis. A χ^2 analysis yields a consistent result for the meridional component, with a marginal significance of the zonal component at the 2-σ level. We monitored the positions along the HPA meridian (see figure 3.6) in our CFHT/ESPaDOnS datasets of Apr. 16 till Apr. 19 (points number: 4, 9, 14, 19, 24, 29, 31, 36, 41, 46 and 51), covering the latitudes from 40°S to 60°N by steps of 10°. We applied a best-fit method to pure meridional wind coefficients (c_m) along this meridian:

$$\bar{v_z} = \frac{\sum[c_{m,i} \cdot v'_{k,i}]/[\sigma^2_{k,i}]}{\sum[c^2_{m,i}/\sigma^2_{k,i}]} \tag{3.11}$$

3.2 Telescope and Instrument description

In this section we present a brief description and overview of the ground telescopes and instruments used in the development of this work: ESPaDOnS at CFHT; HARPS-N and NICS at TNG. Details about the space telescopes and instruments VEx/VIRTIS-M and Akatsuki/UVI can be found in section 4.2.

3.2.1 CFHT / ESPaDOnS

CFHT - Canada France Hawaii Telescope

The Canada France Hawaii Telescope (CFHT) is located in atop the summit of Mauna Kea (as part of the Mauna Kea Observatory), in the island of Hawaii, at 4200 meters altitude. This 3.6 meter optical/infrared telescope, that became operational in 1979, is a joint facility of the *"National Research Council of Canada"* (NRC), the *"Centre National de la Recherche Scientifique"* of France (CNRS) and the *University of Hawaii* (UH). Currently, the following instruments are in use at the CFHT:

- MegaPrime/MegaCam: MegaCam is a wide-field optical and infrared imgager covering a full 1 x 1 square degree field-of-view with a resolution of 0.187 arcsecond per pixel. MegaPrime is a prime focus upper end which includes an image stabilization unit and a guide/autofocus unit with two independent guide CCD detectors.
- WIRCam (Wide-field InfraRed Camera): near infrared mosaic imager with a FOV of 20 square min.
- SITELLE (SpectromÃ¨tre Imageur Ã TransformÃ©e de fourier pour l'Etude en Long et en Large de raies d'Emission): imaging Fourier transform spectrometer (IFTS) with integral field unit (IFU) spectroscopic capabilities in the visible (350 to 900 nm) over an 11 by 11 arcminutes FOV with a variable spectral resolution (R = 2 to R 10000).
- SPIRou (SPectropolarimÃ¨tre InfraROUge): fiber-fed near infrared (0.95 to 2.35 microns) spectropolarimeter with spectral resolution of 75000.

Figure 3.4: CFH Telescope in Mauna Kea Observatory, Hawaii, U.S.A. Credits: www.cfht.hawaii.edu

ESPaDOnS - Echelle SpectroPolarimetric Device for the Observation of Stars

The **E**chelle **S**pectro **P**ol**a**rimetric **D**evice for the **O**bservatio**n** of **S**tars (ESPaDOnS), at CFHT, is a bench-mounted high-resolution echelle spectrograph and spectropolarimeter which was designed to obtain a complete optical spectrum (from 370 to 1 050 nm) in a single exposure.

ESPaDOns consists of two distinct units, each located at a different place with respect to the telescope:

- Cassegrain unit - mounted at Cassegrain focus, includes the calibration/guiding module as well as the polarimeter module;

- Spectroscopic unit - installed in a thermally stable room right at the heart of the telescope building (the *Coudé* room), includes the spectrograph module (the core item of ESPaDOnS in terms of cost and weight) fed from the Cassegrain unit by the fibre link and image slicer module.

The calibration/guiding module includes three components: an atmospheric dispersion corrector (ADC), made of two separate prisms rotating independently from each other, cancelling out the atmospheric refraction in real time; a compact (1k $\times$ 1k) ccd camera looking at the instrument aperture (that can be used to autoguide on the star of interest or on any other star present in the 100" camera FOV); and a calibration wheel that can replace the stellar beam by various sorts of calibration light (such as a tungsten lamp for flat fielding purposes, a Thorium-Argon (Th-Ar) lamp used as a wavelength reference, and fully polarised light to impose known vibration directions as a polarising reference).

The spectrograph apparatus consists of a dual pupil configuration with 190 mm, a double set of high-reflectance collimators, a monolithic grating echelle (R2 type) as the diffraction device, with a size of 200 $\times$ 400 mm and 79 g/mm, a fully dioptric f/2 camera with 388 mm focal length; also in the instrument optical path there is a high dispersion prism cross-disperser and the detector's CCD (2k $\times$ 4.5k) with a pixel size of 0.0135 mm, inside a cryogenic cooling recipient (dewar cooling system). The optical path is the following: the beam bounces from the main collimator to a flat mirror, and then to a transfer collimator, to the double prism cross-disperser, through the fully dioptric camera and, finally, entering the CCD dewar camera, as seen in the diagram of figure 3.5.

The full spectral coverage of the optical domain extends from order number 61, centered at the wavelength of 372 nm, till order 22, centered at 1029 nm, with a spectral resolution of the order of 80 000 (object only mode). The peak throughput of the spectrograph (with ccd detector) is about 40% to 45%, bringing the total instrument peak efficiency at a level of about 15% to 20%.

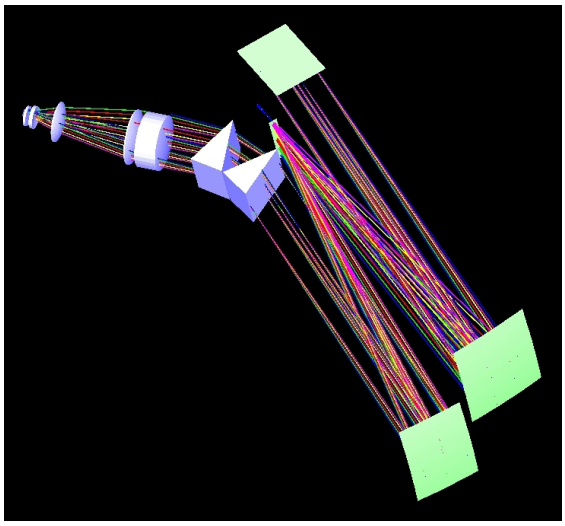

Figure 3.5: ESPaDOnS optical path. (Image from ESPaDOnS website).

Modes

The instrument has three different configurations choices for the 1.6” FOV slits:

- **Spectropolarimetric mode** - The two orthogonal states of a given polarization (either circular or linear) are recorded throughout the whole spectral range simultaneously on the ccd detector with the two sets of orders interleaved. The two fibre images are sliced in 3 at spectrograph entrance, yielding an average spectral resolution of about 68 000;

- **First spectroscopic mode (‘object+sky’)** - The spectra of the target and of the background sky are recorded simultaneously on the ccd detector (with orders interleaved), the two fibre images are sliced in 3 at spectrograph entrance, yielding an average spectral resolution of about 68 000;

- **Second spectroscopic mode (‘object only’)** - In this mode (the one used in this work), only the spectrum from the target is collect, the spectrum from the background sky is neglected (for objects bright enough to outshine the sky background, as is the case of Venus in our observations). The single fibre image is sliced in 6 at spectrograph entrance, bringing the average spectral resolution to about 81 000.

3.2.2 TNG / HARPS-N & NICS

TNG - Telescopio Nazionale Galileo

The 3.58 m telescope is the Italian facility located at the top of the Roque de Los Muchachos Observatory in the canarian island of La Palma, Spain. The Fundación Galileo Galilei, Fundación Canaria (FGG), is a Spanish non-profit institution, which main aim is to promote astrophysical research by managing the TNG together with its scientific, technical and administrative facilities. The financial support is ensured by the Italian Istituto Nazionale di Astrofisica (INAF) (http://www.tng.iac.es/).

TNG handles observing time allotted by answering to four calls: INAF (Italian time and TNG-NOT agreement), CAT (Spanish time), ITP (International Time), and OPTICON. The telescope has currently the following instruments on service:

- HARPS-N (High Accuracy Radial velocity Planet Searcher in North hemisphere): a high-resolution (resolving power R = 115000), high-stability visible spectrograph (383-693 nm). Design for the discovery and characterization of exoplanets, down to Earth-like size ones.
- GIANO: a high-resolution (R=50,000) IR spectrograph, covering the 0.9-2.5 micron range. Used for the characterization of exoplanet astmospheres and for the detailed abundance analysis of stellar atmospheres.
- DOLORES (Device Optimized for the LOw RESolution): a multi-mode imager/spectrometer at visual wavelengths with a FOV of 9'x9' and spectral resolving power from R = 300 to R = 7 000. Well-suited for the monitoring of transient events and extragalactic sources.
- NICS (Near Infrared Camera Spectrometer): a multi-mode imager/spectrometer at infrared wavelengths (0.9-2.5 microns) with a FOV of up to 4.2'x4.2' and spectral resolving power from R=40 to R=2,500. Well-suited for the monitoring of transient events and study of solar systems objects.

HARPS-N

HARPS-N (High-Accuracy Radial-velocity Planetary Searcher - North) is an echelle spectrograph covering the wavelength range between 383 to 693 nm, with a spectral resolution of R = 115000, collected over 69 spectral orders in a single exposure (Cosentino et al., 2012). The two fibres entrances (object + sky or Th-Ar), fed by the Nasmyth B Focus, with a FOV of 1", is re-imaged by the spectrograph optics onto a 4k x 4k back-illuminated CCD with 15 µm square pixels (http://www.tng.iac.es/instruments/harps/).

The design of HARPS-N is based on the experience acquired with HARPS, installed at 3.6 m telescope in La Silla, Chile, designed for the study of exoplanets, measuring Radial Velocities (RV) at highest precision. The HARPS-N Project is a collaboration between the Astronomical Observatory of the Geneva University (lead), the CfA in Cambridge, the Universities of St. Andrews and Edinburgh, the Queens University of Belfast, and the TNG-INAF Observatory.

An automatic data reduction system (DRS) is included with HARPS-N to reduce, shortly after the exposure, observations for "classical" spectroscopy and high-precision Doppler measurements with simultaneous wavelength reference. For science exposures, the DRS outcomes are flat-fielded, wavelength-calibrated spectra and, when possible and requested, barycentric radial velocity of the target. Calibration exposures are used by the DRS to calibrate the instrument for best-quality scientific reduction. The DRS is designed to run automatically like a batch process on the archived frames. All relevant parameters required by the DRS are passed to the DRS through the FITS headers of the archived frames. Results of the DRS are stored in the FITS keywords of reduced frames. The final products of the DRS process are background-subtracted, cosmic-corrected, flat-fielded and wavelength-calibrated spectra (with and without merging of the spectral orders). The possibility to flux-calibrate the spectra is also available. These products are provided also for the reference fiber (sky or simultaneous wavelength calibration) if applicable. In addition to these reduction products, cross-correlation functions of the spectra are also computed to provide high-precision radial velocities.

The work presented here (as in Gonçalves et al. (2020)) was the first observation to use HARPS-N to study the atmosphere of a Solar system body. This opened a new window of opportunity for future solar system observations (Venus or other) using the high-resolution spectrograph HARPS-N.

NICS

The Near Infrared Camera Spectrometer mounted on TNG can work both as a imager or a spectrometer (http://www.tng.iac.es/instruments/nics/). The imager provides a FOV of up to 4.2’ x 4.2’ and a resolving power from R = 40 to R = 2,500

- **Imaging mode:**

  The imaging mode can use a large (LF) or small field (SF) camera. The LF offers a FOV of 4.2’ x 4.2’ with a pixel scale of 0.25"/pix, small enough to properly sample the images under normal seeing conditions. The SF is primarily intended for imaging programs requiring a fine sampling of the point spread function, providing a FOV of 2.2’ x 2.2’ with 0.13"/pix image scale. It has a superb optical quality with negligible field distortion.

The instrument is equipped with a number of broad and narrow band filters from the from K band to metane CH4 filters, ranging respectively from 1.68 to 2.20 μm.

- **Spectroscopic mode:**

  The instruments provides a long slit spectroscopy mode by inserting a slit at the entrance focal plane and a disperser (prism or grism) in the collimated beam. The instrument is equipped with one prism (0.8-2.5 μm) and a number of grism dispersers that range from 0.9 to 2.34 μm for both low (R 500) and high (R 1250) resolution. The available slits' width (all with 4' lenght) vary from 0.5" to 2.0", which corresponds to 2 to 8 pixels respectively. All spectroscopic modes make use of the LF camera with a scale of 0.25"/pixel. It is also possible to perform low resolution spectroscopic observations using the Amici prism in slit-less mode. This provides a FOV of 3.5' x 4.2', a spectral coverage of 0.9-1.75 μm.

3.3 CFHT/ESPaDOnS April 2014

3.3.1 Observations (April 2014)

These observations were made in 16, 17, 18 and 19 April 2014, using the ESPaDOnS in CFHT, in coordination with ESA's Venus Express mission (see section 4.3.1). In addition to coordinating with Venus Express, the choice of observing dates offered the best compromise between the need to (i) maximize the angular diameter of Venus and spatial resolution on the disk, and (ii) minimize Venus phase angle and illuminated fraction as we only observe the day side.

Between the 16^{th} and 19^{th} april, Venus was observed at a phase angle Φ (Sun-Target-Observer) of 77.1°-75.6°, with surface brightness at 1.35-1.33 (mag/arcsec), apparent magnitude from -4,27 to -4.22, illuminated fraction between 61.2%-63.2% and an angular diameter of 19.11-18.61 arcsec (see table 3.6 for more details).

The observing strategy has been to displace the entrance fibre of the spectrograph along points on the dayside hemisphere, while taking a reference point exposure between each sequence (reference point at the intersection of Equator and the null zonal Doppler meridian, as in figure 3.6). Exposure times were adjusted at t = 3 sec to obtain a S/N > 400 on the continuum and avoid saturation. The sequence of observation points (ajusting the fibre of ESPaDOnS to each positions as is figure 3.6) is displayed in table 3.7.

(1) Date	(2) UT	(3) Phase angle Φ (°)	(4) Ill. fraction (%)	(5) Ang. diam. (")	(6) Ob-lon/lat (°)	(7) Airmass	(8) seeing (")
16 Apr	19:00-21:16	77.1	61.2	19.11-19.10	170.7/ -0,43	1.14-1.25	0.9-0.8
17 Apr	16:53-20:47	76.7-76.6	61.5	18.96-18.93	173.1/ -0.38	1.50-1.18	1.0
18 Apr	17:10-20:58	76.2-76.1	62.0	18.79-18.77	175.7/ -0.32	1.41-1.20	1.1-0.6
19 Apr	17:13-20:34	75.7-75.6	62.4	18.63-18.61	178.3/ -0.27	1.39-1.15	1.1-0.6

Table 3.2: Orbital geometry and circumstances of ground-based observations 16-19 Apr 2014: (1-2) Date/UT interval ; (3-5) disk aspect ; (6) sub-observer longitude and latitude (planetocentric) ; (7-9) observing conditions and geometry.

The initial data was reduced and retrieved by a pipeline software named "Libre-ESpRIT", which is available to use in any observational run with the ESPaDOnS. This pipeline produces one file for each point observation in the format *".out"*, which is a text format. The first step in our work was to export (manually) the

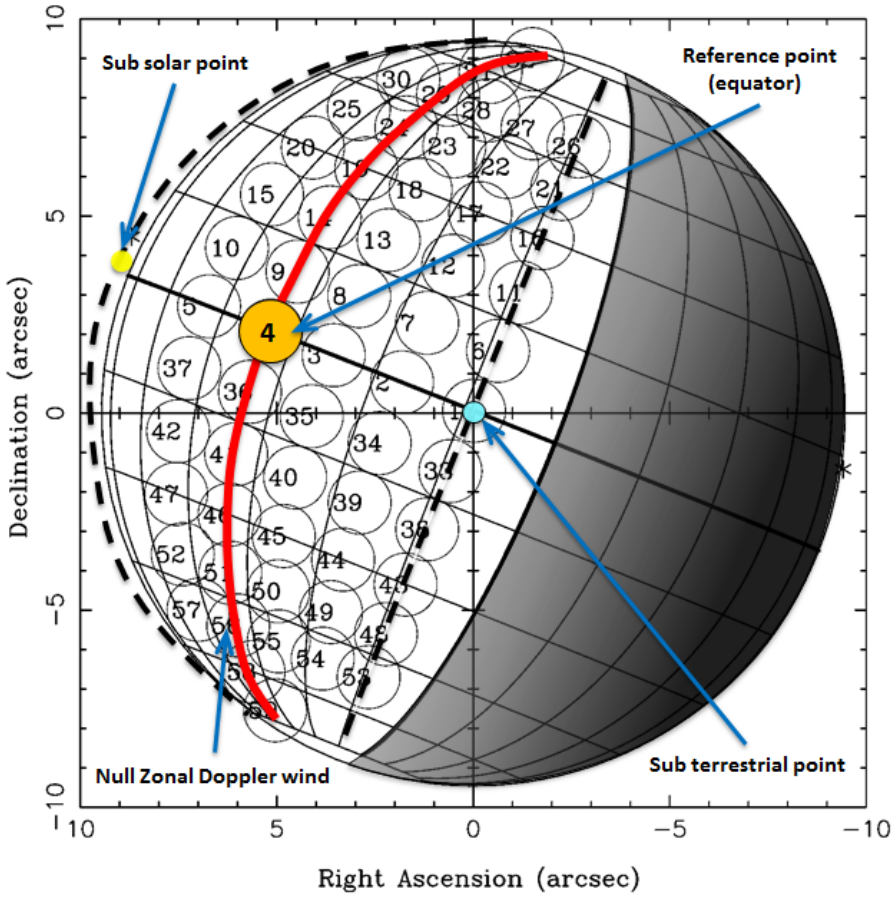

Figure 3.6: Aspect and angular size of Venus as seen from Earth on Apr. 18, 2014, 19h UTC. RA and DEC axis are in arcsec. Celestial North is up. From left to right : (1) thick dashed line is the sub-solar meridian (with the Sun symbol at sub-solar point in yellow) ; (2) red solid line in the half-phase angle (HPA) meridian at $[\phi - \phi_E] = \Phi/2 = 38.2^\circ$; (3) thick dashed-dotted line is the sub-terrestrial meridian (with sub-Earth point as a blue circle) ; (4) local morning terminator is noted as a thick solid grid line east of central meridian. Point numbers as cited in the text are indicated. Planetocentric latitude of sub-Earth and sub-solar points are -0.32° and 1.32°, respectively. The figure illustrates our observing strategy to match CFHT/ESPaDOnS operations (thin black circles) with the respective field of view (1.6”). The point 4 is the reference point (at 0°latitude and 36°longitude) used for the spectral calibration.

(1) Loc.	(2) Time (UT)	(3) Points order
Equator	19:01-19:33	4-4-5-4-3-2-1-4
N lat 10°	19:35-19:58	4-10-10-9-8-7-6-6-4
N lat 20°	19h59-20:25	4-15-14-13-12-12-11-4
N lat 30°	20:26-20:41	4-20-19-18-17-16-4
N lat 40°	20:42-21:03	4-25-24-23-22-21-4
Equator	16:53-17:35	[4]-4-4-5-(4)-[3]-[2]-[1]-4
N lat 10°	17:36-17:55	[4]-10-(10)-9-[8]-[7]-[6]-[4]
N lat 20°	18:00-18:24	4-[15]-14-[13]-4
N lat 30°	18:26-18:43	4-20-19-[18]-[17]-4
N lat 40°	18:50-19:21	4-[25]-24-(24)-23-[22]-[21]-4
S lat 10° - 30°	19:22-20:25	(4)-4-(37)-37-36-47-46-45-44-(43)-[4]-4
$[\phi - \phi_E] = 36°$, N	17:10-17:30	4-9-14-19-24-29-31-32-4
$[\phi - \phi_E] = 36°$, S	17:31-17:55	4-36-41-(46)-46-46-[51]-56-[58]-58-4
$[\phi - \phi_E] = 0°$	17:58-18:37	[4]-[1]-[6]-[11]-[16]-[21]-[4]-[33]-[38]-[43]-[48]-[53]-[4]
$[\phi - \phi_E] = 24°$	19:57-20:58	4-3-8-13-18-[4]-23-28-4-3-4
N lat 20°	17:13-17:29	4-15-14-13-12-11-4
N lat 30°	17:31-17:45	4-20-19-18-17-16-4
N lat 40°	17:46-18:10	4-(25)-[25]-25-24-[23]-23-22-21-21-4
S lat 20°	18:11-18:25	4-42-41-40-39-38-4
S lat 30°	18:27-18:47	4-47-46-46-45-44-43-43-4
S lat 40°	18:48-19:11	4-52-51-51-50-49-48-4
N lat 20°	19:12-19:26	4-15-14-13-12-11-4
N lat 30°	19:27-19:47	4-20-19-18-17-16-16-4
N lat 40°	19:49-20:06	4-25-24-23-22-21-4
S lat 20°	20:16-20:34	4-42-41-41

Table 3.3: Scanning sequences on Venus' dayside hemisphere using CFHT/ESPaDOnS during the Apr. 16-19 (separated by horizontal lines) observing run: (1) location on disk; (3) UT time interval; (4) points acquisition order; points in parenthesis have been observed but not included in the kinematical best fits either for their lower S/N and/or limb or high SZA geometry. Each point is acquired 3 times, with 3 seconds exposure each, to check for internal consistency. Points in brackets were discarded from analysis due to severe drift, seeing or tracking issues.

Date	Mean zonal wind (m s^{-1}) $\bar{v}_z$	reduced χ^2	2σ m s^{-1}	3σ m s^{-1}
16 Apr. 2014	119.6	1.49	$\pm$ 16.5	$\pm$24.8
17 Apr. 2014	122.6	3.38	$\pm$ 31.3	$\pm$62.5
18 Apr. 2014	119.6	2.27	$\pm$ 26.0	$\pm$39.5
19 Apr. 2014	118.1	1.78	$\pm$ 19.5	$\pm$29.5
Date	Meridional velocity (m s^{-1}) $\bar{v}_m$	reduced χ^2	2σ m s^{-1}	3σ m s^{-1}
16-19 Apr. 2014	22.5	1.68	$\pm$15.5	$\pm$20.3

Table 3.4: CFHT/ESPaDOnS mean zonal and mean meridional flow results. - (a) Mean zonal velocity $\bar{v}_z$ on April 16, 17, 18 and 19, 2014 data. The 1-wind regime fit is applied to the entire probed region $v_{z,i}$ data points. Best-fit reduced χ^2 is indicated at 2σ and 3σ confidence. (b) Mean meridional wind velocity $\bar{v}_m$ fit along HPA meridian ($[\phi - \phi_E] = \Phi/2 \simeq$ -38°), obtained at 2σ and 3σ confidence level.

data we needed from each pointing, from each file *.out* to an excel page. Then, we analyzed manually which points suffered an anomaly (such as a telescope drift or passing clouds) and which data may have been compromised. The next step was to run our manually reduced data through *IDL* programs, introducing the theoretical models and calculating the mean wind values (zonal and meridional)

3.3.2 Results (April 2014)

Mean zonal circulation

After applying all the necessary corrections (Young effect and spectral drift), and weighed averaged all the measures of each position for each day, we applied the respective theoretical models, under the assumption of a pure zonal one-wind system, to all data points with latitudes between -50°and +50°(as the model predicts), to estimate the mean zonal wind (parallel to equator).

The results obtained, with the CFHT/ESPaDOnS observations, for the mean zonal and mean meridional winds, with a best-fit reduced χ^2 at 2σ and 3σ confidence, are presented in table 3.4 (results for day-averaged wind velocity $\bar{v}'_i$).

Day-averaged zonal wind

By weigh averaging all the measures for each position, we obtained a single mean value for each position, for all the 4 days. With this data, we produced a color map of the zonal mean velocity for each position, as seen in figure 3.7.

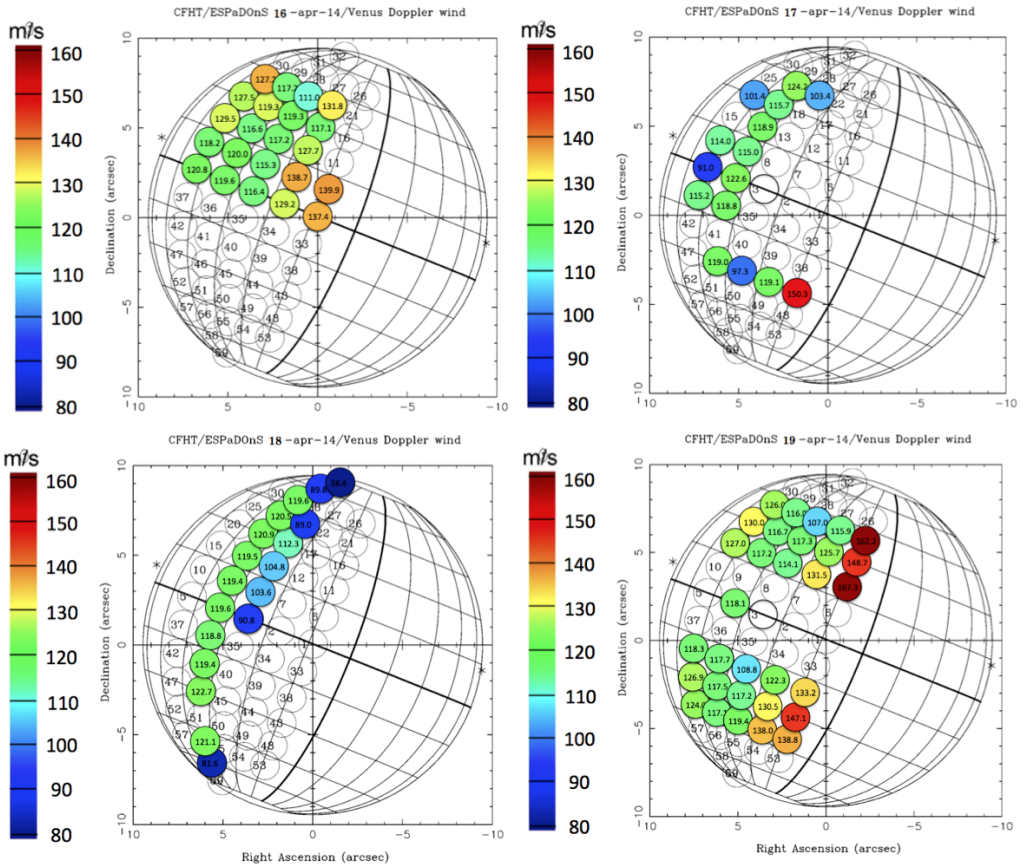

Figure 3.7: Results for day average (16-19 April) wind velocity $\overline{v}_i'$ (ms^{-1}) at latitude/local time points of table 3.7.

CFHT/ESPaDOnS observations took the form of observing sequences between April 16^{th} and 19^{th}. Sequences [1-5] (Apr. 16) were acquired across the dayside hemisphere at latitudinal bands 10-degrees apart at latitude/local time points of table 3.7 in a 2-hours time scale. On this day of observations ESPaDOnS has a projected field of view of 507 km at Venus' disk center. The upper-left of figure 3.7 locates points acquired on that day with the resulting horizontal wind superimposed to each point.

Observed measurements of Apr. 17 (sequences [6-11]) appear in the upper right part of figure 3.7. Observations on Apr. 17 were frequently interrupted

by clouds and this is reflected by the larger confidence interval at 2σ and 3σ appearing in table 3.4 for the mean zonal circulation.

On Apr. 18, 2014 (sequences [12-15] bottom-left part of figure 3.7), our priority was given to repeated observations of the HPA (null-Doppler meridian) in search for the meridional component of the wind (see the following subsection 3.9). The mean-zonal circulation was also retrieved from the available sequences, especially using the 30°S latitude band.

On Apr. 19, 2014 (sequences [16-25]), N and S hemispheres were symetrically explored during a 3:20 period [17:13 UT-20:34 UT] for the monitoring of zonal wind short term variability. This is further described in Section 3.3.2.

The best-fit results for the four days of observations are self-consistent, with $\overline{v}_z$ = (119.6 $\pm$ 16.5) ms^{-1} on Apr. 16, $\overline{v}_z$ = (122.6 $\pm$ 31.3) ms^{-1} on Apr. 17, $\overline{v}_z$ = (119.6 $\pm$ 26.0) ms^{-1} on Apr. 18, and $\overline{v}_z$ = (118.1 $\pm$ 19.5) ms^{-1} on Apr. 19, with a best quality of fit on Apr. 16 and Apr. 19 (S_{min} = 1.49 and 1.78, respectively). Although the overall fit looks reasonable, the fit is statistically poor on Apr. 17 and 18 (S_{min} = 3.38 and 2.27, respectively), suggesting that individual error bars may be underestimated, or that the circulation is more complex than described by the model.

Zonal wind latitudinal profile of CFHT/ESPaDOnS $\overline{v}_{z,i}$ velocities obtained from a weighed average on all data present on our observations (Table 3.5), and consolidated by the observations from all days of observations, are shown in Fig. 3.8.

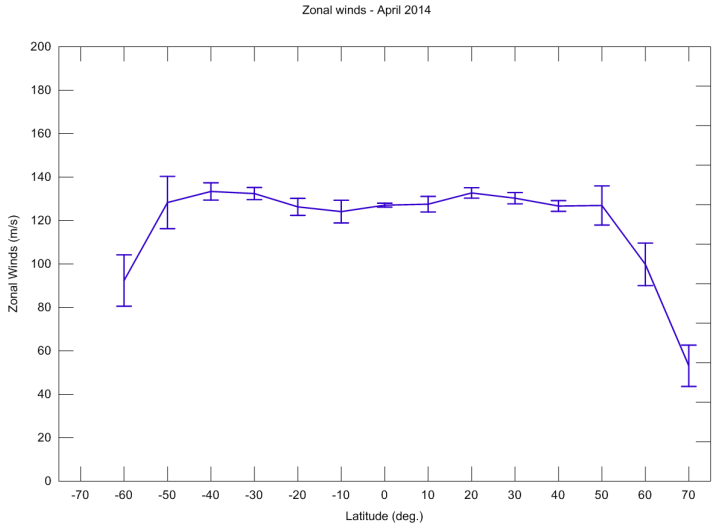

Figure 3.8: Zonal wind latitudinal profile, $\overline{v}_{z,i}$ velocities combine all Apr. 16-19, 2014 CFHT/ESPaDOnS observations of table 3.5). The weighing coefficients reflect the zonally averaged variance of each latitude. We note an almost uniform average zonal wind component ($\overline{v}_{z,i}$) between mid-latitudes, the presence of mid-latitudes jets and a sharp decrease of zonal wind for higher latitudes (higher than 50°).

Meridional wind

The data gathered in day 18^{th} April allowed us, after applying the respective theoretical model, to estimate the meridian wind flow for the Hadley cell, from -50°to +60°latitude. The points in the Null-Zonal Doppler meridian (longitude = 36°) are points in which the Doppler shift effect cancels out, due to the half-angle phase location, as explained earlier. For those points, we assumed that the Doppler measures were due to meridian wind flow caused by the Hadley cell structure.

A poleward meridional wind component is determined within the 2-σ statistical significance by selecting the line-of-sight measurements on half-phase angle meridian HPA. Table 3.4 shows the mean meridional wind velocity $\overline{v}_m$ fit along HPA meridian ($[\phi - \phi_E] = \Phi/2 \simeq$ -38°), obtained at 2σ and 3σ confidence level by combining HPA data from Apr. 16-19 sequences [1-25], analyzing the entire data set with a single meridional model.

For the first time, a meridional wind component at cloud top is simultaneously observed from the ground in the two hemispheres (figure 3.9). Negative velocities in the S hemisphere on figure 3.9 reflects poleward cloud top motion, while positive values in the N hemisphere also indicate a poleward motion. This is in agreement with a Hadley cell's upper branch, were the meridional wind flows from equator region to higher latitudes. We note the almost symmetrical behavior of the meridional flow between N and S hemispheres. The dashed line is a fit to a pure meridional model flow with $\overline{v}_m = (22.5 \pm 15.5)$ m s^{-1} (see table 3.4).

Our meridional wind model is assumed to vary sinusoidally with latitude, having zero velocity at equator and the poles, and a maximum value at 45° latitude. It can be noted that our measurements differ significantly from this model poleward of 50°, meaning lower winds than predicted at high latitudes near the cold collar.

Zonal wind variability (spatial and temporal)

$[\phi - \phi_E]$ longitudinal (local time) variations of zonal wind velocities $\bar{v_{z,i}}$ Here we present the latitudinal profile (fixed latitude) for each day of CFHT/ESPaDOnS zonal wind velocities $\overline{v}_{z,i}$ (days 16, 17, 18, 19 April, 2014). Each presented latitudinal wind velocity results from a weighed average along each latitude band measured on each day of observations. The weighing coefficients were the inverse of the variance associated to each velocity measurement. Figure 3.10 shows a comparison of day-averaged zonal wind $\overline{v}_{z,i}$ at various latitudinal bands on different days of April 2014 observations. On each plot, X-axis is west longitude to sub-terrestrial meridian. $[\phi - \phi_E]$, and the corresponding to local times. Y-axis are $\overline{v}_{z,i}$ determination. Fit results to a pure zonal wind per latitudinal band $\overline{v}_{z,lat}$ are indicated in table 3.5.

Table 3.5 shows 1-wind zonal circulation per latitudinal bands $\overline{v}_{z,lat}$ is fit to

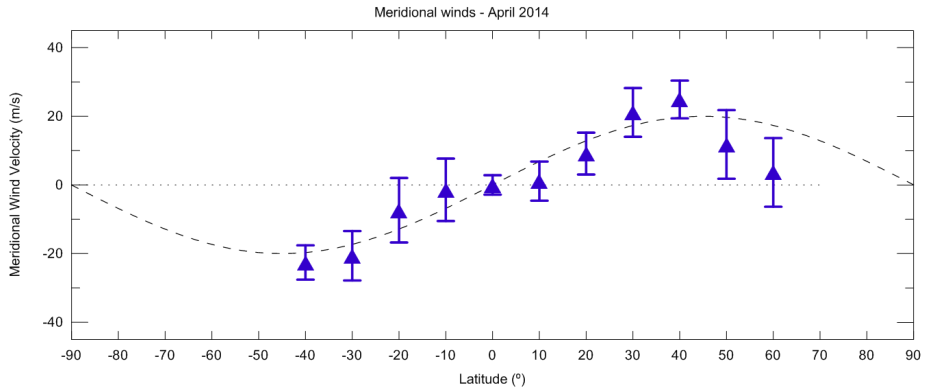

Figure 3.9: Meridional wind component determined e by consolidating the line-of-sight measurements along half-phase angle meridian HPA, averaged over Apr. 16-19 sequences. Negative velocities in southern hemisphere means aerosols motion away from equator, as is the case of the positive values of meridional wind in northern hemisphere (remind that our reference is position number 4, at equator). The dashed line is a fit to a pure meridional model flow with $\overline{v}_m$ = (22.5 $\pm$ 15.5) m s^{-1} (see table 3.4). It is assumed to vary sinusoidally with latitude, having zero velocity at equator and the poles, and a maximum value at 45° latitude.

day-averaged wind values $v_{z,i}$ of figure 3.10, with their statistical significance at the 2-σ level. The weighing coefficients were the inverse of each retrieved velocity's variance.

Figure 3.11 shows latitude bands of day-averaged horizontal zonal wind $\overline{v}_{z,i}$ as in figure 3.10. Fit results to a pure zonal wind per latitudinal band $\overline{v}_{z,lat}$ are indicated in table 3.5.

Temporal variation - By comparing the same latitudinal band for different days (figure 3.10, we can analyze the time evolution and variability of zonal winds. For 40°N and 30°S latitudinal bands, is notorious a slight variation in zonal wind velocity, in the points located at $[\phi - \phi_E]$ = -12° and $[\phi - \phi_E]$ = -24°, respectively. These variations were measured with two and three day intervals for 40°N and 30°S latitudinal bands, respectively. Although these variations are of the order or 20 m/s, they are of the same order of the respective error bars, thus, they may not represent substantial temporal variation. Additional, the variation in the latitudinal bands 30°S may be due to the difficulties faced during the observations of day 17 Apr (high cirrus clouds passing during observations).

Spatial (latitudinal) variation - By comparing all the latitudinal bands of each day-averaged horizontal zonal wind $\overline{v}_{z,i}$ (figure 3.11), no unambiguous spatial variation can be derived, since all latitudinal bands show similar profiles (vari-

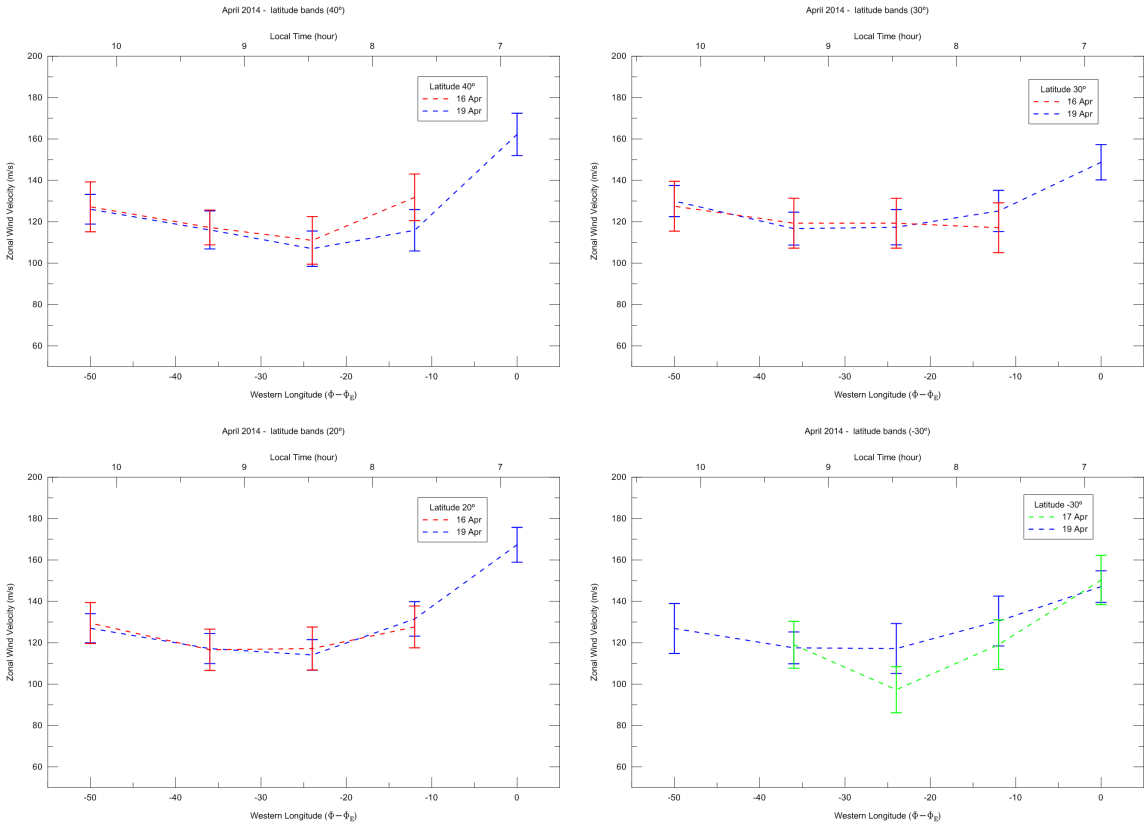

Figure 3.10: Latitude bands of horizontal zonal wind $\overline{v}_{z,i}$ across ESPaDOnS' day-side local-time range between 6:50a and 10:00a. X-axis is west longitude to sub-terrestrial meridian. $[\phi - \phi_E]$, corresponding to local times 6:50a (0°), 7:40a (-12°), 8:30a (-24°), 9:15a (-36°), 10:10a (-50°) from terminator (left) to sub-solar region (right). Y-axis are $\overline{v}_{z,i}$ results. Fit results to a pure zonal wind per latitudinal band $\overline{v}_{z,lat}$ are indicated in table 3.5. Top left: Comparison between day 16 and 19 April, 2014, for 40°N latitude band. Top right: the same but for 30°N. Bottom left: Comparison of 20°N latitude band for day 16 and 19 April, 2014. Bottom right: Comparison of 30°S latitude band for day 17 and 19 April, 2014.

	Dates			
	Apr. 16, 2014	Apr. 17, 2014	Apr. 18, 2014	Apr. 19, 2014
Lat. band	$\overline{v}_{z,lat}$ (m s^{-1})	$\overline{v}_{z,lat}$ (m s^{-1})	$\overline{v}_{z,lat}$ (m s^{-1})	$\overline{v}_{z,lat}$ (m s^{-1})
70°S	-	-	38.4 ± 10.5	-
60°S	-	-	89.8 ± 10.8	-
50°S	-	-	119.6 ± 9.9	-
40°S	121.0 ± 5.2	115.0 ± 6.8	97.8 ± 9.0	123.9 ± 3.9
30°S	120.8 ± 6.0	108.8 ± 8.4	120.1 ± 10.6	127.5 ± 3.7
20°S	122.8 ± 5.0	118.9 ± 11.2	115.3 ± 9.3	129.5 ± 3.4
10°S	123.7 ± 5.1	114.2 ± 10.1	115.4 ± 8.2	-
0°S	120.3 ± 2.0	116.2 ± 6.2	118.6 ± 2.4	118.8 ± 4.8
-10°S	-	-	118.8 ± 16.0	129.6 ± 4.3
-20°S	-	120.5 ± 5.8	119.4 ± 10.3	126.7 ± 4.4
-30°S	-	-	122.7 ± 6.9	-
-40°S	-	-	-	-
-50°S	-	-	121.1 ± 13.2	-
-60°S	-	-	81.6 ± 13.0	-

Table 3.5: 1-wind zonal circulation per latitudinal bands $\overline{v}_{z,lat}$ is fit to day-averaged wind values $v_{z,i}$ of Fig. 6, with their statistical significance at the 2-σ level.

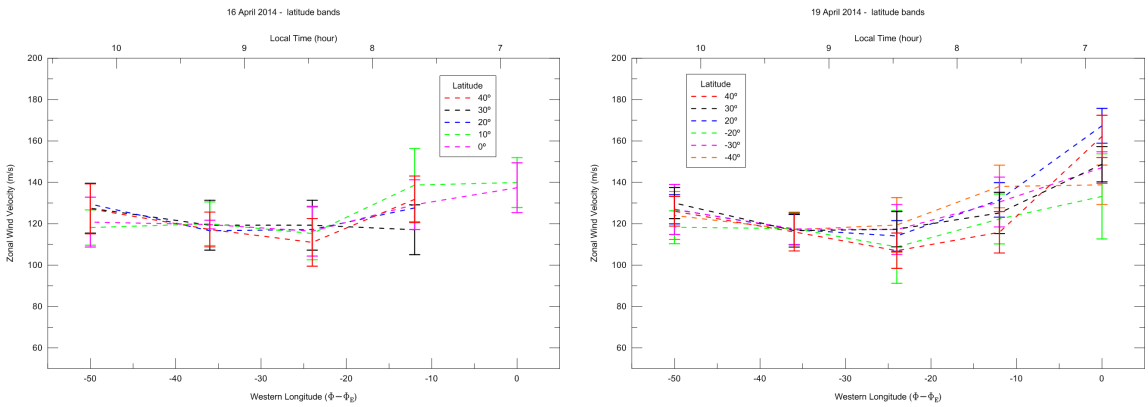

Figure 3.11: Latitude bands of day-averaged horizontal zonal wind $\overline{v}_{z,i}$ as in figure 3.10. Fit results to a pure zonal wind per latitudinal band $\overline{v}_{z,lat}$ are indicated in table 3.5. Left: Latitude bands for day 16 April, 2014. Right: Latitude bands for day 19 April, 2014.

ations in the order of the error bars - 10m/s). The observations made in the 17^{th} and 18^{th} April were more focused on the Half-Phase meridian (longitude -36°), thus, no significant analysis could be done for latitudinal and temporal variation from said data. In both figures(3.10 and 3.11) it is noticeable the very similar profiles with velocities decreasing from the terminator onwards (western longitude direction), with a slight increase at longitude -50°S. The systematic higher wind velocities in the sub-terrestrial meridian ($[\phi - \phi_E] = 0°$) can be interpreted in terms of a thermal solar tide, as stated by Machado et al. (2014) and Sánchez-Lavega et al. (2008).

Latitudinal variations of zonal wind velocities $\overline{v}_{z,i}$ Here we present the longitudinal profile (fixed longitude) for each day of CFHT/ESPaDOnS zonal wind velocities $\overline{v}_{z,i}$ (days 16, 17, 18, 19 April, 2014). Each presented longitudinal wind velocity results from a weighed average along each latitude band measured on each day of observations. The weighing coefficients were the inverse of the variance associated to each velocity measurement.

Comparison from day-averaged longitude bands of zonal wind $\overline{v}_{z,i}$ between observational days, across ESPaDOnS' dayside, are presented in figure 3.12 (X-axis are $\overline{v}_{z,i}$ results and Y-axis is latitudes along Venus). Referred longitudes correspond to west longitude to sub-terrestrial meridian $[\phi - \phi_E]$, where 0° correspond to local time of 6:50a, -12° to 7:40a, -24° to 8:30a, -36° to 9:15a and -50° to 10:10a.

Spatial variability of day-averaged on relative longitudes bands, in solar-fixed coordinates, of zonal wind $\overline{v}_{z,i}$ across ESPaDOnS' dayside, are presented in figure 3.13 (X-axis are $\overline{v}_{z,i}$ results and Y-axis is latitudes along Venus). Referred surveyed longitudes and local times are as in figure 3.12.

Temporal variation - By comparing the same longitudinal band for different days (figure 3.12, we can analyze the time evolution and variability of zonal winds. None of the longitude bands show any unambiguous variation with time, with the exception of longitude -50°(10:10a local hour). However, the wind velocity variations shown in the said longitude band (-50°) may also be due to the adverse observing conditions encountered during the observations of day 17 Apr (high cirrus clouds passing in front of the FOV). The bottom left plot (figure 3.12) shows a highly consistent latitudinal profile along all the 4 days for longitude -36°. This profile clearly shows a steady decrease in wind velocity from 50°latitude (both North and South) towards the poles, as expected from the zonal wind models and in agreement with previous results.

Spatial (longitudinal) variation - By comparing all the longitudinal bands of each day-averaged longitude bands $\overline{v}_{z,i}$ (figure 3.13), the most relevant variation is seen in the bottom right plot (19 Apr.): the 0°profile shows higher wind velocities comparatively to all other longitudinal profiles. As previously stated, this may be explained by a presence of solar tide in the meridians near the terminator. Day 17^{th} Apr. shows, again, some wind velocity variations in the order of 20 m/s.

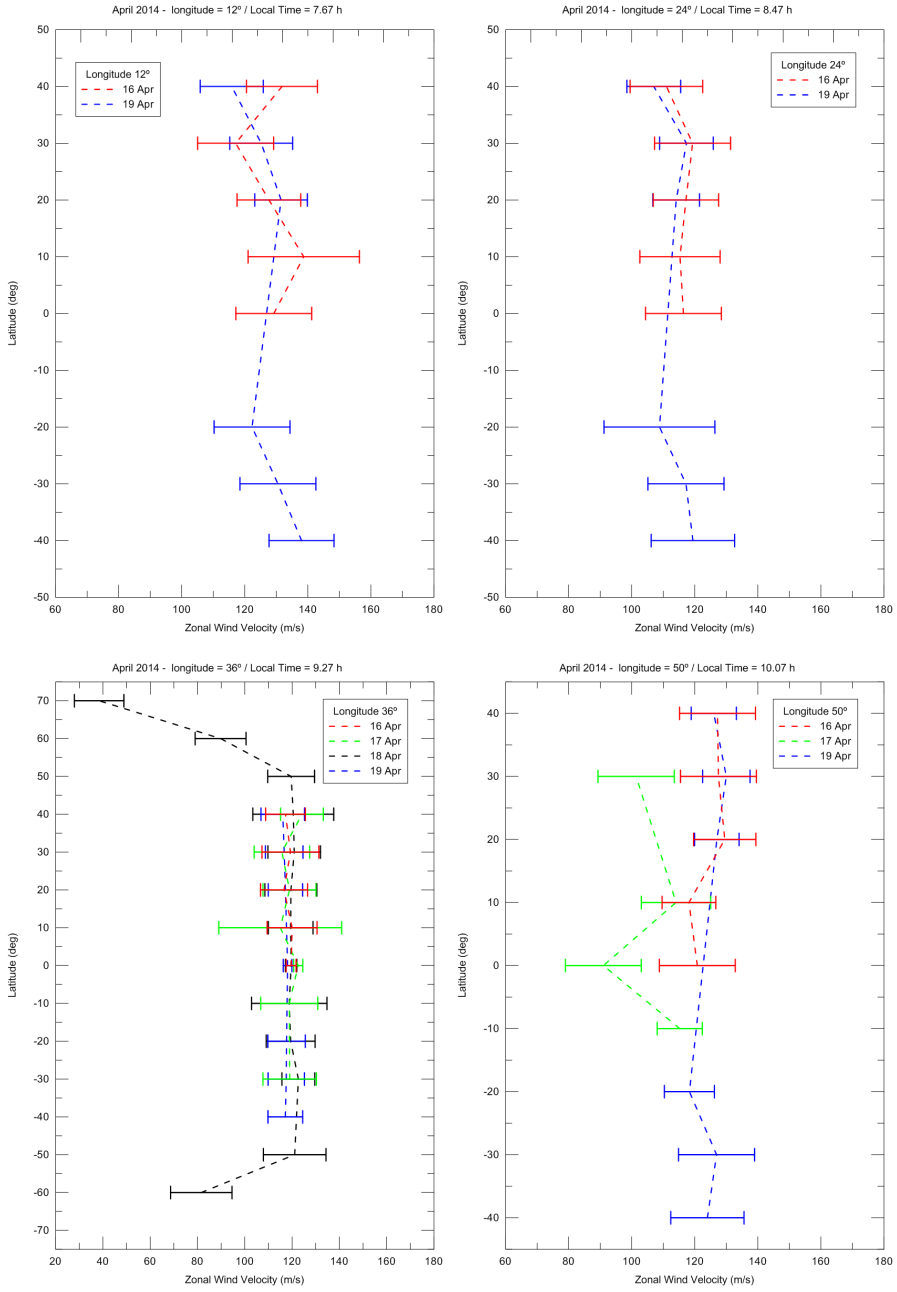

Figure 3.12: Comparison from day-averaged longitude bands of zonal wind $\overline{v}_{z,i}$ between observational days. X-axis are $\overline{v}_{z,i}$ results. Y-axis is latitudes along Venus. Top left: temporal variability study, of zonal wind for local time of 7:40a (-12° western longitude from sub-terrestrial point), between day 16 Apr. and 19 Apr., 2014. Top right: temporal variability, as in precedent case, for 8:30a local time (-24°) between day 16 and 19 Apr. Bottom left: temporal variability of 9:15a (36° western longitude from sub-terrestrial meridian, ESPaDOnS' FOV along this meridian includes the HPA meridian) between days: 16, 17, 18 and 19 Apr. Bottom right: same as precedent but for 10:10a local time (-50° longitude) for days 16, 17 and 19 Apr.

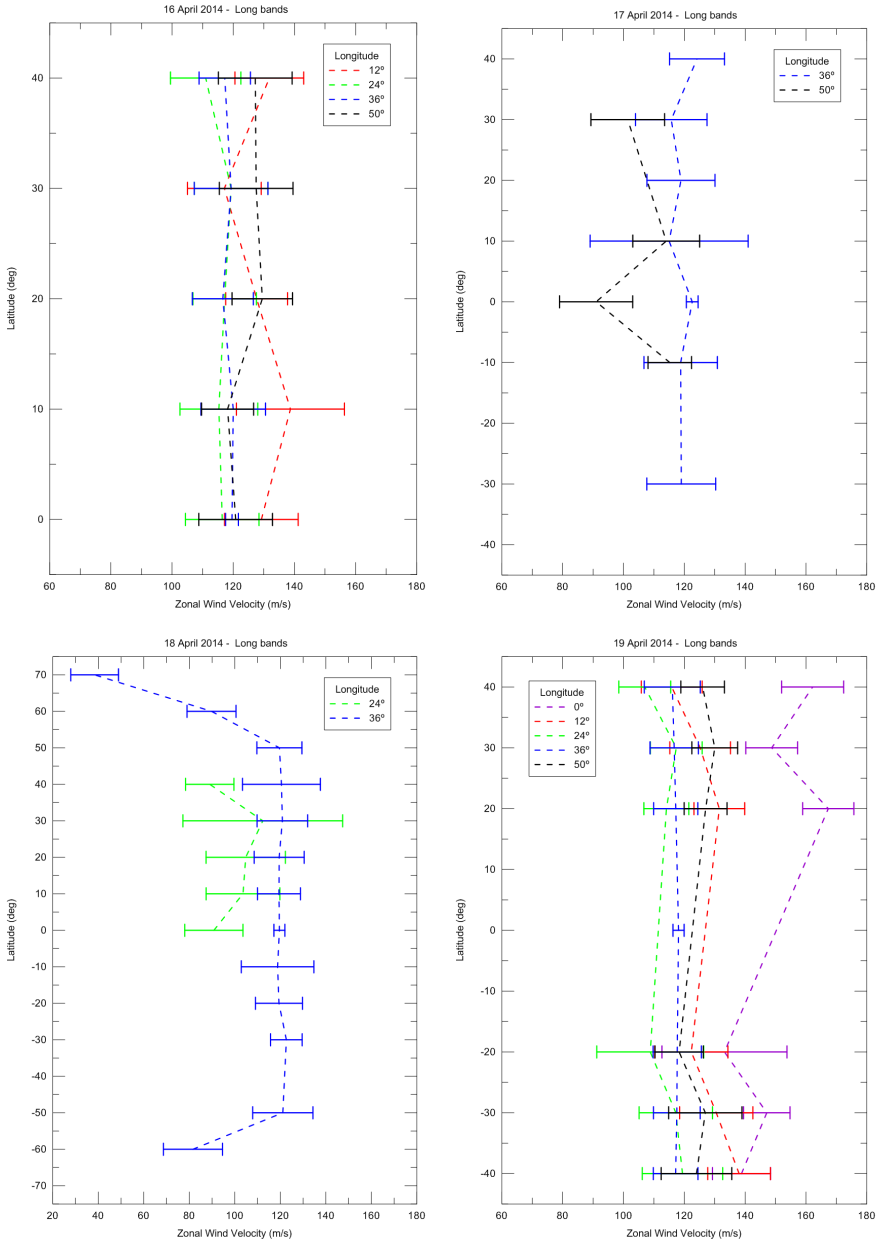

Figure 3.13: Spatial variability study of day-averaged on relative longitudes bands, in solar-fixed coordinates, of zonal wind $\overline{v}_{z,i}$. X-axis are $\overline{v}_{z,i}$ results. Y-axis is latitudes along Venus. Referred surveyed longitudes and local times are as in figure 3.12. Top left: comparison between -12° (7:40a), -24° (8:30a), -36° (9:15a) and -50° (10:10a) at day 16 Apr., 2014. Top right: the same as previous but for -36° (9:15a) and -50° (10:10a) at day 17 Apr. Top right: Bottom left: idem but for -24° (8:30a), -36° (9:15a) at day 18 Apr. Bottom right: ibidem but 0° (6:50a), -12° (7:40a), -24° (8:30a), -36° (9:15a) and -50° (10:10a) at day 19 Apr.

Discussion and Conclusions (April 2014 results)

We report an investigation of the dayside cloud tops dynamical regimes using simultaneous VenusExpress and ground-based Doppler measurements presenting coherent results were obtained on both hemispheres N and S.

The unambiguous detection of a poleward meridional circulation is reported on the morning dayside hemisphere, using optical Doppler velocimetry from the ground at CFHT. We could also perform a monitoring of short time-scale (day-to-day) variability with CFHT, and conclude that their significance remains essentially marginal at the 2-σ level. Since a reliable model of the circulation of Venus requires an accurate characterization of both long and short-term averages, our results are expected to add a new constrain to the mean circulation and eddy motions.

Best-fit results for the four days of observations are generally self-consistent, with $\bar{v}_z$ = (119.6 $\pm$ 16.5) ms^{-1} on Apr. 16, $\bar{v}_z$ = (122.6 $\pm$ 31.3) ms^{-1} on Apr. 17, $\bar{v}_z$ = (119.6 $\pm$ 26.0) ms^{-1} on Apr. 18, and $\bar{v}_z$ = (118.1 $\pm$ 19.5) ms^{-1} on Apr. 19, with a best quality of fit on Apr. 16 and Apr. 19 (S_{min} = 1.49 and 1.78, respectively). Although the overall fit looks reasonable, the fit is statistically poor on Apr. 17 and 18 (S_{min} = 3.38 and 2.27, respectively), suggesting that individual error bars may have been underestimated, or that the circulation is more complex than described by current general circulation models (Lebonnois et al., 2013). An increase of the zonal wind can be seen at all latitudes near the morning terminator, manifesting with particular latitudinal pattern emerging within the 2-σ confidence interval that might be associated to the spatial structure expected for the diurnal solar tide (Peralta et al., 2012). Fig. 3.10, 3.11 and 3.13 show $[\phi - \phi_E]$ longitudinal (local time) variations of the zonal velocity. In Figure 3.10, a general increase of the zonal wind regime near the morning terminator can be inferred at all latitudes observed on the day average, although no particular wind pattern emerges within the 2-σ confidence interval so that specific latitudinal bands equatorward of 40°N/S could be differentiated (Fig. 3.11). No significant assymetry between the two hemispheres can neither be inferred in the daytime zonal wind field, at least on a day-averages. In Figure 3.13, the day-averaged zonal wind is plotted as a latitudinal profile and reflects the stability of the winds relative to solar-fixed coordinates. This is in agreement with previous observations combining several years of observations by VIRTIS-M (Hueso et al., 2015), indicating high zonal speeds in the early morning. Near morning terminator (Fig. 3.13, bottom right) we eventually detect a zonal wind increase of about 20-30 m s^{-1} beyond the confidence level of 2-σ, at the equator and 30° N.

For the first time, a meridional wind component at cloud top is simultaneously observed from the ground in the two hemispheres (Fig. 3.9). The meridional circulation consists of two equator-to-pole cells, with ascending motions at the equator,

subsiding motions over the poles, an upper poleward branch in the middle clouds, which redistributes energy poleward, and a lower equatorward branch in the lower clouds.

We note the almost symmetrical behavior of the meridional flow between N and S hemispheres. The dashed line in Fig. 3.9 corresponds to the fit to a model of meridional circulation of $\bar{v}_m = (22.5 \pm 15.5)$ m s^{-1} (see also Table 3.4). It is generally accepted that meridional winds vary with local time accelerating towards the local afternoon (Hueso et al., 2012, 2015; Khatuntsev et al., 2013).

Our meridional wind model is assumed to vary sinusoidally with latitude, having zero velocity at equator and the poles, and a maximum value at 45° latitude. It can be noted that our measurements differ significantly from this model poleward of 50°, meaning lower winds than predicted at high latitudes near the cold collar. Constraining the meridional wind component at cloud top has long been an issue for diagnosing the maintenance of the super-rotation of the Venus atmosphere by determining the global mean and eddy circulations, as well as the accompanying meridional transports of angular momentum and energy (Limaye and Rengel, 2013). The role of thermal tides that transport angular momentum vertically in the low latitudes was confirmed by recent works (Lebonnois et al., 2010; Takagi and Matsuda, 2007). We also note that the latitudinal distribution of zonal wind at cloud tops may result from an equilibrium between the impact of thermal tides, and the angular momentum transport by the meridional circulation (Lebonnois et al., 2010), providing grounds for future systematic, simultaneous observations of both dynamical regimes.

3.4 TNG/HARPS-N January 2017

3.4.1 Observations January 2017

These observations took place in 28 and 29 of January 2017. Venus was observed at a phase angle Φ (Sun-Target-Observer) of 99.5°-100.3°, with surface brightness at 1.43-1.44 (mag/arcsec), apparent magnitude from -4,71 to -4.72, illuminated fraction between 41.7-41.1% and an angular diameter of 29.58-29.99 arcsec. The observations were made from 18:50 to 20:30 UTC for both days. The observing strategy has been to displace the entrance fibre of the spectrograph along points on the dayside hemisphere (see Fig. 3.14). Exposure times were adjusted at t = 3 sec to obtain a S/N of 250-450 on the continuum and avoid saturation. Table 3.6 summarizes the observing conditions and aspect of Venus at the time of the observations.

(1) Date	(2) UT	(3) Phase angle Φ (°)	(4) Ill. fraction (%)	(5) Ang. diam. (")	(6) Ob-lon/lat (°)	(7) Air-mass	(8) see-ing (")	(9) Pt diameter (km)
28 Jan	18:50-20:30	99.5	41.7	29.58-29.60	251.84/-2.34	1.46-2.52	0.5	409
29 Jan	19:03-20:23	100.3	41.1	29.97-29.99	254.2/-2.49	1.52-2.38	0.7	403

Table 3.6: Orbital geometry and circumstances of ground-based observations, 28-29 January 2017: (1-2) Date/UT interval ; (3-5) disk aspect; (6) sub-observer longitude and latitude (planetocentric); (7-9) observing conditions and geometry.

HARPS-N (High-Accuracy Radial-velocity Planetary Searcher - North) is an echelle spectrograph covering the wavelength range between 383 to 693 nm, with a spectral resolution of R=115000, collected over 69 spectral orders in a single exposure (Cosentino et al., 2012). The design of HARPS-N is based on the experience acquired with HARPS (installed at 3.6 m telescope in La Silla). The instrument was designed for the study of exoplanets, measuring Radial Velocities (RV) at highest precision. This was the first observation to use HARPS-N to study the atmosphere of a Solar system body.

Fig. 3.14 represents the Venus disk as seen from Earth during observations. In this figure is represented each fibre displacement along the upper end Venus disk. The observations of the first day were focused in the central latitudes ($10°N - 10°S$), while the second day of observations focused on points between $55°N$ and

$60°S$ latitude and $[\phi - \phi_E] = -50°$ (where ϕ is the longitude of the given points and ϕ_E is the longitude of the sub-Earth meridian), at the HPA meridian, in order to retrieve meridional wind.

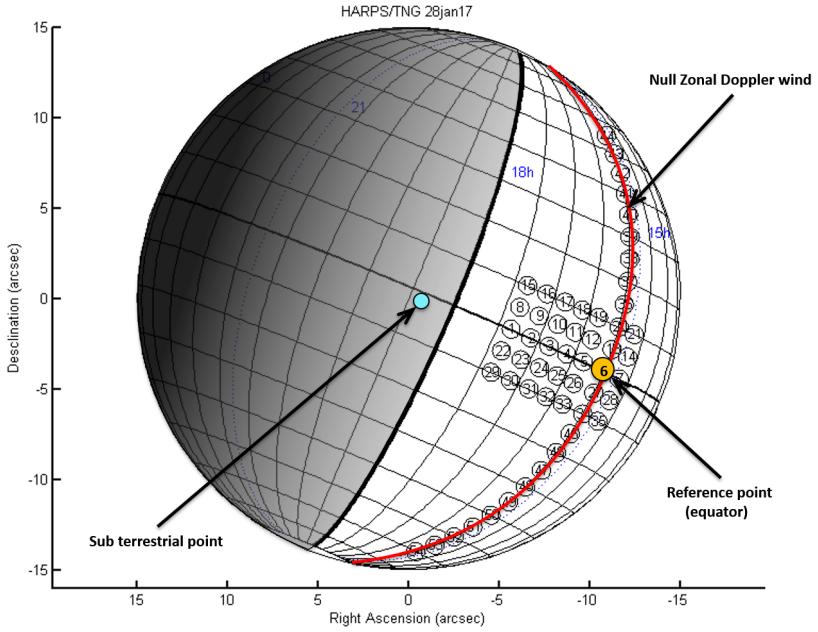

Figure 3.14: Aspect, angular size of Venus and pointing geometry as seen from Earth on 28 of January 2017. RA and DEC axis are in arcsec in relation to the center of Venus. Celestial North is up. Dayside hemisphere on Venus is on the right. Solid black circles represents HARPS-N FOV as seen in Venus disk, in each position observed. Red solid line is along the half-phase angle (HPA) meridian at $[\phi - \phi_E] = \Phi/2 = -50°$; Point numbers correspond to measured regions of Table 3.8.

The scanning sequences on Venus' dayside hemisphere during the 28-29 Jan 2017 observing run is presented in table 3.7. Weather conditions were generally good with a seeing lower than 0.7 arcsec. The sequence number indicates the number of times a full sequence is observed, beginning with the null-Doppler reference point 6. The location on disk (column 2) indicates the telescope manual displacement along the template of observing points for each sequence. Each fibre displacement refered in fig. 3.14 is detailed in table 3.8, where each point has its respective latitude, sub-Earth planetary longitude, local time.

Due to observation time constrains, it was not possible to observe all the positions projected for the first day.

(1) Seq. nb	(2) Loc.	(3) Time span (UT)	(4) Points order
Jan. 28, 2017			
[1]	Equ.	18:59-19:25	6-6-5-4-3-2-1-7
[2]	N lat 5°	19:28-19:48	6-13-12-11-10-9-8-14
[3]	S lat 5°	19:50-20:16	6-27-26-25-24-23-22-28
[4]	N lat 10°	20:19-20:31	6-20-19-6
Jan. 29, 2017			
[6]	10° S lat	19:04-19:17	6-21-35-34-33
[7]	$[\phi - \phi_E]$ = -50°, N lat	19:19-19:50	6-36-37-38-39-40-41-42-43-44
[8]	$[\phi - \phi_E]$ = -50°, S lat	19:52-20:20	6-45-46-47-48-49-50-51-52-53-54-6

Table 3.7: Scanning sequences on Venus' dayside hemisphere using TNG/HARPS-N during the Jan. 28-29, 2017 observing run: (1) sequence number; (2) location on disk; (3) UT time interval; (4) points acquisition order. All points were observed 3 consecutive times, with a 3 second exposure each.

(1) Point	(2) $\phi - \phi_E$ (°)	(3) latitude (°)	(4) Local time (h:m)
1	-23	0	16:28
2	-28	0	16:08
3	-33	0	15:48
4	-38	0	15:28
5	-43	0	15:08
6	-50	0	14:40
7	-56	0	14:16
8	-23	5	16:28
9	-28	5	16:08
10	-33	5	15:48
11	-38	5	15:28
12	-43	5	15:08
13	-50	5	14:40
14	-56	5	14:16
15	-23	10	16:28
16	-28	10	16:08
17	-33	10	15:48
18	-38	10	15:28
19	-43	10	15:08
20	-50	10	14:40
21	-56	10	14:16
22	-23	-5	16:28
23	-28	-5	16:08
24	-33	-5	15:48
25	-38	-5	15:28
26	-43	-5	15:08
27	-50	-5	14:40
28	-56	-5	14:16
29	-23	-10	16:28
30	-28	-10	16:08
31	-33	-10	15:48
32	-38	-10	15:28
33	-43	-10	15:08
34	-50	-10	14:40
35	-56	-10	14:16
36	-50	15	14:40
37	-50	20	14:40
38	-50	25	14:40
39	-50	30	14:40
40	-50	35	14:40
41	-50	40	14:40
42	-50	45	14:40
43	-50	50	14:40
44	-50	55	14:40
45	-50	-15	14:40
46	-50	-20	14:40
47	-50	-25	14:40
48	-50	-30	14:50
49	-50	-35	14:40
50	-50	-40	14:40
51	-50	-45	14:40
52	-50	-50	14:40
53	-50	-55	14:40
54	-50	-60	14:40

Table 3.8: Pointing geometry for TNG/HARPS-N during the January 2017 observations: (1) Point number, also appearing in Fig. 3.14; (2-3) planetocentric longitude $[\phi - \phi_E]$ (relative to sub-terrestrial meridian) and latitude (λ) at point center; (4) local solar time on Venus (LST) at point center.

3.4.2 Results (January 2017)

Zonal wind

The first day of observations was focused on low latitudes (10°S - 10°N), while the second day was focused on HPA meridian (55°S - 55°N), in order to retrieve zonal and meridional wind respectively. After applying the required corrections and weighed averaged all the measures of each position for each day, we applied the respective theoretical models, under the assumption of a pure zonal wind system to all data points with latitudes between 10°S - 10°N, and the same procedure under the assumption of a pure meridional wind system to all points located at the HPA meridian ($[\phi - \phi_E] = -50°$), using the same method as described by Machado et al. (2014, 2017). Due to observation time constrains, it was not possible to retrieve measurements from all the planned FOV pointing.

Fig. 3.15 presents zonal (left panel) and meridional (right panel) wind retrieved for each point observed in Venus' disk, as identified in fig. 3.14. The zonal wind was retrieved for positions numbers [1, 2, 3, 4, 5, 7, 8, 9, 10, 11, 12, 14, 21, 22, 23, 24, 25, 26, 28, 33 and 35] while meridional wind was retrieved for positions numbers [13, 20, 34 and 36-54] (position numbers as in fig. 3.14).

Meridional wind

Since the Doppler measurements from HPA cannot be atributed to zonal wind (see section 3.1.2), we used this data to retrieve a mean meridional wind for those positions, which is presented in fig. 3.16 (positive velocities in the northern hemisphere and negative velocities in the southern hemisphere both reflect poleward motion).

HPA meridian corresponds to points 6, 13, 20, 27, 34 and points from 36 to 54, all located at $[\phi - \phi_E] = -50°$, at the local meridian time of 14h40m (fig. 3.8). A poleward meridional wind component is determined within the 2-σ statistical significance by selecting the line-of-sight measurements on HPA meridian.

A increase in zonal wind velocity fo about 10 ms^{-1} near the evening terminator is noticeable in fig. 3.15 (left panel). As for the meridian circulation, fig. 3.16 presents the most precise meridional wind latitudinal profile ever retrieved. A peak of about 30 ms^{-1} is reached at around 35° in both hemispheres, while a steep decrease is noticeable at 55° in the northern hemisphere.

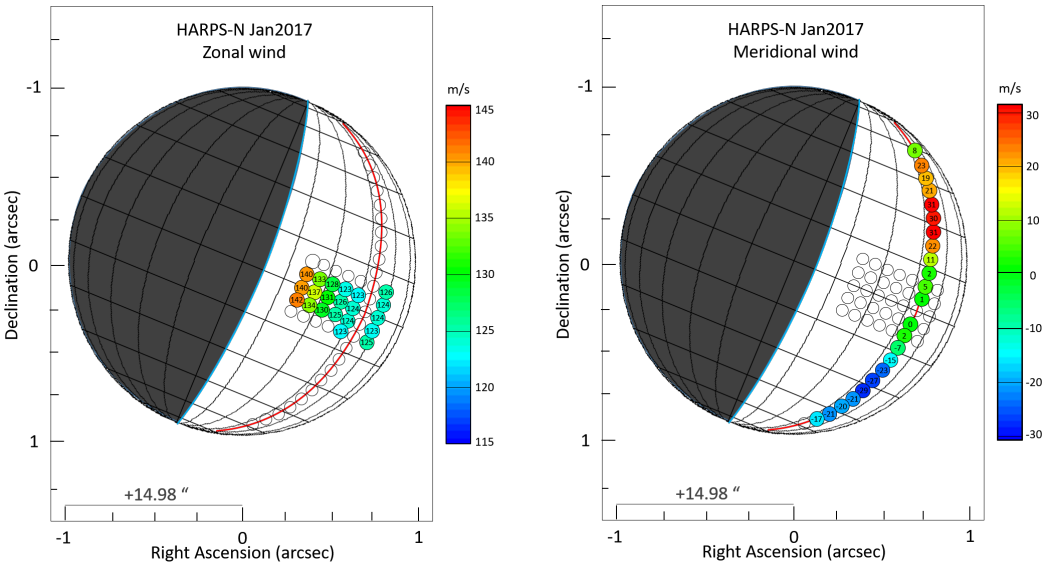

Figure 3.15: Zonal (left panel) and meridional (right panel) wind retrieved by HARPS-N. Each solid circle represents each pointing of the instrument FOV, as identified in fig. 3.14, while the values inside are the respective zonal or meridional wind (rounded to unit). The solid red line is the HPA meridian (see section 3.1.2). Right ascension and declination are relative to the centre of Venus' disk. The meridional wind follows a equator to pole direction, with positive/negative magnitude for the northern/southern hemisphere respectively.

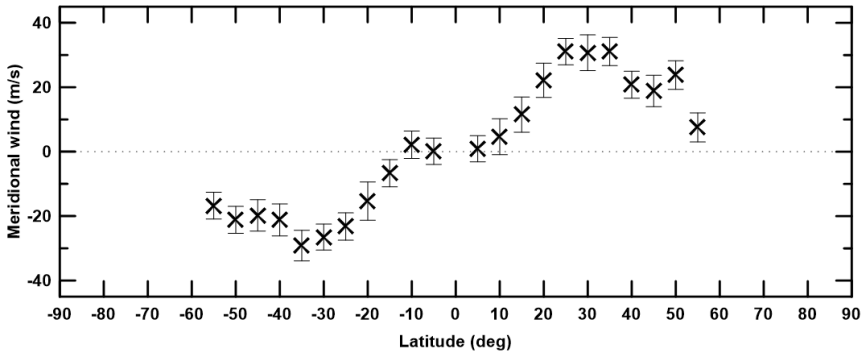

Figure 3.16: Meridional wind latitudinal profile from HARPS-N observations of 28 January. Wind velocity determined within the 2-σ statistical significance by consolidating the line-of-sight measurements along half-phase angle meridian HPA.

Long term comparison

The Doppler velocimetry technique has proven its consistency in both zonal and meridional wind results of Venus' cloud-top, using different telescopes and instruments (Machado et al., 2012, 2014, 2017). In this work we used the same technique as in Machado et al. (2017). Due to the higher spectral resolution of HARPS-N when compared with previous spectrographs used before (Machado et al., 2012, 2014), allied with the excellent seeing during observations, we were able to reach an increased precision in zonal and meridian wind velocity determination. A comparison with previous Doppler zonal and meridional results are presented in fig. 3.17 and fig. 3.18 respectively.

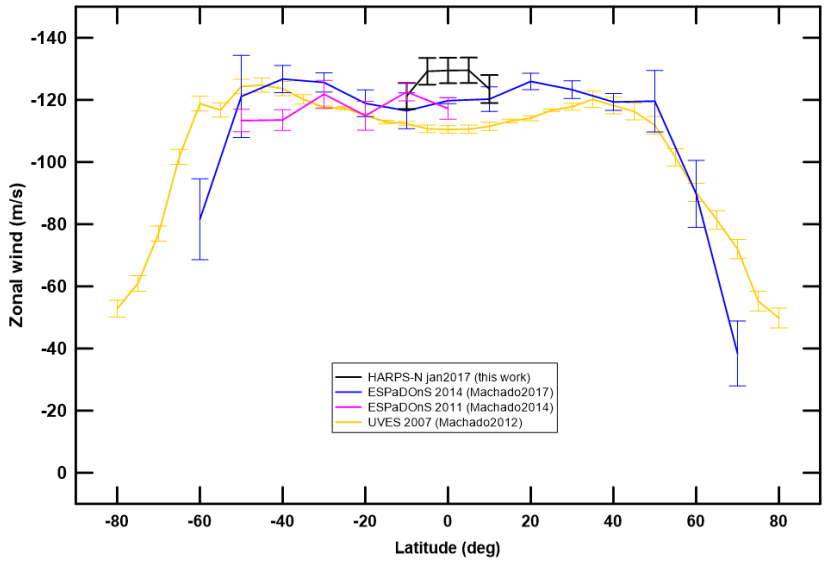

Figure 3.17: Comparison of zonal wind results retrieved from different observations and telescopes/instruments, using the Doppler velocimetry technique. The legend of the figure refers the instrument used, date of observations and respective scientific publication. This work (black) result is presented with a 5° bin in latitude.

The zonal wind obtained from this work, while focused only in low latidudes ($10°S$-$10°N$), is $\sim$10 ms^{-1} higher than the results obtained from previous Doppler observations for the same latitudes. While the previous results points to a lower uniform velocity at mid latitudes ($< 30°$) with higher velocities at around 40°, this work suggests the presence of an equator jet. However, the amount of points along Venus' disk where zonal wind was retrieved was considerably lower than previous Doppler campaigns, as was the time span of observations (one day).

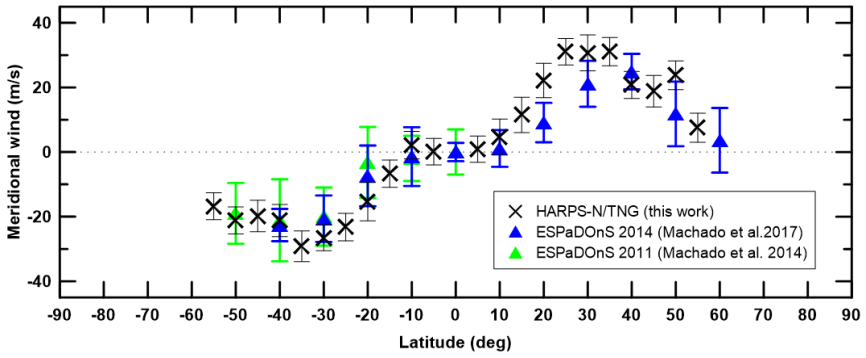

Figure 3.18: Comparison of meridional wind results retrieved from different observations and telescopes/instruments, using the Doppler velocimetry technique. The legend of the figure refers the instrument used, date of observations and respective scientific article.

Thus, additional observations are required to confirm if this is an intrinsic wind variation.

The high quality spectra retrieved by HARPS-N allied with the Doppler velocimetry technique allowed for a meridional wind flow with unprecedent precision. The results in fig. 3.18 show a high consistency in constraining the meridional wind flow, with a almost symmetric profile. The decrease of wind magnitude at 60° is consistent with the presence of the cold colar, the structure which precedes the polar vortex (Luz et al., 2011).

Discussion and Conclusions (January 2017 results)

HARPS-N is a high resolution spectrograph observing the northern skies and it was especially designed for searching extrasolar planets. While it was the first time this spectrograph was used to observe a solar system planetary atmosphere, HARPS-N spectrograph provided unprecedented high quality spectra of Venus atmosphere, allowing the retrieval of wind velocities with and unmatched precision of the order of 3-4 ms^{-1}. This opens a new window of opportunity for future solar system observations using HARPS-N.

Ee note that HARPS-N zonal wind results acquired in the equatorial region between 10°N and 10°S (fig. 3.17) show slightly higher velocities, when compared to the results of Machado et al. (2012, 2014, 2017). Considering that these results are based on a limited temporal and spatial observation (one day of observations and reduced amount of points on Venus disk), additional observations are required to confirm the intrinsic nature of this jet-like feature.

This work presents the most complete and precise meridional wind latitudinal

profile ever retrieved (fig. 3.16). This emphasizes the uniqueness and importance of ground-based Doppler velocimetry technique in the constrain of Venus cloud-top meridional wind circulation, which is of utmost importance to understand and constrain the mechanisms of Venus' super-rotational atmosphere.

Furthermore, although Doppler velocimetry had already proven to be a reference technique in the study of zonal and meridional wind at could-top of Venus' atmosphere (Machado et al., 2012, 2014, 2017), the HARPS-N results demonstrate the high consistency and reliability of the technique, successfully using different telescopes and instruments at different time frames.

3.5 CFHT/ESPaDOnS March 2015

3.5.1 Observations (March 20159

The observations were made on 27-29 March 2015, using the ESPaDOnS at CFHT. We also executed a short observation run (1.5 h) on the 25^{th} with the goal to test and fine tune our observation strategy; but targeting drift and the presence of clouds resulted in low quality spectra, hence no results could be retrieved. Venus was observed at a phase angle Φ (Sun-Target-Observer) of 54.0°-54.9°, with surface brightness 1.16 (mag/arcsec), apparent magnitude -4.0, illuminated fraction between 79.4%78.7% and an angular diameter of 13.5-13.7 arcsec (see table 3.9 for more details). The choice of observing dates offered the best compromise between the need to (i) maximize the angular diameter of Venus and spatial resolution on the disk, and (ii) minimize Venus phase angle (Earth-Sun-Venus) and illuminated fraction as we only observe the day side.

Fig. 3.19 represents the Venus disk as seen from Earth during observations. In this figure is represented each fibre displacement along the upper end Venus disk. The scanning sequences on Venus' dayside hemisphere during the observation run is presented in table 3.10.

The observing strategy has been to displace the entrance fibre of the spectrograph along points on the dayside hemisphere, while taking a reference point exposure between each sequence (reference point number 22, at the intersection of Equator and the null zonal Doppler meridian, as in figure 3.19). Exposure times were adjusted at t = 3 sec to obtain a S/N > 400 on the continuum and avoid saturation. The sequence of observation points (ajusting the fibre of ESPaDOnS to each positions as is figure 3.19) is displayed in table 3.10.

(1) Date	(2) UT	(3) Phase angle Φ (°)	(4) Ill. fraction (%)	(5) Ang. diam. (")	(6) Ob-lon/lat (°)	(7) Airmass	(8) seeing (")
27 Mar	20:00-00:52	54.0	79.4	13.5	22.4/ -1.88	2.5-1.0	0.7-0.9
28 Mar	19:31-00:55	54.4	79.1	13.6	25.0/ -1.93	3.4-1.0	0.8 -1.0
29 Mar	19:32-00:04	54.8	78.8	13.7	27.7/ -1.98	3.4-1.0	0.8-1.0

Table 3.9: Orbital geometry and circumstances of ground-based observations 27-29 Mar 2015: (1-2) Date/UT interval ; (3-5) disk aspect ; (6) sub-observer longitude and latitude (planetocentric) ; (7-9) observing conditions and geometry.

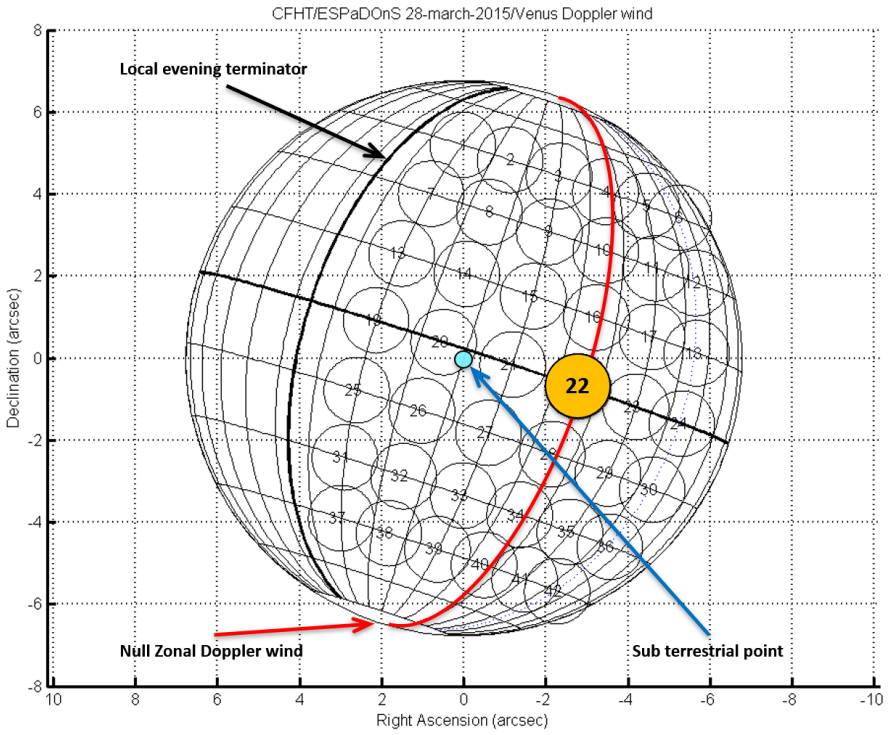

Figure 3.19: Aspect and angular size of Venus as seen from Earth on Mar. 28, 2015, 00h UTC. RA and DEC axis are in arcsec. Celestial North is up. Red solid line in the half-phase angle (HPA) meridian at $[\phi - \phi_E] = \Phi/2 \sim 27°$; Sub-Earth point as a blue circle; Local evening terminator is noted as a thick solid grid line west of central meridian. The grid has steps of 15° latitude and 10° longitude. The reference point 22, used for the spectral calibration, is the as orange solid circle (0°latitude and 25°longitude).

(1) Seq. nb	(2) Loc.	(3) Time span (UT)	(4) Points order	(5) Exp. repetition
Mar. 27				
[1]	Equator	20:00-20:18	23-21-20-19-23-24-22	3 x
[2]	N lat 15°	20:21-20:41	22-16-15-14-13-17-18-22	3 x
[3]	S lat 15°	20:42-20:59	28-22-28-27-26-25-22	3 x
[4]	$[\phi - \phi_E]$ = -25° (HPA)	22:59-23:20	22-16-10-4-22-28-34-40-22	3 x
[5]	$[\phi - \phi_E]$ = 20°, N	23:22-23:39	22-19-19-13-7-1-22	3 x
[6]	$[\phi - \phi_E]$ = 20°, S	23:47-00:10	22-25-31-22-31-37-37-22-22	3 x
[7]	S lat 15°	00:12-00:33	22-28-27-22-26-25-29-30-22	3 x
[8]	S lat 30°	00:34-00:51	22-34-22-33-32-31-22	3 x
Mar. 28				
[9]	Equator	19:31-19:49	22-22-21-20-19-23-24-24	3 x
[10]	S lat 15°	19:51-20:09	22-28-27-26-25-29-30-22	3 x
[11]	S lat 30°	20:10-20:28	22-34-33-32-31-35-36-22	3 x
[9]	S lat 45°	20:29-20:46	22-22-40-39-38-37-41-42-22	3 x
[10]	$[\phi - \phi_E]$ = 20°	20:47-23:08	22-19-13-7-1-25-31-37-22	3 x
[11]	$[\phi - \phi_E]$ = -25 ° (HPA)	23:08-23:26	16-22-10-4-28-34-40-22	3 x
[12]	N lat 15°	23:35-23:54	22-13-14-15-16-17-18-22	3 x
[13]	N lat 30°	23:55-00:13	7-8-22-9-10-11-12	3 x
[14]	N lat 45°	00:14-00:30	22-1-2-3-4-5-[6]	3 x
[15]	Equator°	00:32-00:30	22-21-20-19-22-[22]-[22]	3 x
Mar. 29				
[16]	$[\phi - \phi_E]$ = 20°	19:32-19:54	22-19-13-13-7-1-25-31-37-22	3 x
[17]	$[\phi - \phi_E]$ = -25 (HPA)°	19:56-20:15	22-16-10-4-22-28-34-40-22	3 x
[18]	Equator	20:17-22:42	22-21-22-22-21-20-19-23-24	3 x
[19]	N lat 15°	22:43-23:01	22-16-22-15-14-13-17-18	3 x
[20]	N lat 30°	23:02-23:22	22-10-22-9-8-7-11-12-22	3 x
[21]	N lat 45°	23:33-00:03	22-4-3-2-1-5-22-[22]-[22]-[22]	3 x

Table 3.10: Scanning sequences on Venus' dayside hemisphere using CFHT/ESPaDOnS during the Apr. 16-19, 2014 observing run: (1) sequence number; (2) location on disk; (3) UT time interval; (4) points acquisition order; points in parenthesis have been observed but not included in the kinematical best fits either for their lower S/N and/or limb or high SZA geometry; (5) exposure repetition: each point is acquired 3 times to check for internal consistency. Points in brackets were discarded from analysis due to severe drift, seeing or tracking issues.

3.5.2 Results (March 2015)

Zonal wind

First we applied the required corrections and weighted averaged all the measures of each position of the same day, for each day, using the inverse of the variance associated to each velocity measurement as the weighing coefficients. Then we applied the theoretical models for each wind circulation, (1) zonal wind, under the assumption of a pure zonal wind system to all data points with latitudes between 45°S - 45°N, (2) and the same procedure for meridional wind, under the assumption of a pure meridional wind system to all points located at the HPA meridian ($[\phi - \phi_E] = -25°$), using the same method as described by Machado et al. (2014, 2017); Gonçalves et al. (2020). The zonal wind latitudinal profile of each day of observations, as seen in fig. 3.20, was obtained by weighted averaging each point along the same latitude for each day.

The zonal wind velocities obtained for each FOV positions in each day of observation is displayed in fig. 3.21. Since the zonal component of the wind cannot be retrieved in the HPA (see section 3.1.2), this meridian doesn't present any zonal velocities. The HPA meridian is used to retrieve meridional wind velocities.

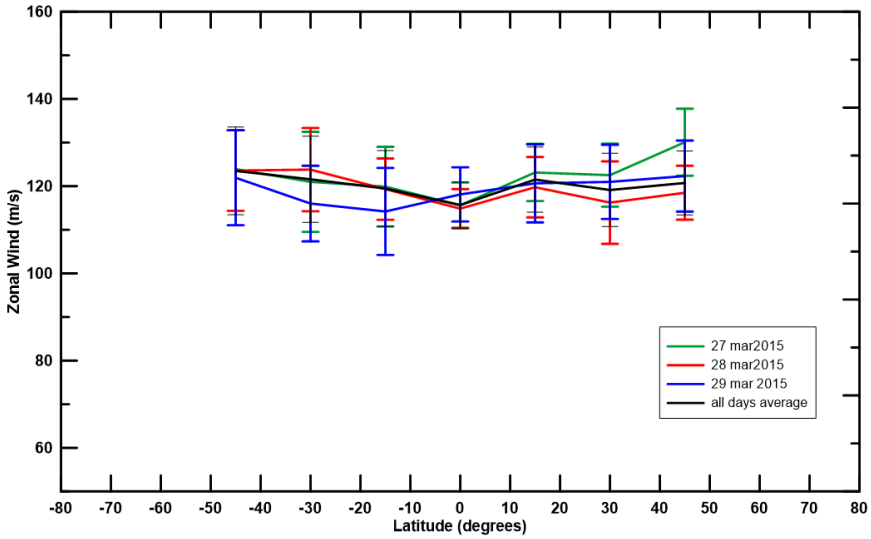

Figure 3.20: Latitudinal profile of zonal wind for each day of observation and the average values of the observation campaign (in black). For each day, we applied a weighted average of all the points at the same latitude, producing a daily latitudinal profile of the zonal wind.

No unambiguous conclusion can be made regarding daily variability of the

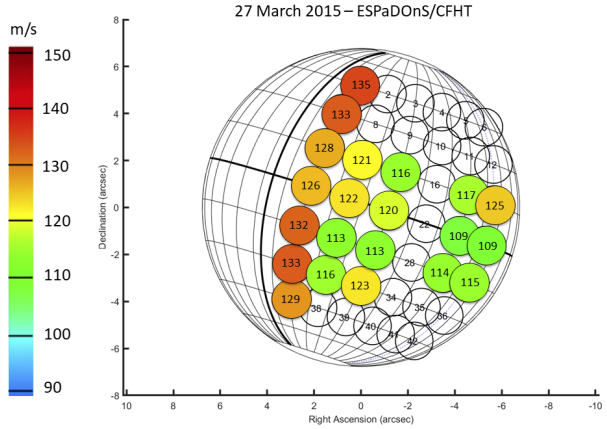

(a)

(b)

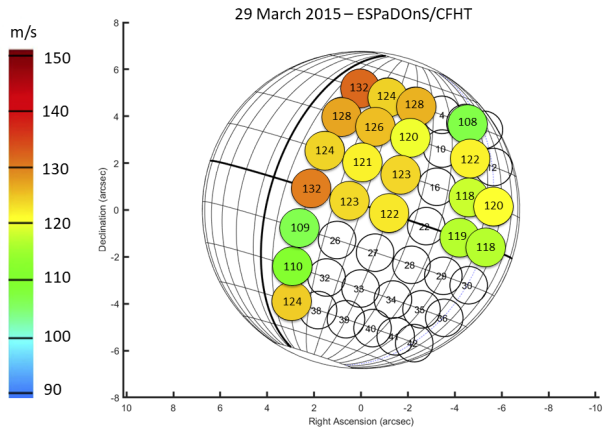

(c)

Figure 3.21: Colour plots of zonal wind for each position observed (as in fig. 3.19) between 27-29 March 2015 (panels a-c, respectively). Zonal wind velocity represented as a color code in a westward direction. The zonal wind velocity is

latitudinal wind profile since all variability present in fig. 3.20 is within the uncertainty of the measurements.

All profiles present lower and homogeneous velocities near equator (latitudes between 10°S-10°N). Although the profile suggests an increase of around $\sim$ 5-10 ms^{-1} up to 45° N and S, these values are within the associated errors, therefore, no unambiguous conclusion can be inferred.

The mean values of the zonal wind velocities (averaged on all points on the same sub-Earth longitude/local time and for all days of observation) are 129, 123, 122, 116 and 118 ms^{-1}, under an uncertainty of the order of 10 ms^{-1}, for the corresponding local time meridians of 16:55, 15:55, 14:55, 12:55 and 11:55. The meridian closer to the evening terminator ($[\phi - \phi_E] = 20°$, 16:55 local time) presents zonal velocities on average higher of up to 15 ms^{-1} when compared with the mean zonal wind measured at meridians within 1h (15° longitude) from the sub-solar meridian (as shown in fig. 3.21). However, for the results from 29 March, this difference is ambiguous and within the uncertainty margin.

Meridional wind

The meridional wind was obtained by observing several points along the HPA meridian. We used this data to retrieve a mean meridional wind for those positions (positive velocities in the northern hemisphere and negative velocities in the southern hemisphere both reflect poleward motion).

HPA meridian corresponds to points 4, 10, 16, 22, 28, 34 and 40, all located at $[\phi - \phi_E] = -25°$ (fig. 3.8). A poleward meridional wind component is determined within the 2-σ statistical significance by selecting the line-of-sight measurements on HPA meridian.

Fig. 3.22 presents the meridional wind for each day of observations (27-29 March 2015) and the average of all days (in black). Although some variability is present, it has no statistical significance considering the respective errors, thus the meridional profile is consistent within all 3 days of observations. The profile presents peak velocities at 45°, in the order of 25 ms^{-1}.

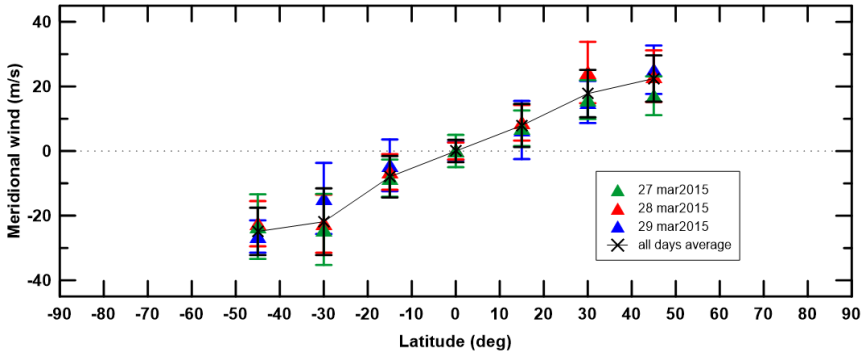

Figure 3.22: Latitudinal profile of Meridional wind for each day of observation (27-29 March 2015). For each day, we applied a weighted average on all the Doppler values at each latitude, producing a daily latitudinal profile of the meridional wind.

Discussion (March 2015)

The Doppler velocimetry method we used is identical to the method used in Machado et al. (2014, 2017) and Gonçalves et al. (2020). Only one adaptation was made regarding the Young effect correction where we introduced an approach suggested by Gaulme et al. (2018).

The latitudinal profile of the zonal wind retrieved in this work is consistent with previous Doppler velocimetry results using the same method, as seen in fig. 3.23. Although this work didn't provide observation at latitudes higher than 45°, the zonal wind profile shows consistency with previous data for the latitudes

observed. There is no significant variability in zonal wind within the associated uncertainty, with the exception of the data from Gonçalves et al. (2020).

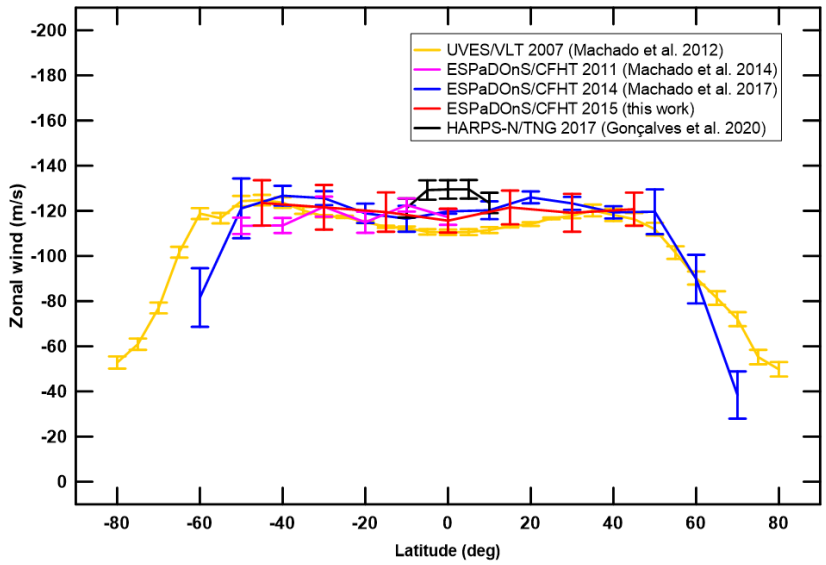

Figure 3.23: Comparison of zonal wind velocities obtained using the Doppler velocimetry technique throughout multiple observations campaigns - Machado et al. (2012) (UVES/VLT) Machado et al. (2014, 2017) (ESPaDOnS/CFHT) and Gonçalves et al. (2020) (HARPS-N/TNG).

Regarding local-time variability, there's evidence of an increase in the magnitude of the zonal wind velocity near the evening terminator (fig. 3.21). The meridian closer to the evening terminator ($[\phi - \phi_E] = 20°$, 16:55 local time) presents zonal velocities on average higher of up to 15 ms^{-1} when compared with the mean zonal winds measured at meridians within 1h (15° sub-Earth longitude) from the sub-solar meridian (as shown in fig. 3.21). The magnitude of this increase is consistent with the zonal wind variation with local time detected by Horinouchi et al. (2018), where an increase of 12-15 ms^{-1} is shown between 12h and 16h local time. Since the averaged zonal wind calculated for each local time band is affected by an uncertainty of at most 10 ms^{-1} in our Doppler velocities, and cloud-tracked averaged zonal winds were obtained by Horinouchi et al. (2018) with an uncertainty of around 4-8 ms^{-1}, we can state that the increase of zonal wind close to the terminator is in fact relevant. A combination of vertical wind shear and local-time dependence of temperature and wind structures associated with the thermal tide may explain this increase in zonal wind closer to the terminator, as already discussed by several authors (Sánchez-Lavega et al., 2008; Hueso et al., 2015; Horinouchi et al., 2018; Takagi et al., 2018).

The meridional wind profile of multiple Doppler velocimetry results are shown in fig. 3.24, where we present results from Machado et al. (2014, 2017) (with ESPaDOnS/CFHT) and Gonçalves et al. (2020) (with HARPS-N/TNG). All these results were retrieved using the same method. This works' meridional profile is consistent with previous Doppler velocimetry measurements, all presenting a profile with (1) peak velocities ($\sim$30 ms^{-1}) at around 40°, (2) wind speed decrease at latitudes higher than 50° and (3) null velocities at lower latitudes (<10°).

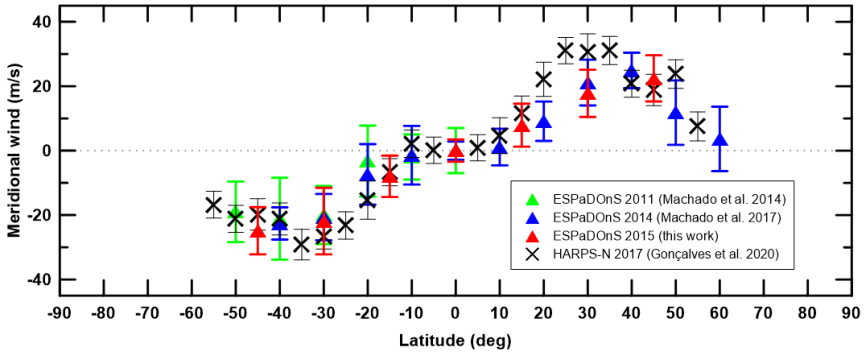

Figure 3.24: Comparison of meridional wind latitudinal profile obtained with Doppler velocimetry technique along several observation campaigns. All results were obtained using the same method and all observations were made with a fibre-fed high-resolution spectrograph - this work and Machado et al. (2014, 2017) used ESPaDOnS at CFHT, Gonçalves et al. (2020) used the HARPS-N/TNG.

The precision of the results obtained were negatively affected by the large size of the FOV of the instrument in comparison with Venus' disk. Observations made with an higher Phase angle (lower illumination fraction) would present a bigger angular diameter of Venus disk, allowing a more precise measure of zonal wind. However, in such conditions (larger phase angle) the HPA meridian would be located further way from the sub-Earth point and closer to the limb, at higher longitudes. This would represent a lower precision in our meridional wind measurements, since the placement of FOV of the instrument along the HPA would be covering a larger area of atmosphere when compared with a meridian closer to sub-Earth geometry.

We note that retrieved winds, both zonal and meridional, are assumed to result from scattering of visible light at a cloud-top altitude of about 65-70 km, where the optical depth is one. However, as suggested by Hueso et al. (2015), Venus cloud top seems to be located in a region (58-70 km) of high vertical wind shear above a region of small wind shear (58-48 km). It is also possible that Doppler observations could be probing altitudes of $\sim$72 km, in a region of even higher vertical wind shear than the regions below, while cloud-tracking UV observations

were probing altitudes of 68-70 km. Considering cloud top Doppler results from Machado et al. (2017), with an average of 120 ms^{-1} placed at 70 km, and cloud-tracking NIR data from Hueso et al. (2015), with an average of 65 ms^{-1} placed at 58 km, we obtain a linear vertical wind shear of about 4.6 ms^{-1} per km. It could be argued that a fraction of wind variations measured at an accuracy of $\sim$10 ms^{-1} could result from a cloud top altitude variation and not necessarily by actual atmospheric circulation. However, considering the different spatial scales involved, both in latitude, longitude and local time, it is likely that such a study would require simultaneous measurements of cloud top height (e.g. from an orbiter mission, Cottini et al. (2012)). Such a study would be of high interest both in modeling and future investigations.

Conclusions (March 2015)

This work is based on three day observations at the CFHT using its ESPaDOnS spectrograph. The Doppler velocimetry method we used is identical to the method used in Machado et al. (2014, 2017) and Gonçalves et al. (2020). This technique has been successfully used to retrieve zonal and meridional wind at Venus cloud top, where the velocity of the superrotation regime peaks. This new zonal and meridional wind measurements presents new an opportunity to access (1) daily and spatial (latitude and local-time) zonal wind variability (2) wind variability along time, (3) consistency of results provided by Doppler velocimetry method.

These March 2015 measurements provide valuable and unique data to constrain horizontal winds at cloud top, since Doppler velocimetry was the only available method to do so in a period when no space mission was orbiting Venus - between VenusExpress end, in January 2015, and Akatsuki orbit insertion, in December 2015. The frequent survey of horizontal winds is essential to constrain both short and long term variability, allowing a more comprehensive understanding of the dynamics of Venus atmosphere.

Spatial variability of zonal wind is also shown, with an increase of velocities up to 15 ms^{-1} near the evening terminator, at $[\phi - \phi_E] = 20^\circ$. This is consistent with previous works, both with observational data and modelization, as in Sánchez-Lavega et al. (2008); Hueso et al. (2015); Horinouchi et al. (2018); Takagi et al. (2018).

Daily zonal wind variability cannot be unambiguously inferred from our results (fig. 3.21), since the variability shown (around 5 ms^{-1}) is contained within the uncertainty interval. This is also the case for meridional wind daily variability, no variability can be inferred considering the associated errors.

The latitudinal profile of meridional wind presents null velocities at lower latitudes, below 10°N-S., and peak velocities of $\sim$30 ms^{-1}) at around 40°, consistent with previous Doppler results (fig 3.24).

Both zonal and meridional wind profiles are consistent with our previous Doppler velocimetry studies, using the same observing technique and retrieval method. This demonstrates the efficiency and viability of the method in the retrieval of wind velocities at cloud top Venus' atmosphere and the robustness of our detection and characterization of meridional wind latitudinal profile.

When comparing this work's results with previous Doppler observations, with the exception of the 2017 data from Gonçalves et al. (2020) there's an absence of unambiguous temporal variability (figures 3.23 and 3.24). This suggest a long-term stability of the Venus dynamics for the period of time under study, 2011-2015.

Additional measurements of horizontal winds with a wide spatial coverage would be extremely relevant to the study of zonal wind variation with local time and to address what is the behaviour of the wind when crossing from the night hemisphere to the dayside and vice-versa. Further dynamical studies will also help to (i) constrain long term variability of zonal wind, (ii) constrain zonal wind variation with local time, in particular near terminator (evening and morning), (ii) characterize meridional flow and its contribution to the superrotation of Venus' atmosphere.

Chapter 4

Cloud Tracking

4.1 Method: Cloud-Tracking

4.1.1 Method Summary

At cloud top, an unknown UV absorber is responsible for high contrast clouds at UV and visible wavelengths. Although some variability in the cloud-top altitude is known (Lee et al., 2012), the UV images, centered around 380-385 nm, track cloud features located around 68-71 km (Esposito et al., 1997; Ignatiev, 2009). To measure wind velocities by tracking the displacement of contrasting features on the observed atmospheric layer of a planet, a high level of accuracy on the geographical position of such features is paramount. Hence, image navigation, which is the assignment of a latitude and longitude coordinate to each pixel of a planetary image, is a necessary step to ensure the reliability and high precision of our wind velocities retrieval method. The precision of wind velocity retrieval depends on the accurate determination of cloud features location along Venus' disk and along time. The navigation of the original VenusExpress/VIRTIS-M and Akatsuki/UVI images was processed using information computed from SPICE kernels (Spacecraft Planet Instrument C-matrix Event) (Acton , 1995) - a software developed by NASA's Navigation and Ancillary Information Facility(NAIF) to assist scientists in planning and interpreting scientific observations from space-based instruments onboard planetary spacecraft like Venus Express or Akatsuki and it's also used in engineering tasks associated with space missions. SPICE uses a wealth of available data on the ephemerides of a great number of objects in the solar system. Each image pair was processed to enhance the contrast by applying a combination of unsharp mask and Butterworth filters. The processed image was geometrically projected into a cylindrical or polar projections, with an angular resolution compatible with the image of worst spatial resolution of the pair, in order to search for low latitude or high latitude cloud features, respectively. The projected image was again processed with an unsharp mask to increase cloud details in the new geometry. The apparent motions of UV upper cloud features were measured manually on projected and processed images of the same day. Figure 4.1 is an animation of a pair of UVI images already cylindrically projected and processed, ready for the process of selecting cloud tracers.

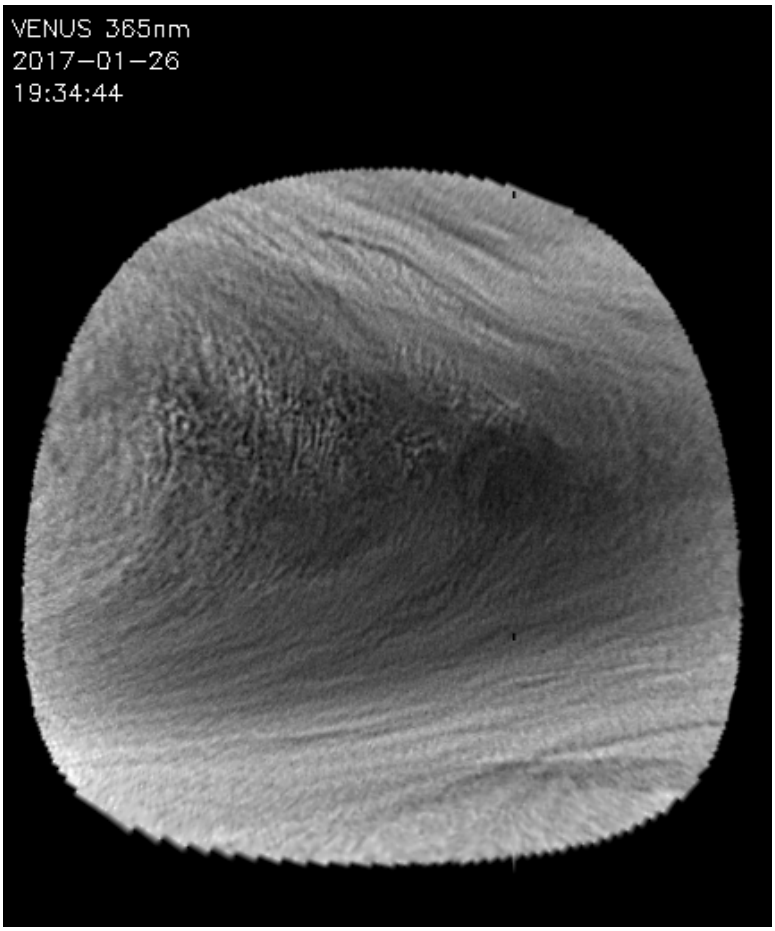

Figure 4.1: Akatsuki/UVI (385 nm filter) images taken on 26 January 2017. Both images were cylindrically projeted and processed to retrieve cloud tracers.

Generally, cloud-tracking methods use pairs of images typically separated by 2 hours (Hueso et al., 2015; Machado et al., 2017; Horinouchi et al., 2018), since for these intervals cloud features remain coherent and can be clearly identified in consecutive images. Theoretically, cloud tracking would benefit from using data separated by a larger temporal lapse (Δt) due to the reduced error associated with the respective Δt, however, most of the fine structures and details do not survive such time difference.

The zonal and meridional wind component were calculated using the following expressions:

$$u = (R+h) \cdot \cos\lambda \cdot \frac{\Delta\phi}{\Delta t} \cdot \frac{\pi}{180} \tag{4.1}$$

$$v = (R+h) \cdot \frac{\Delta\lambda}{\Delta t} \cdot \frac{\pi}{180} \tag{4.2}$$

where R is the Venus radius, h is the height above the surface ($\sim 70km$), ϕ and λ are the longitude and latitude in degrees, and Δt is the temporal lapse (in seconds) between the two images. Considering that the error in time δt is negligible, the absolute errors for both components of the winds will be given by the next expressions following the general expressions given by Bevington et al. (1992),

$$\delta u \approx \delta X / \Delta t \tag{4.3}$$

$$\delta v \approx \delta Y / \Delta t \tag{4.4}$$

where δX and δY are absolute errors for the spatial displacement of the clouds.

4.1.2 VenusExpress/VIRTIS-M

Venus Express had the capability of could tracking different depths of the cloud deck, depending on the wavelenght measured.

- UV (300-400 nm): dayside, from sunlight reflectivity ($\sim$65-70 km)
- NIR ($\sim$950nm)($\sim$950nm): dayside, from sunlight reflectivity ($\sim$61-65 km)
- IR (1.74 and 2.3 μm): nightside, thermal emission ($\sim$45-50 km)
- IR (3.8-5.1 μm): nightside, thermal emission ($\sim$65 km)

The results presented in this work were retrieved by VEx/VIRTIS-M, UV-visible channel at 380nm (center wavelength).

The CT method we used was based on a software developed by Hueso et al. (2010) called PLIA (Planetary Laboratory ImageAnalysis), which is an integrated set of programs written in IDL with a fully operational Graphic User Interface (GUI) The navigation is obtained from geometric files (also data cubes) produced by the European Space Agency which are read by the software automatically with the data cube. The navigation is computed from ephemeris information by the SPICE kernels.

Regarding that the cloud features seen in UV are due to markers in the top cloud layer (approximately the same altitude surveyed by ESPaDOnS/CFHT) the cloud tracking techniques enabled by those cloud contrast (Moissl et al., 2009; Sánchez-Lavega et al., 2008) will produce wind velocity fields that can be compared with the ones obtained with Doppler velocimetry methods that rely in the

observations made with ESPaDOnS/CFHT. Also, this coincidence permits to compare magnitudes and variability between ESPaDOnS/CFHT, UVES/VLT (Machado et al., 2012, 2014) results and the ones from cloud tracking of UV markings as is the case for VEx/VIRTIS-M, Pioneer Venus/OCPP and Galileo/SSI.

The Visible and InfraRed Thermal Imaging Spectrometer (VIRTIS) is a two-channel imaging spectrometer that operates in the visible range (0.3 to 1 μm) and in the near infrared (1 to 5 μm) (Drossart et al., 2007). In this work we took advantage of VIRTIS-M visible channel, that senses the solar radiation ultraviolet wavelengths, of about 380 nm, back-scattered at cloud tops probing the heights of 66-73 km Venus' dayside.

Due to the the highly elliptical polar orbit of Venus Express with apocenter located at south pole side allied with the long integration time needed to obtain an entire VIRTIS data cube, the privileged region where VIRTIS-M operated was Venus' southern hemisphere. The achieved spatial resolution on the analysed images strongly varies between 15 km per pixel for high latitudes and about 45 km per pixel for low latitudes.

The pairs of VIRTIS-M images for the cloud-tracking were selected in order to maximize both the time interval and the overlapping area among them, so that we optimize the velocity accuracy and the number of vectors, respectively. As a result, the pairs were separated by 80 minutes for the orbit 2918 and shorter times for the case of 2923. The original VIRTIS-M images were navigated and processed to improve the S/N ratio in the same way as described by Machado et al. (2014).

The original VIRTIS-M images were navigated and processed to improve the signal-to-noise ratio using the convolution with the directional filter described by Hueso et al. (2010).

Depending on the latitudinal coverage, the couple of image were cylindrically or polar projected with an angular resolution compatible with the image of worst spatial resolution of the pair. We measured the wind speed using visual cloud tracking, as in Machado et al. (2014).

4.1.3 Akatsuki/UVI

The UltraViolet Imager (UVI) on board Akatsuki VCO (Venus Climate Orbiter) is a two-channel imaging spectrometer operating in the ultra violet range (283-365 nm) (Yamazaki et al., 2018), using a Si CCD with 1024 $\times$ 1024 pixels. At cloud top, an unknown UV absorber is responsible for high contrast clouds at UV and visible wavelengths. Although some variability in the cloud-top altitude is known (Lee et al., 2012), the 385 nm UVI images track cloud features at about

68-71 km (Esposito et al., 1997; Ignatiev, 2009). Akatsuki equatorial orbit allows to retrive images from both hemispheres simultaneously (figure 4.2. In this work, we used a cloud-tracking technique based in a phase correlation method between images developed by Peralta et al. (2018).

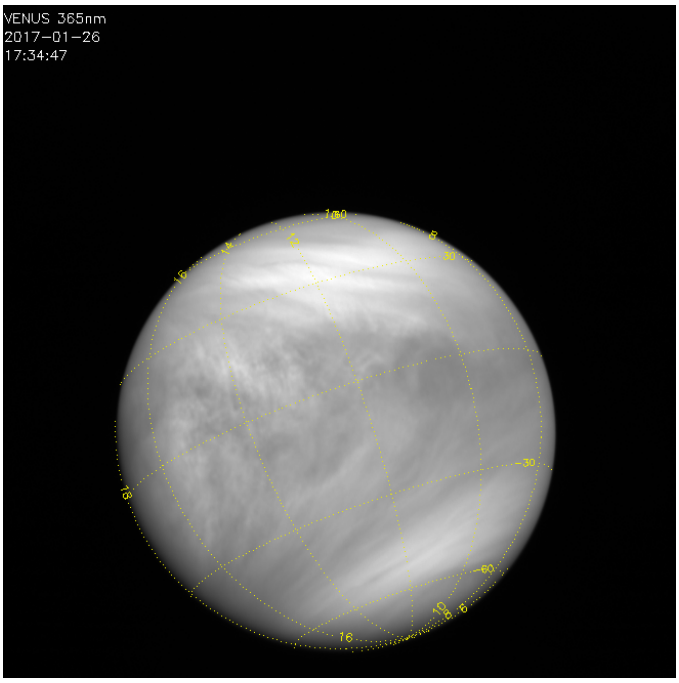

Figure 4.2: Original unprocessed Venus' image from Akatsuki UVI, taken at 17:34:47 on the 26 January 2017. The yellow lines are a grid of latitude (North-South direction) and local time (East-West direction), with steps of 30° and 2 h, respectively.

The original UVI images were navigated using SPICE. By using a limb fitting method (Ogohara et al., 2017), the position error from SPICE image navigation on these observations were of the order of a centimetre. An overview of the navigation correction of Akatsuki's data is presented in Ogohara et al. (2017). Each image pair was processed to enhance the contrast by applying a combination of unsharp mask and Butterworth filters. The processed images were geometrically projected into a cylindrical or polar projections, with an angular resolution compatible with the image of worst spatial resolution of the pair, in order to search for low latitude or high latitude cloud features, respectively. Figure 4.3 is a screenshot of the cloud-tracking software developed by Peralta et al. (2018), during the process of cloud feature selection and respective automatic retrieval of zonal and meridional winds, from Akatsuki/UVI images (385 nm filter) taken on 26 January 2017. Depending on the image resolution, a grid with a spatial resolution of

0.2-0.7 arcsec/pixel was employed, corresponding to 34-76 km/pixel at disk centre. The projected image was again processed with an unsharp mask to increase cloud details in the new geometry. The apparent motions of UV upper cloud features were measured manually on projected and processed images of the same day. This task was done by three of the co-authors in order to reduce any bias and to increase the total number of cloud tracers used, thus, increasing the statistical strength of the results. A total of 4035 cloud tracers were identified to carry out the calculation of the wind velocities, for the entire observations.

The images used for cloud tracking had a spatial resolution of 0.36 to 0.79 arcsec/pixel along X (longitude) and Y axes (latitude), so, since the method's uncertainties are due to spatial resolution of the images (and the negligible error of image time) the absolute errors for the spatial displacement of the clouds were about between 38.5 to 84.7 km (see table 4.2). This implied wind speed measurements errors of 5-10 ms^{-1}, depending on the resolution of the images used, for both components of the wind.

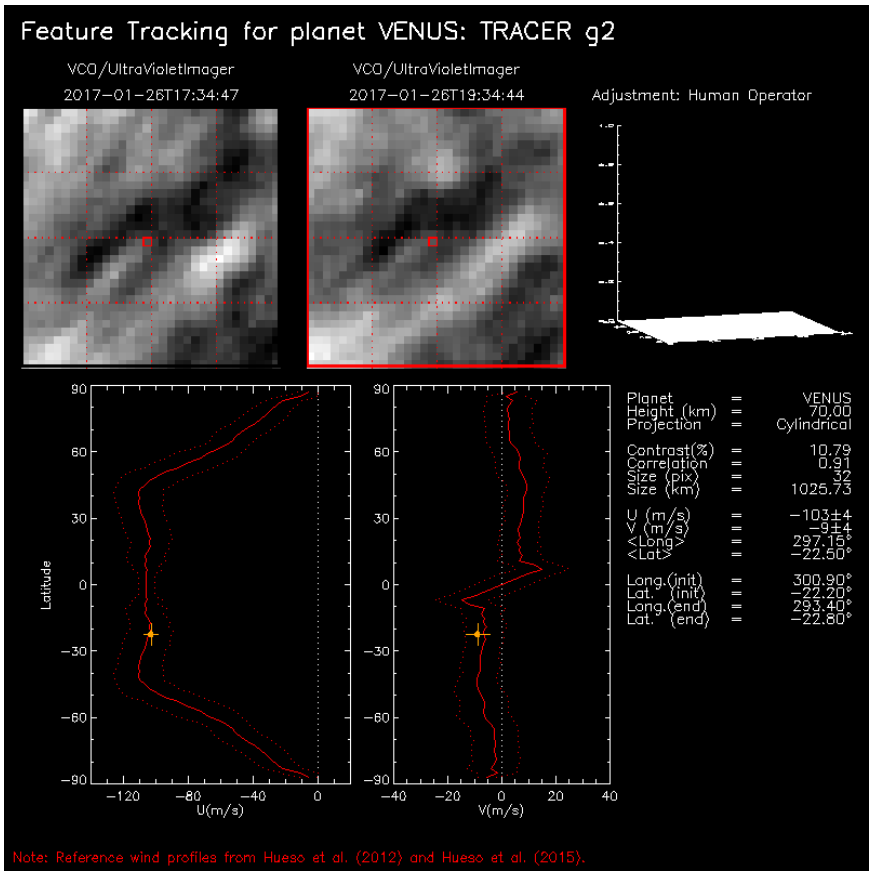

Figure 4.3: Screenshot of the cloud-tracking software developed by Peralta et al. (2018), during the process of cloud feature selection and subsequent automatic retrieval of zonal and meridional winds, from Akatsuki/UVI images (385 nm filter) taken on 27 January 2017. The images are separated by 2h. The red square at the center of the image is the selected cloud feature to be used. At the bottom, the zonal (left) and meridional (right) measurements of the tracer are plotted on a latitudinal profile based on VenusExpress measurements from Hueso et al. (2010, 2015). On the right hand side, the automatic retrieval of zonal and meridional wind velocity (U and V), longitude and latitude of the tracer.

4.2 Space missions description

In this section we present a brief description and overview of the space missions and respective instruments used in the development of this work: VIRTIS-M at VenusExpress and UVI at Akatsuki.

4.2.1 Venus Express

Mission Summary

The ESA launched, on November 9 2005, its first Venus exploration mission Venus Express (VEx). The spacecraft arrived at Venus in April 2006 with the task of conducting studies under the general circulation of the atmosphere, the chemistry of clouds and the atmospheric escape processes of several different volatiles, as well as the interactions between the surface and the atmosphere, with emphasis on the Venusian volcanism.

The orbital period was of 24 hours. The orbital design was elliptical, highly eccentric, with a planetary close pericentre of 250 km and an apocentre of 66 000 km. This orbit configuration provided optimal coverage of planetary latitudes and solar local time. The highly elliptic orbit allows global large scale investigations, as high spatial resolution detailed studies of localized phenomena, at pericentric close approach.

After eight years in orbit and with propellant for its propulsion system running low, Venus Express was tasked in mid-2014 with a daring aerobraking campaign, during which it dipped progressively lower into the atmosphere on its closest approaches to the planet. This unique adventure was aimed at reducing the altitude and allowing an exploration of previously uncharted regions of the atmosphere. The lowest point of the orbit was gradually reduced to about 130-135 km altitude. The campaign also provided important experience for future missions - aerobraking can be used to enter orbit around planets with atmospheres without having to carry quite so much propellant. During an orbit maneuver to raise the spacecraft's altitude in the hopes of extending the mission's lifetime, the spacecraft's remaining fuel was exhausted and the contact with the spacecraft was lost on November 28, 2014. The mission was officially declared over by ESA on December 16, 2014.

Instruments

In this section we present a resume of the instruments aboard VEx orbiter. Figure 4.5 illustrates the size and location of instruments on the spacecraft.

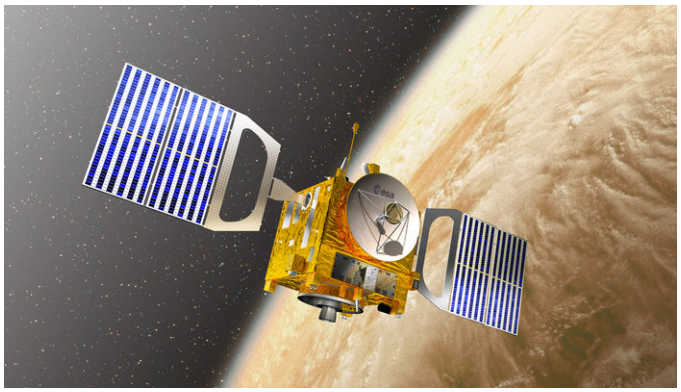

Figure 4.4: Artist's view of Venus Express probe in orbit around Venus (image: ESA's Venus Express mission website).

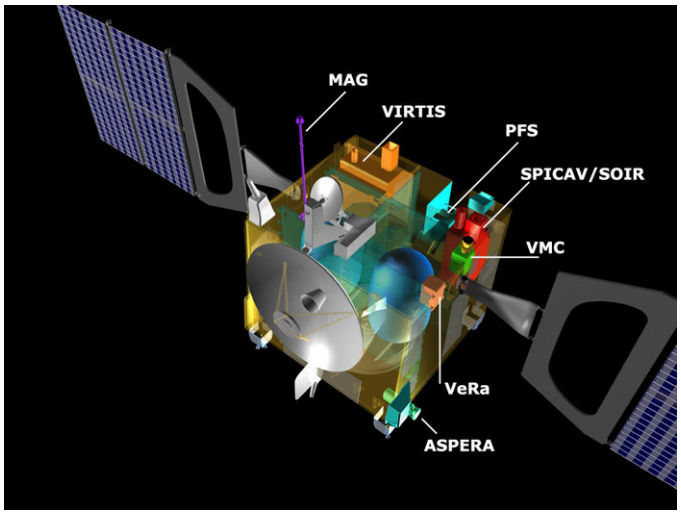

Figure 4.5: A cutaway diagram showing size and locations of Venus Express instruments: MAG, VIRTIS, PFS, SPICAM/SOIR, VMC, VeRa and ASPERA.

- MAG (Venus Express Magnetometer): Venus has no detectable internal magnetic field, and the field that exists around the planet is entirely due to the interaction between the solar wind and the atmosphere. The MAG magnetometer studied this process and contributed to the understanding the effect this has on Venus' atmosphere, for instance the atmospheric escape process.

- VIRTIS (Visible and Infrared Thermal Imaging Spectrometer): (Drossart et al., 2007) The instrument combines a double capability: a high-resolution imaging in the visible-infrared range (0.28-5 μm) at moderate spectral resolution (VIRTIS-M channel) and a high-resolution spectroscopy in the 2-5 μm range (VIRTIS-H channel). The scientific objectives of VIRTIS cover a large field and span from the study of the thermal emission of the surface up to the composition and dynamics of the upper atmosphere

- PFS (Planetary Fourier Spectrometer): was able to measure the temperature of the atmosphere between altitudes of 55-100 km at a very high resolution. It was also be able to measure the surface temperature and therefore be able to search for volcanic activity. In addition to its temperature measurements, PFS made composition measurements of the atmosphere.

- SPICAV/SOIR (Ultraviolet and Infrared Atmospheric Spectrometer): was designed to assist in the analysis of Venus' atmosphere. In particular, searching for the small quantities of water expected to exist in the Venusian atmosphere, looking for sulphur compounds and molecular oxygen in the atmosphere and determining the density and temperature of the atmosphere at 80-180 km altitude.

- VMC (Venus Monitoring Camera): is a wide-angle multi-channel camera that was able to take images of the planet in the near infrared, ultraviolet and visible wavelengths. VMC was able to make global images and studied the cloud dynamics and image the surface. In addition it assisted in the identification of phenomena seen by other instruments.

- VeRa (Venus Radio Science Experiment): used the powerful radio link between the spacecraft and Earth to investigate the conditions prevalent in the ionosphere of Venus. Scientists used it to study the density, temperature, and pressure of the atmosphere from 35-40 km up to 100 km from the surface, and to determine roughness and electrical properties of the surface. It also allowed investigations of the conditions of the solar wind in the inner part of the Solar System.

- ASPERA (Analyser of Space Plasma and Energetic Atoms): was designed to investigate the interaction between the solar wind and the atmosphere of Venus by measuring outflowing particles from the planet's atmosphere and the particles making up the solar wind. It studied how the molecules and ions escape the planet.

4.2.2 Akatsuki

Mission Summary

The AKATSUKI spacecraft was launched in May 2010 (Nakamura et al., 2007). After its smooth flight, JAXA attempted to insert the orbiter into the orbit circling around Venus on December 7, 2010, but it failed as the main engine for orbit control was broken. JAXA established an investigation team to find the cause of the failure while studying a feasible plan for a second attempt. The spacecraft - whose name means "Dawn" in Japanese - had been circling the sun for five years, waiting for another shot at Venus. On Dec. 7, 2015, JAXA successfully inserted the orbiter into the Venus orbit by emitting thrust from the attitude control engine (Nakamura et al., 2016).

Akatsuki's current path takes it as close as 400 km to Venus, and as far away as 440 000 km. This orbit is much more elliptical than the one Akatsuki was supposed to achieve in 2010, which featured a period of 30 hours and an apoapsis (most distant point from Venus) of about 80 000 km.

Akatsuki is the second interplanetary mission in Japan's history. The country's first, the Nozomi Mars probe, failed to arrive as planned at Mars in 2003. In 2007, Japan's Kaguya orbiter successfully launched to the moon to study the lunar surface from orbit. Kaguya's mission ended in 2009 and it ultimately crashed into the moon's surface.

Coordinated observations between ground-based and Akatsuki probe were made in January 2017, in order to study and measure wind velocity at could top of Venus' atmosphere, using both could-tracking (Akatsuki/UVI) and Dopppler velocimetry (TNG/HARPS-N) (Gonçalves et al., 2020). The previous ground and space coordinated observations with VEx granted our team experience and expertise that should contribute for the success of the current Akatsuki collaboration.

Instruments

As an observatory satellite orbiting Venus, Akatsuki consists of five cameras that allow for obtaining images of Venusian atmosphere at various wavelengths between ultraviolet and long-wave infrared, as well as an ultra-stable oscillator used to measure vertical profiles of temperature, pressure, and so on. The five cameras are all installed facing the same orientation so as to enable simultaneous observation of Venusian atmosphere (Nakamura et al., 2011). In fig. 4.6 one can see the Akatsuki spacecraft with the respective location of its instruments.

- UVI (UltraViolet Imager): It consists of two channels: 283 nm (dayside: sulfur dioxide at cloud top) and 365 nm (dayside: unidentified absorbent

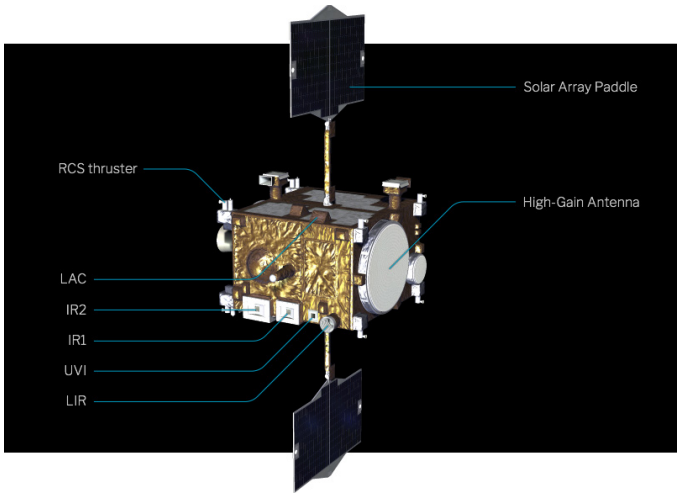

Figure 4.6: Artistic image of Akatsuki probe and its respective instruments (credits: http://akatsuki.isas.jaxa.jp/en/mission/spacecraft/).

substances), with a FOV of 12°x 12 °and Si CCD (1024x1024 pixels) detector. UVI was designed for two purposes: (1) map the SO2 absorption at 283 nm and (2) detect contrast from the unknown UV absorber at 365 nm. Acquires ultraviolet images, allowing to obtain the distribution of sulfur dioxide, which is related to the cloud formation, and the distribution of unidentified chemical substances which absorbs the ultraviolet rays (UV absorber). It can also measure the wind speed at the cloud tops by tracing the dark-and-light pattern due to the scattering of ultraviolet rays in sunlight by Venusian clouds.

- IR1 (InfraRed camera 1): By utilizing the wavelength bands around 1 μm (0.90-1.01 μm), which allows for seeing below clouds and near the surface of Venus, and by comparing infrared intensities of different bands, it can be used to investigate the movement of clouds in the lower atmosphere, the distribution of water vapor, the mineral composition of the surface, and can check for the presence of active volcanoes (Iwagami et al., 2011).

- IR2 (InfraRed camera 2): The camera studied the night side lower clouds' opacity to the thermal emission from the surface and deeper atmosphere (1.74-2.32 μm). It also sensed on the day side the CO2 band at 2.02 μm, which can be used to infer the altitude of the top of the clouds. Finally, the 1.65 μm filter was used during the cruise phase to study the zodiacal light.

- LIR (Longwave InfraRed camera): Detects thermal emission from the cloud top in a wavelengthregion 8-12 μm to map the cloud-top temperature, which

is typically at around 230 K. Unlike other imagers onboard Akatsuki, LIR is able to take images of both dayside and nightside with equal quality (Taguchi et al., 2007).

- LAC (Lightning and Airglow Camera): This camera searches for lightning flashes and maps airglow emissions on the nightside disk of Venus when Akatsuki is located in the eclipse (umbra) of Venus. It has a FOV of 16°x 16°and filters centered at 777.4 nm (nightside: lightning discharge), 480-605 nm (nightside: airglow from oxygen molecules), 557.7 nm (nightside: airglow from oxygen atoms) and 545 nm (for calibration use).

4.3 VEx/VIRTIS-M April 2014

4.3.1 Observations (VEx 2014)

These ESA's Venus Express observations were were carried out in coordination with ground-based Doppler velocimetry observations (CFHT/ESPaDONs April 2014, see section 3.3), extending for three orbits, from 2918 to 2921. Since Venus Express had a polar orbit, some of the instruments onboard the spacecraft demanded long exposure times and they were, thus, unable to carry out observations close to the pericenter. For this reason, ground-based observations were chosen to be coincident with VEx apocentric observations of the south hemisphere of Venus.

Several sets of ultraviolet images - able to sense the cloud tops through the scattered/absorbed radiation at about 70 km (Ignatiev, 2009) - were acquired with the Visible and InfraRed Thermal Imaging Spectrometer (VIRTIS-M) (Drossart et al., 2007) and the Venus Monitoring Camera (VMC) (Markiewicz et al., 2007). Wavelengths of 380 and 365 nm were chosen for VIRTIS-M and VMC, respectively. As VMC required shorter exposure times, it also acquired short-time sets of high spatial resolution images (typically less than 10 minutes in each orbit) closer to VEx pericenter (thus not strictly simultaneous with ESPaDoNS) and covering the northern hemisphere of Venus. Unfortunately, the S/N of VMC apocentric observations during these orbits was low and not trustable for cloud-tracking, while the high velocity of VEx during these pericentric observations didn't allow enough spatial overlap to track cloud features between pairs of images. In the case of the VIRTIS-M, apocentric observations were made only during orbits 2918 and 2923, with the first being the only one coincident with our observations. Although two days after our ground-based observation, the images from the orbit 2923 were also analyzed since they were the closest in time and permitted to have a control about the wind variability with time.

The detailed information about the VIRTIS-M images used in this work can be found in table 4.1, and a comparison of the spatial coverage for VIRTIS-M and ESPaDoNS can be seen in figure 4.7. In addition to clear temporal changes in the cloud morphology as seen from VIRTIS-M images, we also checked from VIRTIS-M and VMC observations that there was an intense wave activity apparent on the albedo of the cloud tops during all the days of ESPaDoNS observations (see figure 4.8), with wavelengths ranging from tens (figure 4.8a-c) to hundreds of km (figure 4.8d) which are consistent with gravity waves (Peralta et al., 2014).

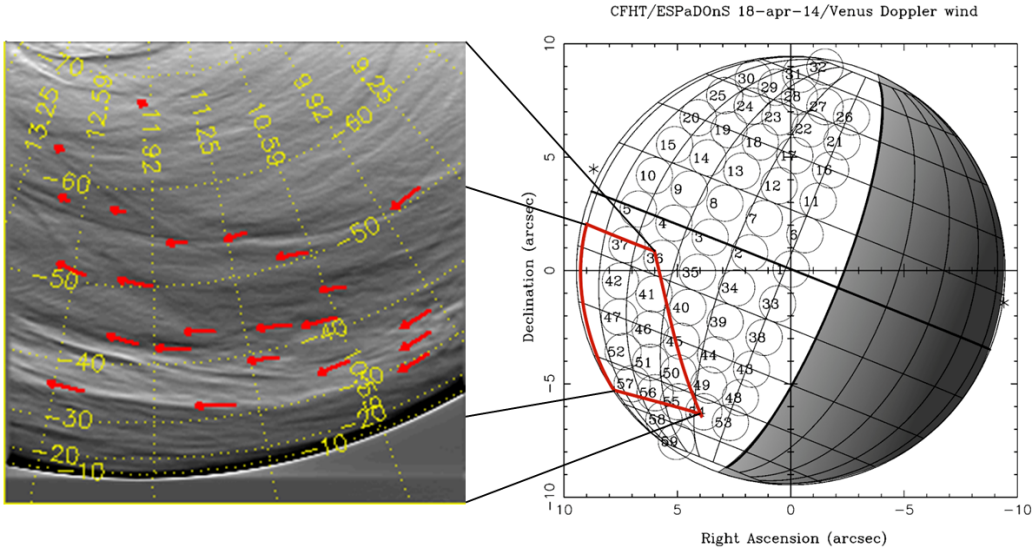

Figure 4.7: Right side: aspect of Venus disk as seen from Earth (as in figure 3.6) with superimposed Venus-Express VIRTIS instrument's FOV. The figure illustrates our observing strategy to match CFHT/ESPaDOnS operations (thin black circles) and ESA/Venus Express VIRTIS-M instrument FOV (red distorted rectangle) during orbit 2923. Left side: zoom-out of an image (VV2923_08) obtained with VIRTIS-M at 21 Apr. 2014 (orbit 2923), the latitudes covered the range from 10°S to 50°S and the local time spans from 10h till 13h. On the zoomed image (VV2923_08) we can see tracers (red arrows) marked on cloud features that will correspond to matching cloud features on this image's pair (VV2923_11) obtained 48 minutes later.

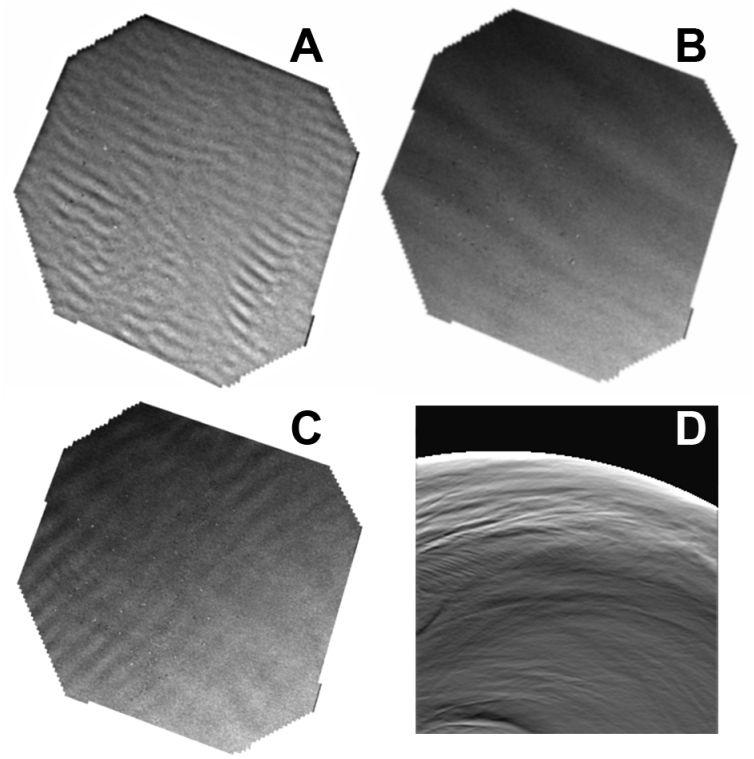

Figure 4.8: Examples of recurrent presence of gravity waves on the dayside cloud tops during our observations: (A) waves at 70°N and 10:31 LT in a VMC image with spatial resolution of 147 m and taken on 17 of April 2014, (B) waves at 73°N and 10:37 LT in VMC image with resolution 135 m during 18 April 2014, (C) waves at 77°N and 10:43 LT in VMC image with resolution of 132 m during 19 April 2014, and (D) waves at 45°S and 12:30 LT in VIRTIS-M image with resolution of 19 km during 21 April 2014.

(1) VEx orbit	(2) Qubes pairs	(3) Date (yyyy/mm/dd)	(4) Time interval (min)	(5) Latitude range	(6) Local time range	(7) Number of points
2918	VV2918_04 VV2918_09	2014/04/16	80	50°S-90°S	10h−14h	08
2918	VV2918_06 VV2918_11	2014/04/16	80	20°S-50°S	12h−15h	11
2918	VV2918_07 VV2918_12	2014/04/16	80	20°S-70°S	09h−12h	14
2918	VV2918_13 VV2918_16	2014/04/16	80	10°S-40°S	11h−13h	10
2923	VV2923_00 VV2923_03	2014/04/21	60	40°S-90°S	09h−14h	13
2923	VV2923_04 VV2923_07	2014/04/21	60	20°S-70°S	09h−13h	23
2923	VV2923_08 VV2923_11	2014/04/21	48	10°S-50°S	10h−13h	25

Table 4.1: Tehcnical details of the April 2014 observation by ESA Venus Express/VIRTIS-M UV-visible channel at 380 nm: (1) orbit number ; (2) VEx-VIRTIS hyper-spectral images or "Qubes" pairs as defined by Cardesín (2010) ; (3) UT date ; (4) time interval between selected image pairs ; (5-6) corresponding latitude and local time range. The imaging spatial resolution varies between 15 km per pixel for polar latitudes and about 45 km per pixel for equatorial ones ; (7) number of cloud tracers identified in image pairs. The observations from 16 Apr., 2014, are coordinated with ESPaDOnS' ones, which allows us to directly compare winds measurements from same time, same location, upon Venus. The VIRTIS-M observations from 21 Apr. will permit us to better address temporal variability of the Venus' winds, regarding that this observing date increases, considerably the time span of our investigation in this run.

4.3.2 Results (Vex 2014)

In this section we analyse the results from the VIRTIS-M cloud-tracking technique based on measurements from 16 and 21 April 2014. As many as 104 wind measurements were obtained with cloud-tracking on the VIRTIS-M images, as detailed in Table 4.1. When confronted with mean profiles of the winds from VEx/VIRTIS-M (Hueso et al., 2015), the zonal and meridional wind speeds display, as expected (Peralta et al., 2007), a clear decrease of the zonal component poleward of mid-latitudes and a weak meridional circulation towards the polar region (see figure 4.9).

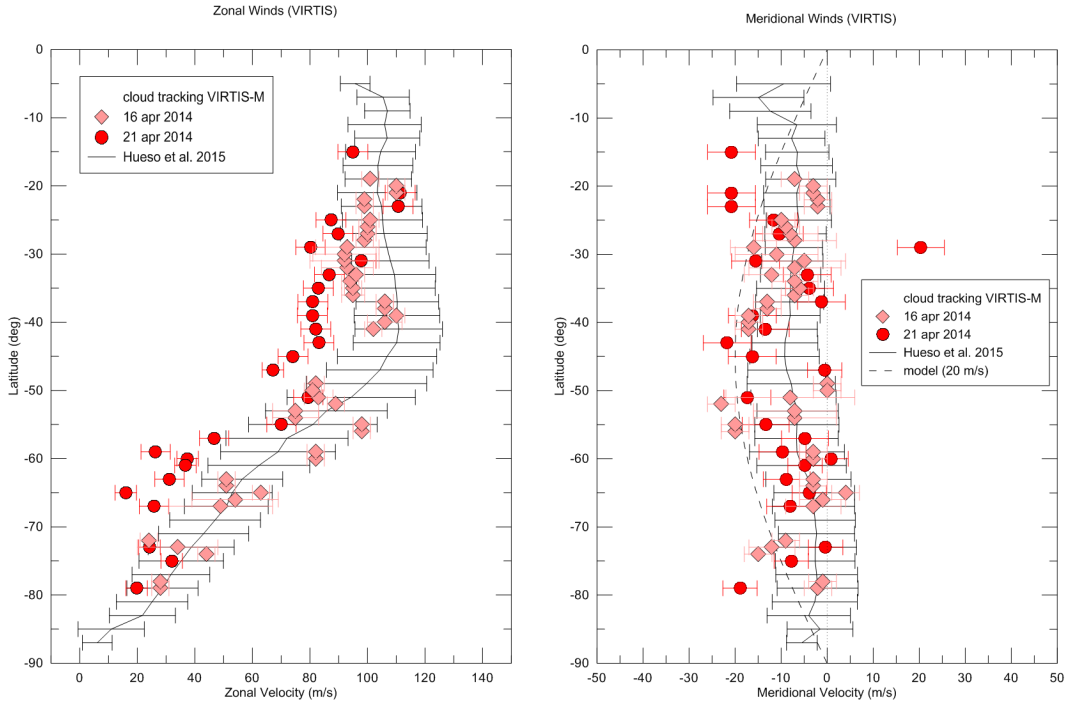

Figure 4.9: Zonal and meridional wind speeds measured with cloud-tracking using VIRTIS-M images taken at 380 nm during the VEx orbits 2918 (diamonds) and 2923 (circles), corresponding to dates 16 and 21 of April 2014. Zonally averaged winds from VIRTIS-M long-term studies are also displayed as reference with black solid line (Hueso et al., 2015). In the case of the meridional winds, the dashed line is a fit to a pure meridional model flow with $\overline{v}_m = (22.5 \pm 15.5)$ m s^{-1} (see table 3.4) as in figure 3.9.

Discussion and Conclusions

An investigation of the dayside cloud tops dynamical regimes using simultaneous ground and space-based measurements was undertaken, yielding coherent results on both N and S hemispheres.

Mean latitudinal distribution of the zonal wind profile by VEx/VIRTIS-M is in agreement with general VIRTIS-M (Peralta et al., 2007; Hueso et al., 2012, 2015; Machado et al., 2014) and VEx/VMC cloud-tracked results (Khatuntsev et al., 2013): zonal circulation is characterized by almost uniform velocity up to the middle latitudes (near 50°N-S), where the wind speed tends to show a weak maximum.

The decrease of the zonal component poleward of mid-latitudes and a weak meridional circulation towards the polar region are clearly seen in our VIRTIS 2014 data (Fig. 4.9). Poleward from about 50° latitude, the zonal wind velocity quickly decrease.

The meridional shear of the wind between 50° and 80° S is - 0.4 m s^{-1} deg^{-1}. Fig. 4.9 indicates how well our 16-21 Apr. VIRTIS measurements compare with zonally-averaged winds from VIRTIS-M 2006-2015 long-term mean zonal circulation. We can note that VIRTIS-M data from a single orbit typically cover a relatively small portion of the dayside within a limited longitudinal range. Also, we can observe that the winds obtained during VEx orbit 2923 (Apr. 21) display more disperse values in both components, suggestive of winds being affected by the presence of stronger wave activity (see fig. 4.8).

4.4 Akatsuki/UVI January 2017

4.4.1 Observations (Akatsuki 2017)

The space observations by JAXA's Akatsuki mission were made between 26 and 31 January 2017, during orbit number 39. We also carried out coordinated ground-based Doppler velocimetry observations using the TNG/HARPS-N between 28-29 January (see section 3.4.1). The sets of ultraviolet images (3 images per day of observation) were acquired with the UltraViolet Imager (UVI) using the 365 nm centre wavelength filter (Yamazaki et al., 2018). The original UVI images (fig. 4.2 were processed to improve the signal-to-noise ratio, using a semi-automatic method, evolved from a phase correlation method between images developed by Peralta et al. (2018)).

For each one of the six days of observations we had 3 images (hereinafter refered as images a, b and c, as in table 4.2), separated by $\approx$ 2 hours each. Cloud tracking method is based on the analysis of the apparent movement of cloud features retrieving zonal and meridional mean velocities along the time interval between two images. Therefore, we used 3 pairs of images per day: pair P_1 (image a and b), pair P_2 (image b and c) and pair P_3 (image a and c). Pairs P_1 and P_2 both consist in images with a time interval of $\approx$ 2 hours, while the images in pair P_3 have an interval of $\approx$ 4 hours.

A total of 4035 cloud tracers were identified to carry out the calculation of the wind velocities, for all the images. Table 4.3 shows the number of cloud tracers used for each pair of images.

Generally, cloud-tracking methods use pairs of images typically separated by 2 hours (Hueso et al., 2015; Machado et al., 2017; Horinouchi et al., 2018), since for these intervals cloud features remain coherent and can be clearly identified in consecutive images. We opted to also use the pairs of images separated by 4 hours, however, most of the fine structures and details do not survive such time difference, as is reflected by the reduced number of tracers tracked in those pairs of images (table 4.3).

4.4.2 Results (Akatsuki 2017)

Zonal wind

In this section we present the results for zonal wind velocities retrieved with Akatsuki/UVI observations. Fig. 4.10 shows the daily latitudinal zonal wind profile, weighted averaged with a binning of 5° in latitude, while also presenting each cloud related wind measurement. A total of 758, 599, 669, 675, 693 and 642 cloud tracers were used to retrieve wind velocities for day 26^{th} to 31^{th} respectively. In

(1) Date and time UT	(2) arcsec/px	(3) km/px	(4) latitude	(5) local time	(6) distance (km)	(7) diameter (°)	(8) code
26-01-2017 17:34:46	0.361	38.564	$72°N - 88°S$	7:30-18:00	139281	5.04	a
26-01-2017 19:34:44	0.392	41.866	$72°N - 88°S$	7:30-18:00	150410	4.67	b
26-01-2017 21:34:46	0.421	44.955	$72°N - 88°S$	7:30-18:00	160935	4.36	c
27-01-2017 17:04:44	0.542	57.962	$75°N - 85°S$	8:00-18:00	241464	2.91	a
27-01-2017 19:04:45	0.556	59.423	$75°N - 85°S$	8:00-18:00	248056	2.83	b
27-01-2017 21:04:43	0.569	60.811	$75°N - 85°S$	8:00-18:00	254403	2.76	c
28-01-2017 18:04:44	0.679	72.499	$75°N - 85°S$	8:30-18:00	308741	2.27	a
28-01-2017 20:04:46	0.687	73.368	$75°N - 85°S$	8:30-18:00	312904	2.24	b
28-01-2017 22:04:44	0.694	74.157	$75°N - 85°S$	8:30-18:00	316909	2.21	c
29-01-2017 18:54:44	0.754	80.534	$75°N - 85°S$	9:00-18:00	350172	2.00	a
29-01-2017 20:54:45	0.758	80.974	$75°N - 85°S$	9:00-18:00	352612	1.99	b
29-01-2017 22:54:43	0.762	81.386	$75°N - 85°S$	9:00-18:00	354927	1.98	c
30-01-2017 18:04:45	0.784	83.755	$75°N - 85°S$	9:15-18:00	371094	1.89	a
30-01-2017 20:04:44	0.785	83.858	$75°N - 85°S$	9:15-18:00	372172	1.88	b
30-01-2017 22:04:44	0.786	83.929	$75°N - 85°S$	9:15-18:00	373138	1.88	c
31-01-2017 17:24:43	0.785	83.904	$70°N - 80°S$	9:50-18:00	376765	1.86	a
31-01-2017 19:24:45	0.784	83.796	$70°N - 80°S$	9:50-18:00	376553	1.86	b
31-01-2017 21:24:42	0.783	83.650	$70°N - 80°S$	9:50-18:00	376230	1.86	c

Table 4.2: List of images from Akatsuki observations, 26-31 January 2017, of Venus' dayside: (1) Date and time UTC; (2) mean resolution in deg/px; (3) mean resolution in km/px; (4) latitude range of Venus' visible disk; (5) local time range of Venus' visible dayside; (6) distance between VCO and Venus in km; (7) Venus' apparent angular diameter in deg; (8) coded letter attributed while pairing images. For each day, we analised tracers from 3 pairs of images: a+b, b+c, and a+c.

(1) Date	(2) pair	(3) images	(4) tracers
26-01-2017	P_1	a+b	284
26-01-2017	P_2	b+c	310
26-01-2017	P_3	a+c	164
27-01-2017	P_1	a+b	168
27-01-2017	P_2	b+c	255
27-01-2017	P_3	a+c	176
28-01-2017	P_1	a+b	252
28-01-2017	P_2	b+c	215
28-01-2017	P_3	a+c	201
29-01-2017	P_1	a+b	257
29-01-2017	P_2	b+c	264
29-01-2017	P_3	a+c	154
30-01-2017	P_1	a+b	288
30-01-2017	P_2	b+c	235
30-01-2017	P_3	a+c	170
31-01-2017	P_1	a+b	201
31-01-2017	P_2	b+c	262
31-01-2017	P_3	a+c	179

Table 4.3: List of Akatsuki image pairs used to in cloud-tracking on 2017 observations: (1) Date; (2) designation of image pairs; (3) images used in the pair (as designated in table 4.2; (4) total tracers obtained for each pair

fig. 4.11 we present the mean zonal velocity in a latitudinal profile of the full observation campaign of January 2017 considering a 5° binning n latitude.

The latitudinal zonal wind profile obtained (fig. 4.11) is consistent with previous cloud-tracking results from Akatsuki/UVI (Horinouchi et al., 2018) and VenusExpress/VIRTIS (Sánchez-Lavega et al., 2008; Hueso et al., 2015). It shows an almost uniform velocity up to 50° N-S, where a maximum is reached, and a steep decrease at higher latitudes.

Both spatial and time variability of the zonal winds can be analysed, as a first approach, in fig. 4.12, where we used a polynomial interpolation of the data to produce a contour plot, using a grid of 60 lines and 40 columns, corresponding to a resolution of about 2.0° latitude and 0.3 h local time. The results in fig. 4.12 show a general daily variability of about 5-10 ms^{-1}. There is evidence of a north-south asymmetry, more obvious on the measures of day one (26^{th}) but also clear in the mean values (fig. 4.10, 4.11 and 4.12). This equator asymmetry, with southern velocities higher about 10 ms^{-1}, is consistent with Horinouchi et al. (2018) results - which were obtained between October 2016 - March 2017 and using the same instrument and filter as this work (UVI, 365 nm filter). Both temporal coverage, instrument used and asymmetry detected are consistent. The results also present an increase in wind velocity towards the evening terminator, more noticeable in the results of day 28^{th} January in fig. 4.12. This increasing of zonal velocity of up to 10 ms^{-1} near evening terminator was already observed by other authors(such as Hueso et al. (2015); Machado et al. (2017); Horinouchi et al. (2018)). However, due to the low number of points and days observed, we cannot properly disentangle the contributions from atmospheric waves (such as the Y-feature wave) and solar tides (Kouyama et al., 2013).

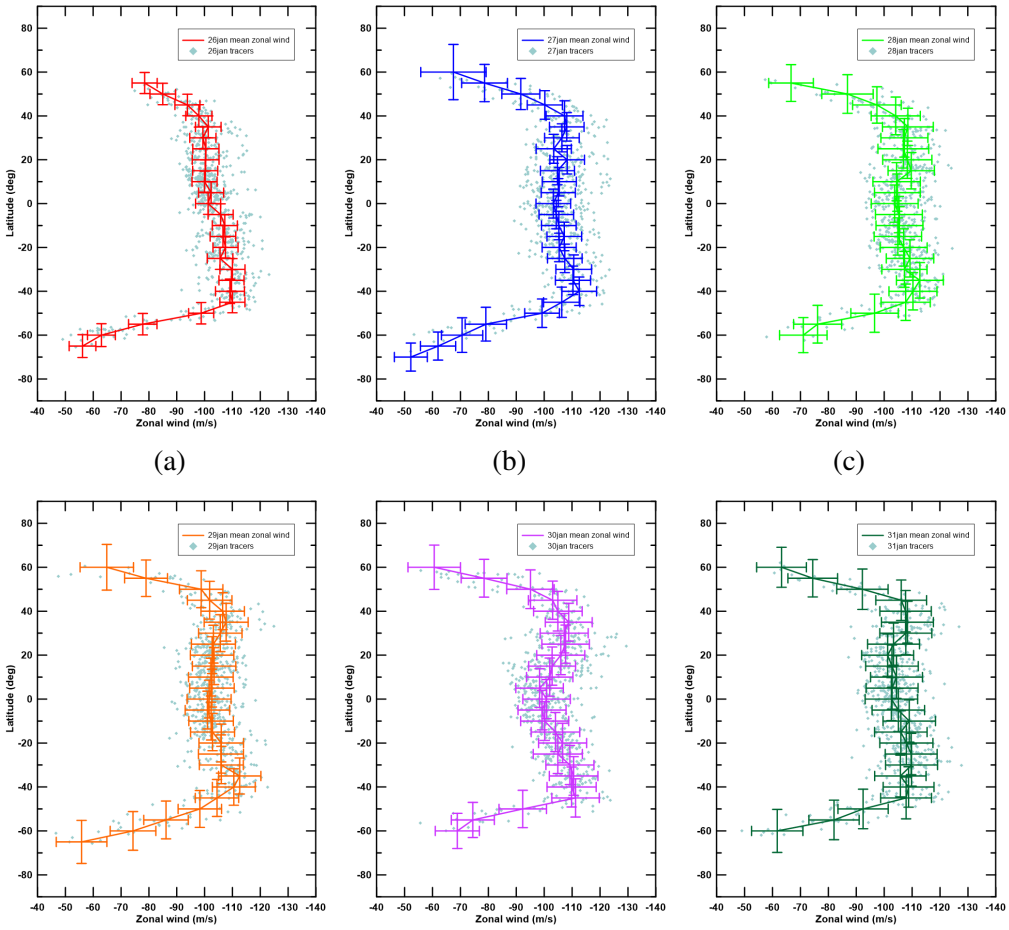

Figure 4.10: Daily zonal wind latitudinal profiles of Akatsuki/UVI resuts for each of the six days of observations (26 to 31 January, in panel *a* to *f*, respectively). The values presented are a weighted average of each day, with a binning of 5° in latitude. Cloud tracers are represented as grey diamonds, while the colored solid line represents the mean wind latitudinal profile and its respective error bars (see section 4.1)

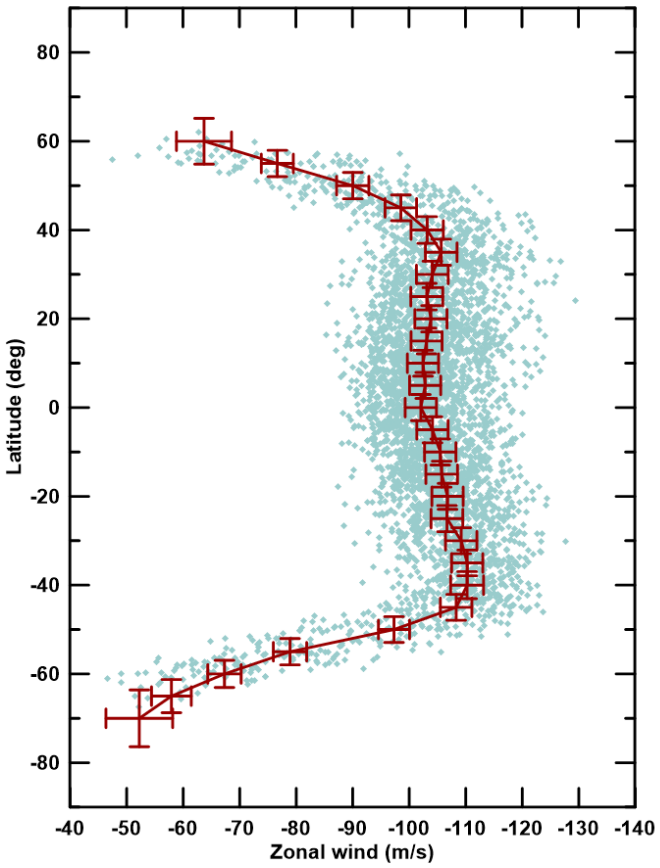

Figure 4.11: Mean zonal wind latitudinal profile of Akatsuki/UVI results. Mean of each latitude band for all days with a binning of 5° latitude. Cloud tracers are represented as grey diamonds.. See section 4.1 for detailed definition of the associated error.

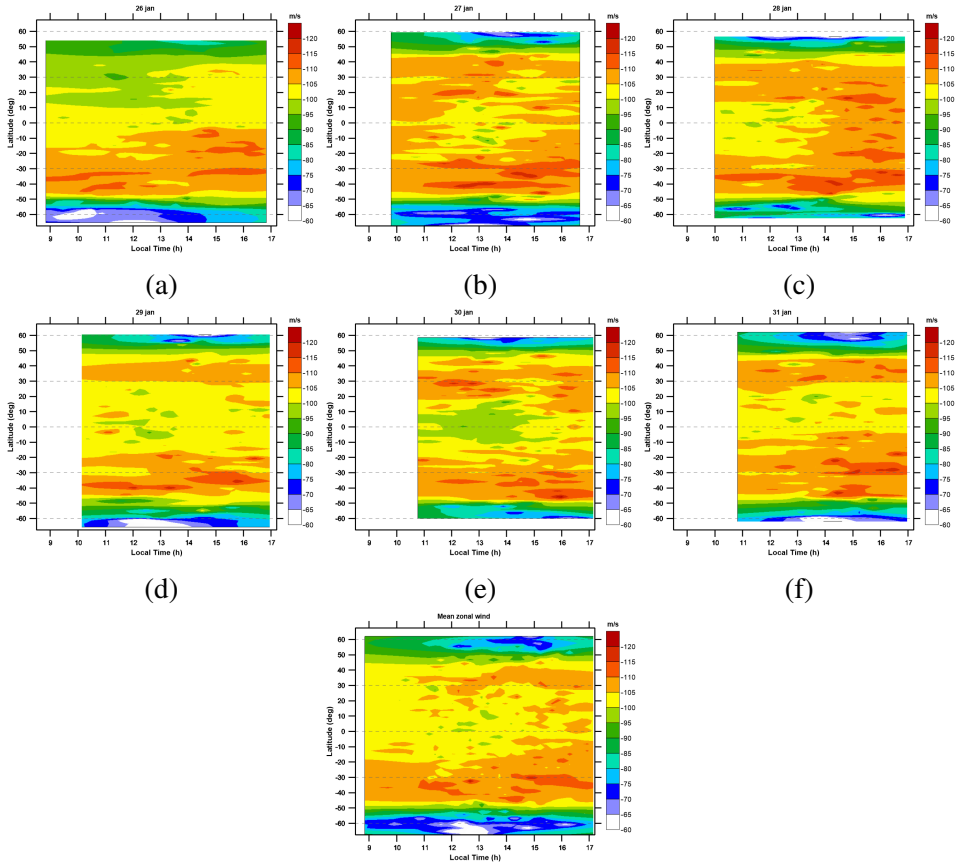

(a) (b) (c)

(d) (e) (f)

(g)

Figure 4.12: Contour plots of zonal wind in function of latitude and local time from Akatsuki/UVI results. Panels a-f are daily results (26-31 January respectively), panel g is the mean contour plot of all the observation campaign. Zonal wind velocity represented as a color code in a westward direction. Polinomial interpolation with a grid of 60 lines and 40 columns, corresponding to a resolution of about 2.0° latitude and 0.3 h local time.

Meridional wind

To study the meridional wind profile we applied the same procedure as stated for the zonal wind - weighted average all measures applying a binning of 5° latitude. The mean meridional wind of the observation campaign is presented in fig. 4.13. The meridional wind contour plot (fig. 4.14) was also retrieved using the same procedure as described for the zonal wind contour plot.

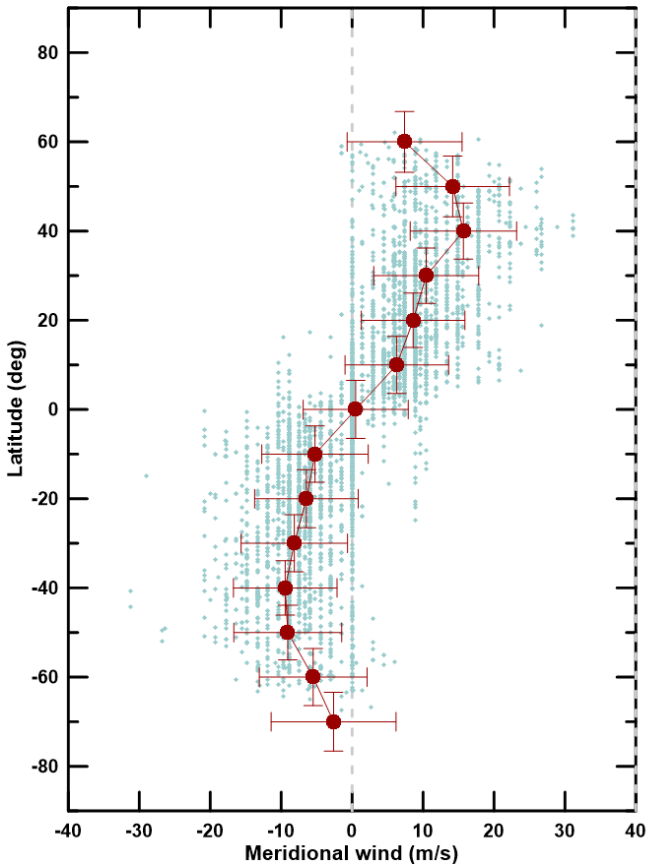

Figure 4.13: Mean meridional wind latitudinal profile from Akatsuki/UVI observations (dark red circles). The tracers used for the mean values are represented in gray diamonds. Weighted average of all the latitudinal profiles of all days, with a binning of 5° latitude.

A day-to-day variability around 4-8 m^{-1} is noticeable on the meridional wind (fig. 4.14). It is also clear a N-S assymmetry with velocities higher up to 8 ms^{-1} on the northern hemisphere, particulary on the first day (26^{th}). However, this assymmetry is opposite of the one detected for zonal wind velocities, suggesting they should be correlated.

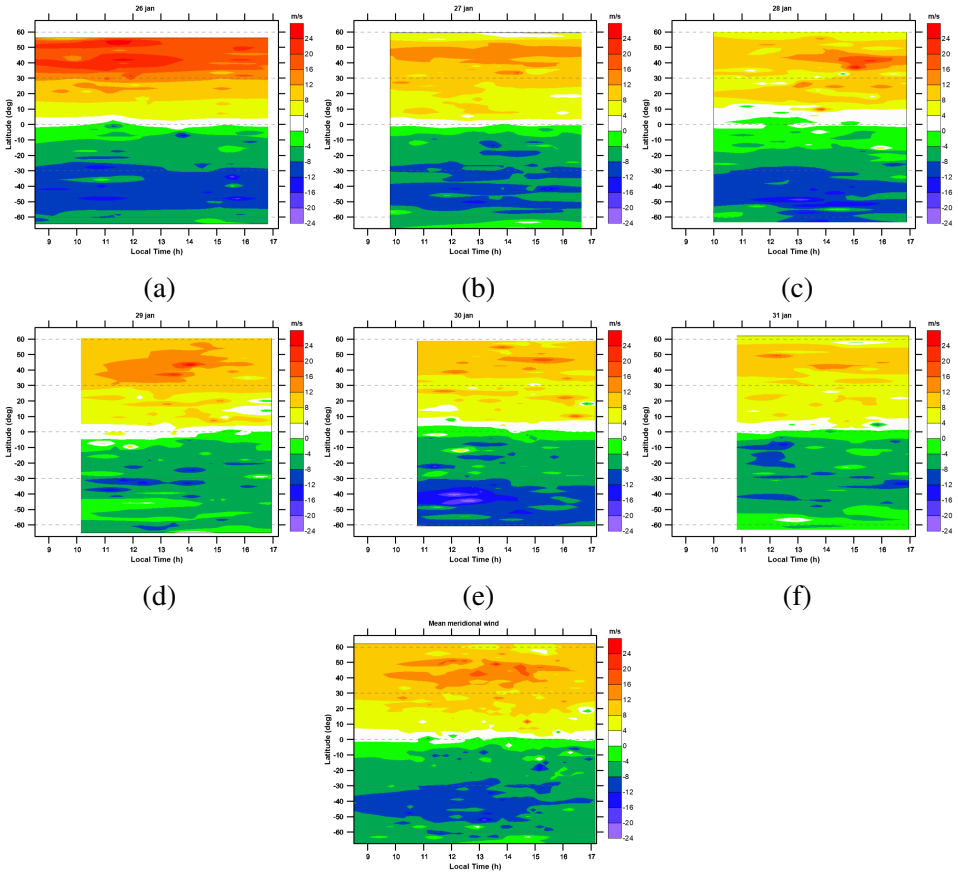

Figure 4.14: Contour plots of meridional wind in function of latitude and local time from Akatsuki/UVI results. Panels a-f are daily results (26-31 January respectively), panel g is the mean contour plot of all the observation campaign. Wind velocities are represented in a color code in a poleward direction, positive velocities towards north pole and negative velocities towards south pole). Polynomial interpolation with a grid of 60 lines and 40 columns, corresponding to a resolution of about 2.0° latitude and 0.3 h local time.

At some latitudes, there is evidence of a decrease in meridional wind velocity towards the evening terminator, in the order of $\sim 5\ ms^{-1}$. This decay in meridional wind magnitude near the evening terminator was already analysed by other works (Hueso et al., 2015; Horinouchi et al., 2018), although it is not possible, with such a low amount of data, to properly disentangle contributions from atmospheric waves and solar tide. However, this data suggest that the decay in meridional wind could be correlated with the higher zonal wind velocities near the evening terminator.

Long term comparison

We present a comparison of zonal and meridional wind results from previous space observations in fig. 4.15 and fig. 4.16 respectively. This comparison includes results from Hueso et al. (2015) (VenusExpress/VIRTIS) and Horinouchi et al. (2018) (Akatsuki/UVI).

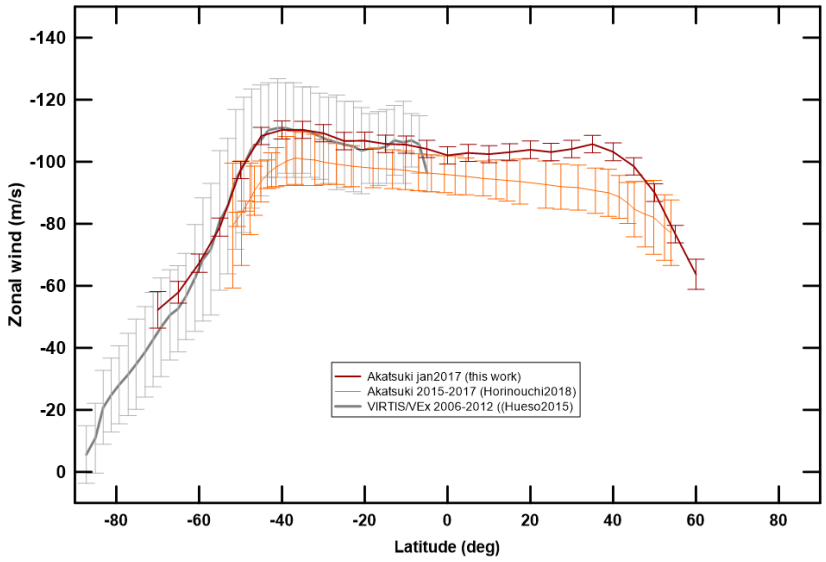

Figure 4.15: Comparison of zonal wind results from different cloud-tracking space observations. The legend of the figure refers the mission/instrument, date of observations and respective scientific article. . See section 4.1 and Hueso et al. (2015); Horinouchi et al. (2018) for detailed definitions of the error bars

The equatorial orbit of Akatsuki presents an opportunity to study winds at both hemispheres simultaneously, contrasting with the VenusExpress's polar orbit, which cloud tracked measurements covered only the southern hemisphere. This allowed for the detection on a zonal wind N-S assymmetry, as noticeable on this

work's results and in Horinouchi et al. (2018). Along the south hemisphere, the latitudinal profile of this work is more similar to the profile from VenusExpress than to the Akatsuki's Horinouchi et al. (2018) wind profile. However, both Hueso et al. (2015) and Horinouchi et al. (2018) profiles presented in fig. 4.15 correspond to velocities, retrieved using an automatic cloud-tracking method, averaged over a large time span data set (2006-2012 and 2015-2017 respectively), while this work's results were obtained using a semi-automatic method, averaged over 6 days of observations. Althoug the latitudinal zonal wind profile of Venus' cloud-top shows some variability along the years of study, the profile remains coherent with a nearly constant zonal wind velocity a latitudes below 30°, with a steep decrease in wind magnitude at higher latitudes, around 40°-50°, in both hemispheres.

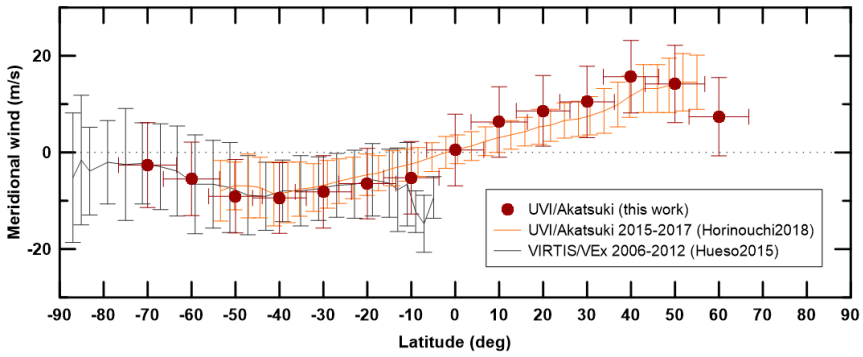

Figure 4.16: Comparison of meridional wind results from different cloud-tracking space observations. The legend of the figure refers the mission/instrument, date of observations and respective scientific article (this work, Hueso et al. (2015) and Horinouchi et al. (2018)).

As for the meridional wind, the latitudinal profile obtained is highly consistent with previous space observations - wind velocity peaks at around 40°-50° with a magnitude of about 15 ms^{-1}, with a steep decrease at 60°. However, the associated errors are of the same order of magnitude as the meridional wind velocities.

Discussion (Akatsuki 2017)

The Akatsuki/UVI results presented in this work show evidence of an asymmetry on zonal wind speed between northern and southern hemisphere, particulary on the first day (26 January) - velocities on the southern hemisphere are generally higher, in the order of ~ 10 ms^{-1} (fig. 4.12). This N-S asymmetry was also evidenced by Horinouchi et al. (2018) based on Akatsuki UVI observations from October 2016 - March 2017 (therefore encompassing this work's Akatsuki/UVI

observations). Yet, previous data sets extending from December 2015 to August 2016 did not show any evidence of N-S asymmetry. This may suggest the existence of a time-variable phenomena or episodic event. Additionally, our analysis also evidences a N-S asymmetry of the meridional wind component (fig. 4.14), with higher velocities in the northern hemisphere. This asymmetrical behaviour (zonal and meridional, North & South hemisphere) appears to be anti-correlated. It may be the result of a persistent vertical shear and hemispheric asymmetry of the altitude of the upper cloud features, as discussed by Horinouchi et al. (2018). It might also be the result of 3-dimensional structures of wind and temperature associated with the thermal tides (Takagi et al., 2018). However, we cannot properly disentangle the contributions from atmospheric waves (such as the Y-feature wave) and solar tides, thus, additional zonal wind measurements acquired simultaneously on both hemispheres, based on ground-based observations on longer periods, will be required to constrain and study the amplitude and time dependency of this asymmetry.

Regarding spatial variability, we find evidence of an increases in the magnitude of the zonal wind velocity near the evening terminator (fig. 4.12). We also find evidence of a decrease (about 5 ms^{-1}) in the magnitude of meridional wind with local time, at some latitudes. The decrease of meridional wind velocities and the increase of zonal wind velocities close to the evening terminator may, again, reflect a combination of a vertical wind shear and local-time dependence of temperature and wind structures associated with the thermal tide, as already been discussed by several authors (Sánchez-Lavega et al., 2008; Hueso et al., 2015; Horinouchi et al., 2018; Takagi et al., 2018).

In order to study the effects of Venus' topography on the wind velocity, through gravity waves and vertical wind shear, we compared the number of cloud tracers (daily and total) and the zonal wind velocity (daily and mean) against surface topography. Bertaux et al. (2016) studied an apparent correlation between zonal wind at cloud-top and surface topography over Aphrodite Terra region, however, we didn't detect any evidence between surface level and zonal wind nor number of tracers. Considering the short temporal coverage of our observations, additional studies are required to determine such correlation.

Chapter 5

Venus' cloud-top: DV and CT comparison

5.1 Altitude determination

The determination of the altitude level originates from early polarization and photometry studies undertaken by Henson and Hovenier (1974). On the other hand, cloud tops 365 nm UV markings were estimated by Kawabata et al. (1980) to probe the same altitude level (Gierasch et al., 1997; Widemann et al., 2007, 2008).

As discussed by Widemann et al. (2007), the Kawabata et al. (1980) model consists of a main cloud, with particle size of 1.05 μm, underlain by and partly mixed with a haze with $\simeq 0.2$ μm particle size. The optical depth of the haze is about 0.6 at 40 mbar, and varies roughly as $\lambda^{-1.7}$, meaning a $\tau = 1$ level is reached within one scale height of the clouds top at 70 km of altitude (Ignatiev, 2009). This is also the altitude of the UV cloud markers that enables the cloud tracking wind's measurements technique (Moissl et al., 2009). This coincidence allows to compare magnitudes and variability between ground based DV results and the ones from tracking of UV markings methods as is the case for VEx/VIRTIS-M, Akatsuki/UVI (385 nm), Pioneer/OCPP (*Orbiter Cloud Photopolarimeter*) and Galileo/SSI (*Solid State Imager*).

The cloud top morphology is extensively discussed by Markiewicz et al. (2007) and Titov et al. (2012). The Venus' clouds are mainly composed of H_2SO_4 droplets produced photochemically through hydration of SO_3 above 60 km. The sulfuric acid gas condenses into droplets, which grow and move downward by diffusion and sedimentation.

Based on photometry and polarization, Henson and Hovenier (1974) determined that cloud top altitude, at visible range, is located at about 65-70 km, where an optical depth of unity ($\tau = 1$) is reached. Kawabata et al. (1980) indicated that this level is about 40 mb pressure and 70 km altitude, based on a detailed analysis of Pioneer Venus OCPP UV and visible data. Using the depth of CO_2 bands in VEx/VIRTIS-M combined with VEx/VMC UV images, Ignatiev (2009) stated that the optical depth of the cloud haze is nearly 0.6 at 40 mbar, and varies as $\lambda^{-1.7}$, implying that a $\tau = 1$ level is reached within one scale height of the clouds top roughly at 70 km of altitude. Fedorova et al. (2016) using SPICAV/VEx Vis-IR observations demonstrated that, for a fixed upper aerosol scale height for all latitudes, the cloud top altitude varies from 68 to 73 km at latitudes from $40^{\circ}S$ to $40^{\circ}N$ with an average of 70.2 ± 0.8 km based on CO_2 bands in the range of 1.4-1.6 μm.

Since the Doppler velocimetry technique is based on solar light scattered on Venus dayside, the altitude of the retrieved horizontal velocities is where optical depth unity is reached, which corresponds to the cloud top at around 70 km. (Henson and Hovenier, 1974; Kawabata et al., 1980; Ignatiev, 2009).

At cloud top, an unknown absorber is responsible for high contrast clouds at

UV and visible wavelengths. Although some variability in the cloud-top altitude is known (Lee et al., 2012), both the 365 nm filter Akatsuki/UVI and the 380 nm channel VEx/VIRTIS-M images track cloud features at the cloud-top level, which is estimated at about 68-71 km (Esposito et al., 1997; Ignatiev, 2009; Fedorova et al., 2016).

These altitude determinations allows for a magnitude and variability comparison between (i) Doppler velocimetry results from VLT/UVES (Machado et al., 2012), CFHT/ESPaDOnS (Machado et al., 2014, 2017) and TNG/HARPS-N (Gonçalves et al., 2020) and (ii) the results from UV cloud tracking as from VEx/VIRTIS-M (Sánchez-Lavega et al., 2008; Hueso et al., 2012; Machado et al., 2014; Hueso et al., 2015; Machado et al., 2017) and Akatsuki/UVI (Gonçalves et al. (2020) and Horinouchi et al. (2018)).

5.2 Results comparison

5.2.1 April 2014: CFHT/ESPaDONs - VEx/VIRTIS

In this section we compare results from the coordinated observations with CFHT/ESPaDOnS and VEx/VIRTIS-M, as in Machado et al. (2017). In figure 5.1 we compare the median zonal wind for each day of observations. Each presented latitudinal wind profile results from a weighed average along each latitude band measured on each day of observations. The weighing coefficients were the inverse of the variance associated to each velocity measurement.

In figure 5.2 we compare the median zonal wind profile of the entire observation campaign from CFHT/ESPaDOnS and Vex/VIRTIS-M 2014 observations (Machado et al., 2017) with the median zonal wind profile from 2011 observations (previous work, Machado et al. (2014).

It is noteworthy the consistency of Doppler velocimetry results from different data sets (3 years apart), both in zonal and meridional winds. Regarding the VIRTIS-M results, there is a higher dispersion both in zonal and meridional winds.

It is also noticeable that zonal wind velocities retrieved by DV are about $\sim 10 ms^{-1}$ higher relatively to the velocities retrieved by CT technique. This is seen for both observation campaigns, as is Machado et al. (2014) and Machado et al. (2017). Further analysis of this gap in zonal wind velocities from both used techniques can be seen in section 5.3.

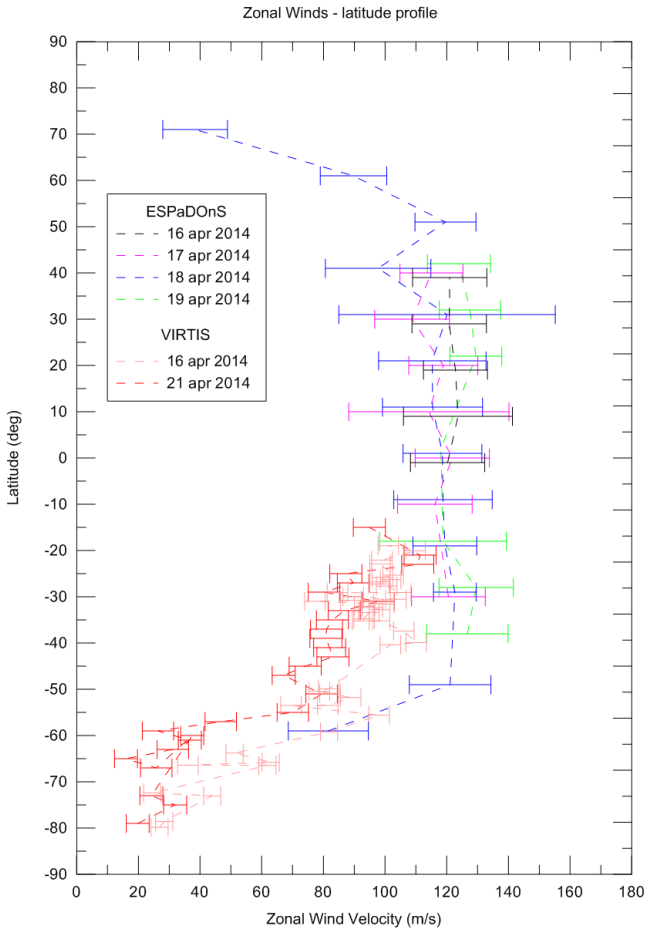

Figure 5.1: Zonal wind velocities $\overline{v}_{z,i}$. Latitudinal profile for each day of observations with CFHT/ESPaDOnS (days 16, 17, 18, 19 April, 2014), and space-based observations with VEx/VIRTIS-M on 16 and 21 April, 2014.

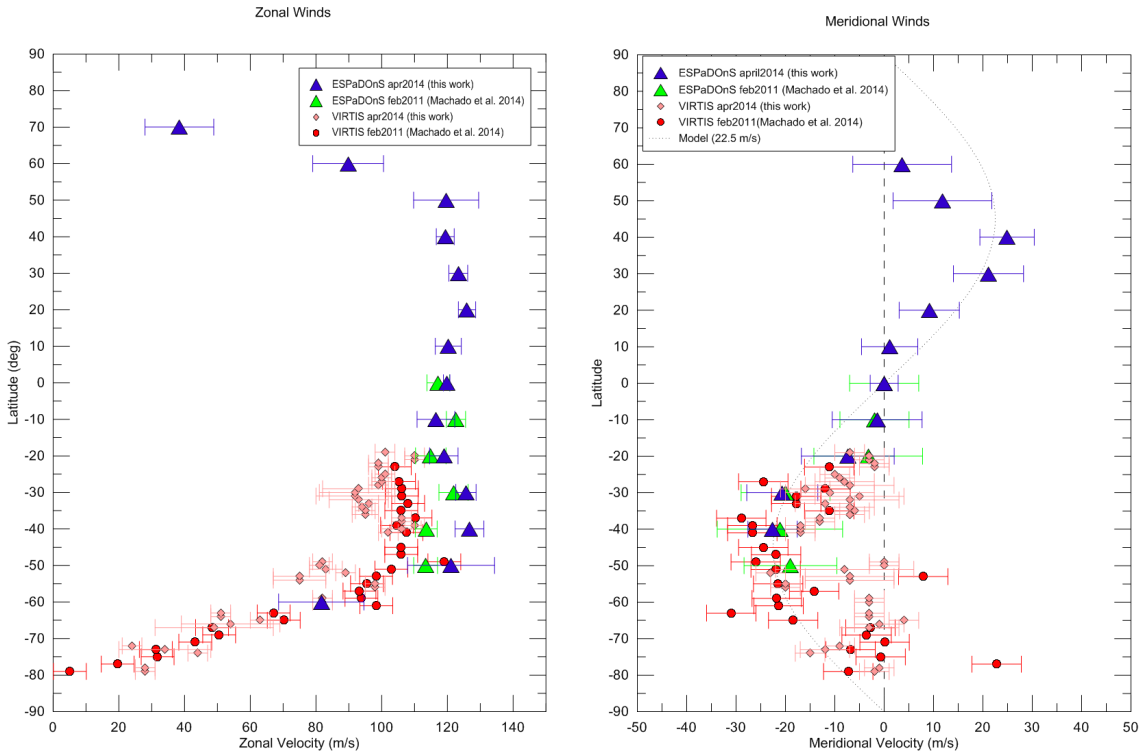

Figure 5.2: Comparison from coordinated CFHT/ESPaDOnS and VEx/VIRTIS-M simultaneous observations. We can compare two distinct runs: April 2014 CFHT/ESPaDOnS' run (blue triangles) and VEx/VIRTIS-M (pink diamonds) show this work latitudinal profile of zonal (left) and meridional (right). We can also compare with the coordinated results from Machado et al. (2014), where green triangles show zonal wind latitudinal profile retrieved from CFHT/ESPaDOnS' observations from February 2011, and red circles come from VEx/VIRTIS-M coordinated observations.

5.2.2 January 2017: TNG/HARPS-N - Akatsuki/UVI

In this section we will compare the results from the coordinated observations with TNG/HARPS-N and Akatsuki/UVI (365 nm filter), as in Gonçalves et al. (2020). The January 2017 HARPS-N observations were focused mainly on the HPA in order to retrieve meridional wind velocities. Therefore, the zonal wind was retrieved for latitudes between 10°N and 10°S with a 5° step. Figure 5.3 presents the mean zonal wind latitudinal profile for both observations, Akatsuki/UVI using CT and TNG/HARPS-N using DV. The velocities were weighed average along each latitude band (with a 5° latitude bin for CT results) measured on each day of observations, followed by a mean value of all the observation campaign. The weighing coefficients were the inverse of the variance associated to each velocity measurement.

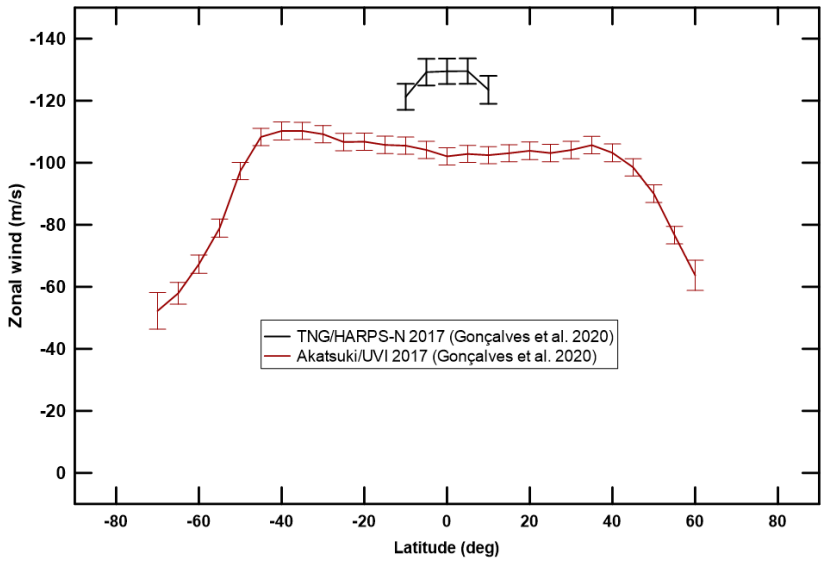

Figure 5.3: Mean latitudinal profile of zonal wind for TNG/HAPRS-N and Akatsuki/UVI (365 nm filter) from January 2017 results.

As for the meridional wind, the same weighted averaging process was conducted as in zonal wind. The comparison is presented in fig. 5.4.

The comparison of zonal wind shows a difference of about 20 ms^{-1}. However, the Doppler zonal results were retreieved using between 10°N and 10°S with a 5° step. This high velocities could represent an equatorial jet or a short term variability. Additional measurements with the TNG/HAPRS-N would contribute to a better understanding of any variability or unseen bias behind the results we obtained. As for the meridional wind, while CT wind velocities reach as high

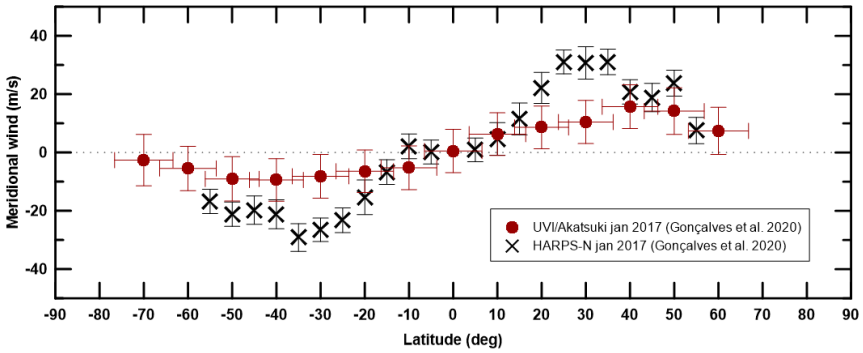

Figure 5.4: Mean latitudinal profile of meridional wind for TNG/HAPRS-N and Akatsuki/UVI (365 nm filter) from Janurary 2017 observations.

as around 10 ms^{-1} on latitudes between 40° to 50° in both hemispheres, DV meridional winds reach about 30 ms^{-1} at around 35°.

Both zonal and meridional wind comparison suggest that CT and DV techniques, apart from probing different features and phenomena at the clouds, might also be probing different altitudes on Venus' atmosphere.

5.2.3 Long term comparison

In this section we will directly compare ground-based DV results with space-based CT results, from datasets gathered along several years.

Our team has conducted several ground observations, with multiple telescopes and spectrographs, using DV to retreive zonal and meridional wind at Venus' cloud top. Some of the ground observations were coordinated with space observations, using CT, with both VenusExpress and Akatsuki missions. Both DV and CT have provided, along several years, valuable measurements of horizontal wind circulation on Venus' cloud-top, where the retrograde zonal wind velocity peaks due to atmospheric superrotation. While the techniques are substantially different they are complimentary and probe similar altitudes at cloud-top (see section 5.1. Figure 5.5 presents a long term comparison of cloud-top zonal latitudinal profile retrieved from multiple observation campaigns using both ground telescopes, DV technique (Machado et al., 2012, 2014, 2017; Gonçalves et al., 2020) and space missions using CT technique (Hueso et al., 2015; Horinouchi et al., 2018; Gonçalves et al., 2020).

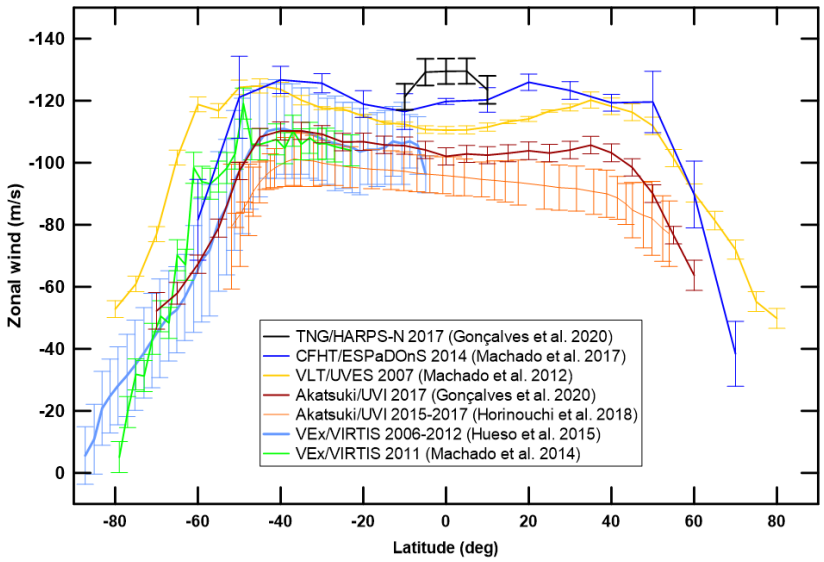

Figure 5.5: Venu's cloud top zonal wind velocities from different observation campaigns, using CT from space observations and DV from ground observations. The dataset and respective article are presented in the legend of the plot.

Figure 5.6 presents a long term comparison of latitudinal profile of meridional wind from cloud-top retrieved from multiple ground and space observations, using DV and CT respectively.

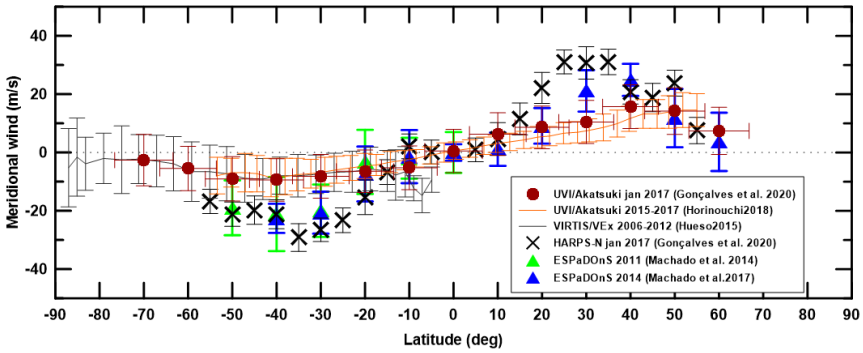

Figure 5.6: Venu's cloud top meridional wind velocities from different observation campaigns, using CT from space observations and DV from ground observations. The dataset and respective article are presented in the legend of the plot: top 3 being CT space observations and bottom 3 being DV ground observations.

In general, all profiles present a uniform wind velocity at lower latitudes with higher velocity jets at around 40° in both hemispheres, followed by a steep decrease in wind speed at higher latitudes, poleward.

Despite consistent results and similar zonal wind profile throughout multiple campaigns, the long term comparison suggests a systematic gap between DV and CT winds, with velocities higher about $10-15ms^{-1}$ for DV results. While CT winds reach as high as $110ms^{-1}$, DV winds. See the discussion section (5.3 for a detailed analysis of these comparisons.

5.2.4 UVI filters: 283 nm - 365 nm

In section 4.4.2 we presented CT results from observations made with Akatsuki/UVI 365 nm filter. With the 365-nm filter, UVI provides cloud images contrasted by the unknown UV absorber, comparable to VenusExpress/VIRTIS ultraviolet images centred at 380 nm (Sánchez-Lavega et al., 2008; Hueso et al., 2012). In Gonçalves et al. (2020) we used the 365 nm filter in order to compare the results directly with DV results (see section 5.1, as this filter probes UV features at cloud-top. While the UVI 365 nm centred filter tracks cloud features produced by an unkwon UV absorber, the 283 nm filter is designed to match and probe an SO_2 absorption band (Horinouchi et al., 2018). However, SO_2 vertical distribution, as well as the variabiality of concentration along local time and latitude, is still not fully constrain Encrenaz et al. (2013, 2020).

Our team also retrieved zonal winds, from the same Akatsuki observations used in Gonçalves et al. (2020), using the 283 nm centered filter, in order to compare both filter results with our DV results. The results we are presenting are still preliminary, as part of the in preparation work Machado et al. 2020b. Figure 5.7 presents and compares zonal wind profiles (5° bin in latitude) from both UVI filters (365 nm as in Gonçalves et al. (2020) and also the 283 nm filter), retrieved from Akatsuki observations made between 26-31 January 2017. As described in section 4.4.1, we used an semi-automatic based on phase correlation method between images developed by Peralta et al. (2018).

Fig. 5.7 shows that the 283 nm filter results present consistently higher zonal wind velocities than the results retrieved by the 365 nm filter, in the order of 10 ms^{-1}. As mentioned by Horinouchi et al. (2018), the 283-nm images likely reflect cloud features at higher altitude than the 365-nm images.

5.2.5 DV, CT and GCM

Following the evidence of a difference in altitudes probed by DV, CT, and both of UVI filters, we proceeded to compare DV and CT wind measurements with Venus' GCM predictions for zonal wind velocity at cloud-top. Figure 5.8 presents a zonal wind comparison between (i) DV results (Machado et al., 2014, 2017) from multiple observations using CFHT/ESPaDOnS, (ii) CT results from January 2017 observations using the 283 nm filter from UVI (Machado et. al 2020b, in preparation), (iii) Venus' GCM predictions for 70 and 72 km altitude, from LMD model (Gilli et al., 2017). Figure 5.9 shows a comparison between zonal wind profile retrieved using CT, both VenusExpress/VIRTIS-M (Machado et al., 2017; Hueso et al., 2015) and Akatsuki/UVI 385 nm filter (Horinouchi et al., 2018; Gonçalves et al., 2020) and the prediction for zonal wind at 68 km altitude by the LMD Venus' GCM (Gilli et al., 2017).

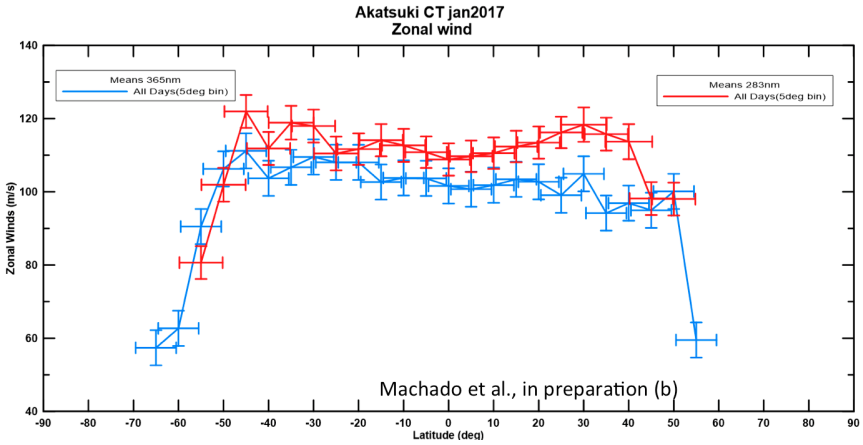

Figure 5.7: Zonal wind velocities using CT with both UVI filters from Akatsuki 2017 observations. The observations were made from 26 to 31 January 2017. Red solid line is the mean zonal wind in a latitudinal profile (with a 5° bining) from the 283 nm filter. Blue solid line is the mean zonal wind in a latitudinal profile (with a 5° bining) from the 365 nm filter (as in Gonçalves et al. (2020)). This work is in preparation as Machado et al. (2020b in preparation).

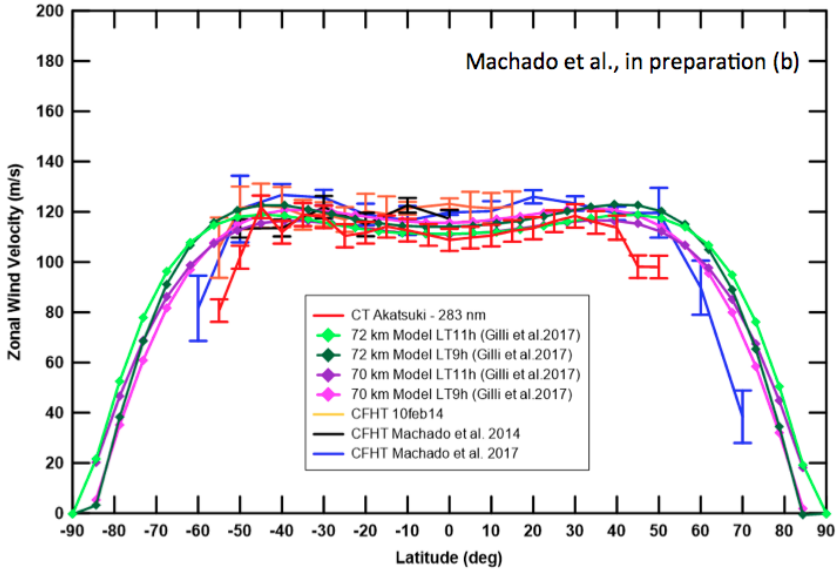

Figure 5.8: Comparison between DV (Machado et al., 2014, 2017), CT with UVI 283 nm filter (Machado et al., 2020b in preparation) and Venus' GCM for 70-72 km altitude (Gilli et al., 2017). CT zonal profile is a mean daily zonal velocity weighted average with a bining of 5°.

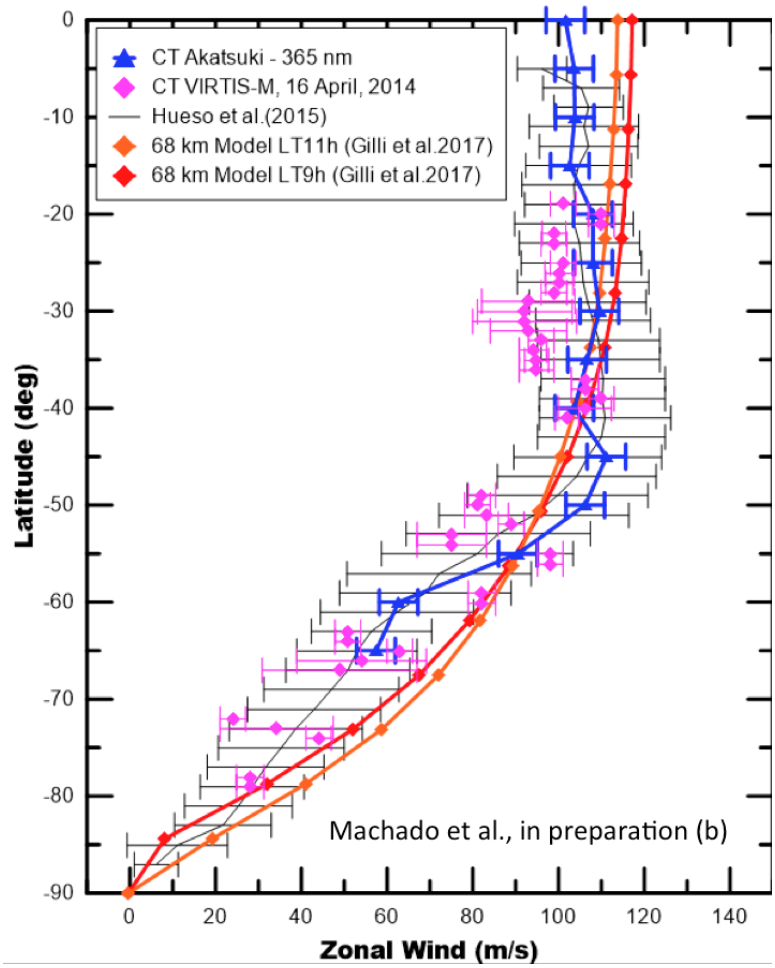

Figure 5.9: Comparison between CT results from VenusExpress/VIRTIS-M (Machado et al., 2017; Hueso et al., 2015), Akatsuki/UVI 365 nm filter (Horinouchi et al., 2018; Gonçalves et al., 2020) and Venus' LMD GCM zonal wind prediction for 68 km altitude (Gilli et al., 2017).

5.3 Discussion

The results presented show evidence of a systematic difference in zonal wind velocity, of up to 15 ms^{-1}, higher for DV ground results when compared with CT space results. This is noticeable across the results of all coordinated ground and space observations, as in Machado et al. (2017) and Gonçalves et al. (2020), also when comparing multiple observation campaigns along several years (as in fig. 5.5). To understand this difference in zonal wind veloctity from the two techniques, one must first comprehend the core differences between the techniques.

Venus' cloud top is dominated by the superrotaional state of Venus' atmosphere, where the westward zonal winds reach the peak velocity at around 120 ms^{-1}. Winds derived by the CT technique used in space missions, such as Venus Express and Akatsuki, do not necessarily trace the true circulation, since clouds are affected by traveling thermal and gravity waves, and could show an apparent displacement different from the true motion of the gas or particles, thus, CT measurements are an indication of the speed of iso-pressure regions, rather than the speed of the actual cloud particles. Winds derived using this technique do not reflect instantaneous wind velocity neither its variability at time scales shorter than the time interval between images A and B ($\approx$ 120 minutes, in the case of this work). Additional uncertainties of tracking cloud features include difficulties to interpret them as passive tracers of the wind, since they may reflect the phase speed of an atmospheric condensation wave, possibly with contributions from atmospheric waves, eddy, the combination of horizontal flow with vertical mixing, or just chemical processes associated with the temporal variation of cloud features. It should also be noted that the instantaneous velocity fluctuations measured with cloud tracking involve eddy and wave motions and the cloud top altitude where the winds are measured varies with latitude, decreasing in particular near the poles (Ignatiev, 2009; Titov et al., 2012). Also, Peralta et al. (2017) estimated the vertical profile of the zonal winds during the second Venus flyby of NASA's Messenger spacecraft, and its results suggest that, on the dayside, the altitude at which the zonal wind peaks seems to vary over time. In addition, tracked UV features may be positioned at a variety of altitude within the upper cloud top layers. Therefore, the unknown nature of the UV absorber may lead to an uncertainty in the altitude of the cloud features of several kilometres.

On the other hand, the DV technique provides instantaneous velocities using visible Fraunhofer lines scattered by Venus' cloud tops, obtained through a bolometric measure along the FOV at the altitude where optical depth reaches unity (around 70 km). Thus, our technique constitutes a complementary way of probing the Venus' atmosphere, and a unique approach from the ground, seen that this method measures directly the aerosol particles motion, and the retrieved wind velocities are instantaneous measurements.

The equivalence of confidence levels between cloud-tracked winds from VEx and Akatsuki on one side, and ground-based Doppler velocimetry on the other side is maintained in the long term. However, by analysing zonal wind measurements from both techniques in a long-term comparison (fig. 5.5), we note a systematic difference, with wind velocities generally higher for ground-based Doppler velocimetry results in the order of 10-15 ms^{-1}. A difference in wind velocities is also noted on the meridional circulation, where the Doppler results present velocities higher up to about 10 ms^{-1}, at 30° N and S, when compared with cloud-tracking results (fig. 5.6. It has been long discussed (e.g. Gierasch et al. (1997), Kawabata et al. (1980), Widemann et al. (2007), Ignatiev (2009), Machado et al. (2014), Machado et al. (2017), Peralta et al. (2017)) whether this is caused by a difference in the averaged altitude probed by the cloud-tracking technique, examined for instance with both VEx/VIRTIS (Sánchez-Lavega et al., 2008; Hueso et al., 2012, 2015) and Akatsuki/UVI (Horinouchi et al., 2018), and the Doppler velocimetry method. Horinouchi et al. (2018) also states that the 283-nm filter UVI images could reflect cloud features at higher altitude than the 365-nm images. The SO_2 vertical is still not fully constrain, while it's know it has horizontal variability along local time and latitude Horinouchi et al. (2018); Encrenaz et al. (2013, 2020). Our results suggest that the altitude probed by UVI 283 nm filter, during the Janurary 2017 observations, is consistent with the altitude probed by several DV observations. Machado et al. (2020b in preparation) will further address this subject, providing additional observation data and an comprehensive comparison with several GCMs.

The results presented here, despite not constituting a unambiguous proof by themselves, do show evidence that (1) the altitude of zonal wind probed by DV technique is highly consistent with both the UVI 283 nm filter and the prediction of the Venus' LMD GCM for 70-72 km (Gilli et al., 2017); (2) the altitude of CT results, from both VenusExpress/VIRTIS-M (Hueso et al., 2015; Machado et al., 2017) and Akatsuki/UVI 385 nm filter (Horinouchi et al., 2018; Gonçalves et al., 2020), are highly consistent with Venus' LMD GCM prediction for altitudes around 68 km (Gilli et al., 2017). Therefore, a difference in altitude of up to 2-3 km could be enough explain the difference in the measurements of zonal wind from DV and CT.

Chapter 6

Ground-based Cloud-Tracking on Venus night side

6.1 Summary

Venus is completely covered by thick clouds in a superrotational state. The rotation of the solid body (with a period of 243 terrestrial days) is much slower than that of the clouds, which circle the planet in only 4.4 days at 70 km altitude and about 6 days at 48 km. The cloud-top of Venus' atmosphere, at around 70 km, is where the retrograde zonal wind velocities peak, dominated by the superrotation circulation. The cloud deck extends in altitude from 45 to 70 km, and can be divided into three main regions, centred at 48, 54 and 60 km (Esposito et al., 1997). The lowest of these is the lower cloud, where fundamental dynamical exchanges that help maintain the superrotation are thought to occur (Lebonnois et al., 2010).

The lower venusian atmosphere is a strong source of thermal radiation, with the gaseous CO_2 component allowing radiation to escape in windows at 1.74 and 2.28 µm. At these wavelengths radiation originates below 35 km, and unit opacity $\tau$is reached at the lower cloud level, close to 48 km. Therefore, in these windows it is possible to observe the horizontal cloud structure, with thicker clouds seen silhouetted against the bright thermal background from the low atmosphere on the nightside hemisphere. By continuous monitoring of the horizontal cloud structure at 2.28 µm (NICS, k filter), it is possible to determine horizontal wind velocities using the CT technique. These measurements will provide a complementary view of the winds at the lower cloud, allowing to construct the latitudinal profile of zonal wind at that level and to search for variability relative to previous measurements. The relative importance of the transport of angular momentum by the Hadley circulation and the equator-ward transport by eddies could also be studied. A flat profile (Belton et al., 1991) should indicate that eddies are highly efficient at balancing the meridional circulation, whereas a profile with mid-latitude jets (Limaye, 1982) should indicate weaker eddy activity.

In this chapter we present preliminary results Machado et al. (2020a submitted) based on observations carried out on July 2012 with the Near Infrared Camera and Spectrograph (NICS) at the Telescopio Nazionale Galileo (TNG), in La Palma, along with coordinated space-based VEx/VIRTIS observations. The ground observations were also coordinated with VenusExpress observations using VMC (Venus Monitoring Camera).

Our objectives were to measure the horizontal wind field in order to (i) characterize the latitudinal zonal and meridional wind profile, (ii) to study variability, (iii) to help constrain the effect of large scale planetary waves in the maintenance of superrotation, and (iv) to map the cloud distribution.

6.2 Observations

Our group observed Venus with the NICS at TNG (La Palma) for periods of 2.5 hours starting just before dawn, for three consecutive nights, 11, 12 and 13 of July, acquiring sets of images of the night side of Venus with the continuum K filter at 2.28 μm. The Venus apparent diameter at observational dates was greater than 32" allowing a high spatial precision. The 0.13" pixel scale of the the NICS narrow field camera allowed to resolve 3-pixel displacements. The absolute spatial resolution on the disk was 100 km/px at disk center and the 0.8-1" seeing-limited resolution was 400 km/px.

By co-adding the best images and cross-correlating regions of clouds the effective resolution was significantly better than the seeing-limited resolution. The best 10% of images have been selected, registered to a common coordinate system and co-added to form image *A*. A subsequent series were taken at a later time, around 2 h time interval, forming image *B*, as shown in fig. 6.1. Cloud displacements in the night side of Venus, between images A and B, can be computed using both an automated technique and a visual one. This observing strategy was similar to the one used previously by Young et al. (2008) and Tavener et al. (2008) at IRTF. With a 2 hr baseline we expect to obtain about 10 m/s resolution on cloud feature velocities, which provides a basis for comparison with VEX-VIRTIS measurements.

We used a semi-authomatic method based on a phase correlation between images, developed by Peralta et al. (2007). The CT process was conducted by three researchers in order to reduce any individual bias and to increase the total number of cloud tracers used, thus, increasing the statistical strength of the results. A total of 696 tracers were identified in the images pairs and used to measure zonal wind for the tree days of observations: 171 tracers for the image pair of 11 July, 259 for 12 July and 266 for 13 July.

In order to correct for scattered light from the (saturated) day side crescent into the night side, a set of observations with the Brγfilter were performed (see fig. 6.2). Cloud features are invisible at this wavelength due to the high optical depth of the gaseous CO2 component, and this technique allows for a good correction of scattered light.

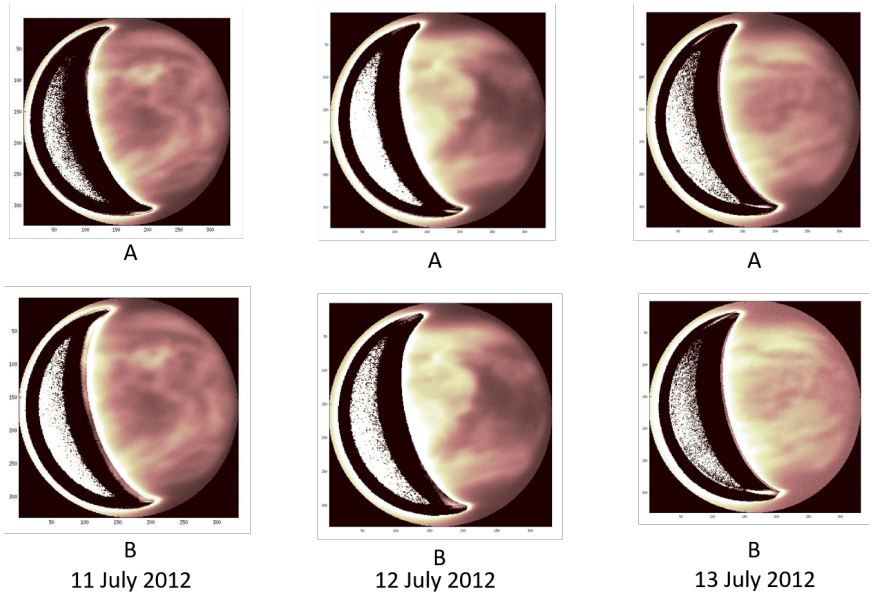

Figure 6.1: Pairs of Venus' images as observed using NICS camera. Images A and B were obtained by stacking multiples images of Venus at the beginning and end of the observation run, respectively, for each day (11-13 July). Image from Machado et al. (2020a submitted).

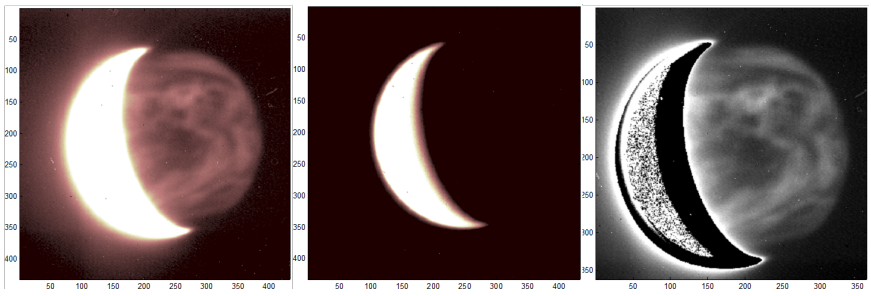

Figure 6.2: Venus' images as observed using NICS camera on July 2012 observations. From left to right: i) continuum-K image, ii) a Bracket-gamma image, iii) the result of subtracting a scaled bracket-gamma image from the on taken in continuum-K. The dark regions are clouds and the bright regions are optically thinner areas between the clouds that allow thermal emission from lower layers to escape. The out-lied crescent is the saturated day-side of Venus. Image from Machado et al. (2020a submitted).

6.3 Preliminary Results

The results presented in this section are still in a preliminary phase, while the article is still in preparation and should be submitted later this year (Machado et al. 2020b). We will present zonal wind velocities retrieved using CT based on ground TNG/NICS observations.

The results presented in fig. 6.3 are daily latitudinal profiles of zonal wind. The values presented are weighted averages with a binning of 5° latitude, while the weighing coefficients are the inverse of the variance associated to each measurement. While there is small variability of about 5 ms^{-1} on the 3^{rd} day, the winds are within the error margin and the tracers used in that day were about a third less than the amount of tracers used in each of the other 2 days of observations.

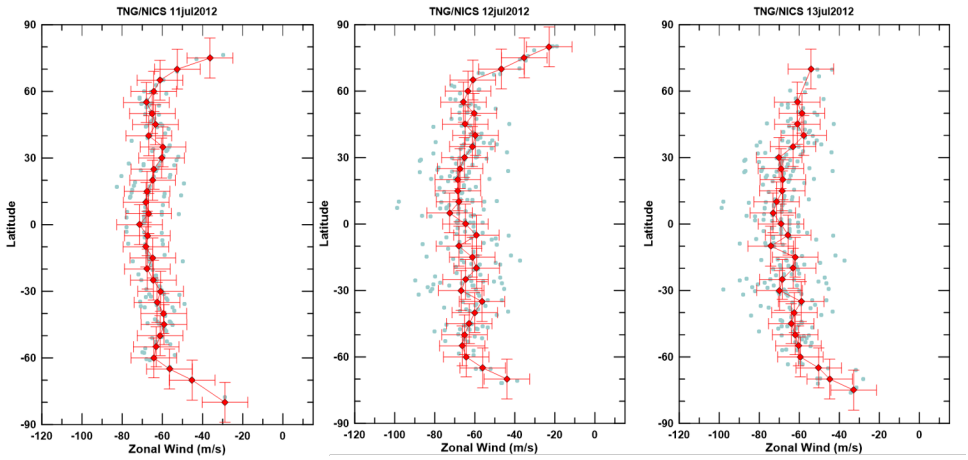

Figure 6.3: Latitudinal profile of zonal wind for each day of observation from TNG/NICS 2012 observations, with a binning of 5°. Gray-blue dots represent each cloud feature tracked; red solid line is the weighted overage of each day. Figure from Machado et al. (2020a submitted).

In fig. 6.4 we compare the median zonal wind profile retrieved with CT from our observations at TNG/NICS with the zonal wind results retrieved by VEx/VIRTIS, as in Sánchez-Lavega et al. (2008) and Hueso et al. (2012). While our ground observations were centered at 2.28 µm using NICS, space observations with VIRTIS-M images were focused on 1.74 µm. However, both observation should probe the lower cloud deck about the same altitude, 44-48 km (Sánchez-Lavega et al., 2008; Bastow et al. , 2012). While VenusExpress results are only from the southern hemisphere, due to the geometry of its eccentric polar orbit, both results present similar and consistent profile with higher wind velocity, in the order of 5-7 ms^{-1}, at around 60° with a steep decrease polar-ward.

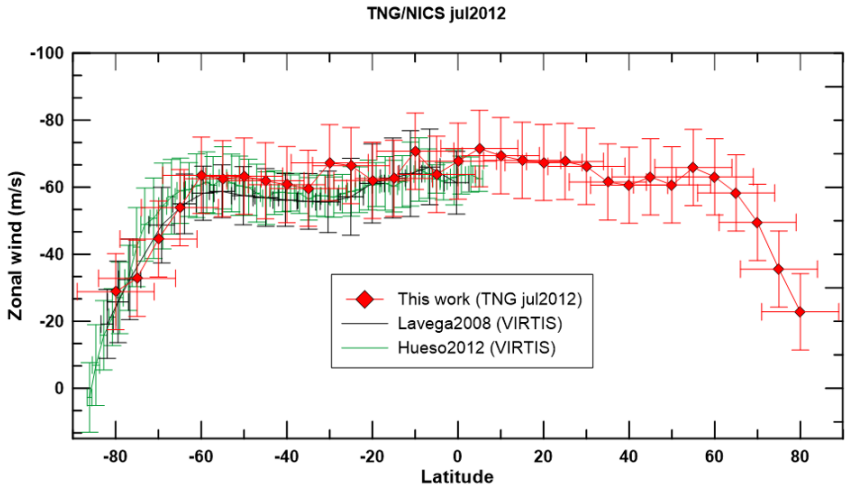

Figure 6.4: Latitudinal profile of zonal wind comparison between this work (TNG/NICS) and VenusExpress/VIRTIS-M results (2012 observations), with binning of 5°. In solid red, this work; in solid black, results from Sánchez-Lavega et al. (2008); in solid green, results from Hueso et al. (2012). Gray-blue dots represent each cloud feature tracked; red solid line is the weighted overage of each day. Figure from Machado et al. (2020a submitted).

6.4 Conclusions

Our team retrieved zonal wind velocities from Venus' lower cloud deck (∼48 km) night-side, using CT on ground-based observations at the TNG/NICS. The 2.28 μm window allows to probe the lower cloud deck, where the bright thermal background from lower layers contrasts with thicker clouds at around 48 km altitude, which can be visible at the night hemisphere of Venus with IR cameras, such as NICS (k filter) at TNG.

We used a semi-automatic CT technique based on a phase correlation between two images Peralta et al. (2012). Our zonal wind results present the same order of magnitude of zonal wind from previous measurements at the same altitude (Sánchez-Lavega et al., 2008; Hueso et al., 2012). The mean latitudinal profile of zonal wind is symmetrical (N-S) and presents an almost constant velocity of 60-65 ms^{-1}, with higher jets at around 60° in the order of 5 ms^{-1}, followed by a steep decrease poleward. The profile it's consistent with measurements from VenusExpress, using VIRTIS-M (1.74 μm filter).

Regarding meridional wind circulation, the magnitude of the wind velocity was similar to the uncertainty of the measurements. Therefore, we could not retrieve a clear unambiguous profile of meridional circulation.

Our results have proven the usefulness and viability of the CT method using ground-based observations, yielding results and precision comparable with the results provided by space observations. This opens new opportunities for coordinated ground and space observations of Venus' lower deck on the night side.

Chapter 7

Solar System and Exoplanets

7.1 Solar System planets

The study of Venus' atmosphere allowed us to further develop and fine tune both DV and CT - two powerful techniques in the retrieval of horizontal winds at both cloud top day-side and lower clouds night-side, using ground and space observations. Tthe study of Venus atmosphere is essential in our understanding of 1) the mechanisms that drive the superrotational state, 2) the variability of horizontal winds on multiple time scales, 3) the differences between Earth and Venus' atmospheres evolution in comparative climatology, 4) Venus as an Earth-like planet and the subsequent understanding and (re) definition of Habitable zone and future characterization of exoplanets atmospheres. However, our team is committed to apply the skills and tools we have acquired and develop on the study of Venus to the study of other SS atmospheres, as well as contributing to the much needed synergy between SS and Exoplanets, by improving modelling and characterization of exoplanets' atmospheres.

The basis of CT, as so the software used, can be easily applied to retrieve horizontal winds from Jupiter (García-Melendo et al., 2011) and Saturn (Hueso et al., 2020) atmospheres using images from orbiting space missions (HST, Juno and Cassini-Huygens). However, while CT strongly depends on high resolution images provided by space missions closely orbiting the planet, DV relies on high-resolution spectroscopy provided by some of the ground based instruments mounted on the biggest telescopes in the world. Furthermore, the next generation of ground telescopes and instruments, such as the 39 meters diameter ELT (Extremely Large Telescope), will further increase the potential of DV in the study of SS atmospheres. Thus, after successfully using Venus as a field laboratory to develop DV, our team has been adapting and applying DV in the study of other SS atmospheres, such as Mars, Jupiter and Saturn.

With the goal of adapting DV to the study other planets atmospheric dynamics, we have conducted observation on:

- Mars: VLT/UVES observations on June 2018
- Jupiter: VLT/ESPRESSO observations on July 2019
- Saturn: CAHA/CARMENES observations on June 2017

My personal contribution to each project was as follow:

- Mars observations: preparation of the observations (co-authorship of the ESO's observational proposal) and data reduction. Further tasks may include velocity retrieval, data analysis and co-authorship of the manuscript.

- Jupiter observations: preparation of observations (co-authorship of the ESO's observational proposal), *in situ* observations (at the VLT), data reduction, spectra analysis (to obtain a median spectra, as described in section 7.2.3). Further tasks will include velocity retrieval, data analysis and co-authorship of two manuscripts (one for horizontal velocities with DV, the other for observing Jupiter as an exoplanet).

- Saturn observations: data reduction with focus on retrieving the planetocentric latitude and longitude of each fibre position as observed. Further tasks may include velocity retrieval, data analysis and co-authorship of the manuscript.

7.1.1 Mars

Objectives

We have conducted Mars observations using the UVES spectrograph at the VLT, Chile. The goal was to retrieve horizontal winds using Doppler vlocimetry during the 2018 global dust storm on Mars. These events are known to sporadically occur on Mars, which have a strong impact in its atmospheric thermal and dynamical structures. These are referred to multi-regional dust storm events that spread mineral dust in the atmosphere at all longitudes, thus, covering the planet at global scale for several months (Montabone and Forget 2017, Montabone et al. 2015). Although dust storms are Mars most notable meteorological phenomenon, many aspects of their structure and dynamics remain mysterious (Heaven et al. 2017). Since the Martian atmosphere is tenuous and cloud coverage is sparse, CT, that proofed to be effective in other Solar System targets, is not the best option for Mars. However, during this massive storm event, high resolution visible spectroscopic observations of backscattered radiation in the dust layer presents an unique opportunity to study the dynamics of the global dust storm.

The observations were conducted on 20 June 2018 for a total of 2 hours, using the high-resolution UVES, mounted at the VLT, in Chile. The spectrograph's slit was positioned perpendicular to Mars rotation axis,

Observing Mars with VLT/UVES during one of the most intense dust storm ever observed on the Red Planet, represented a unique moment to study its atmospheres dynamics. These successful observations will allow the retrieval of horizontal winds by using an adaptation of the DV method detailed by Machado et al. (2012), where the same instrument was used to observe Venus.

The results of this work are being developed by Machado et al 2021 (in preparation).

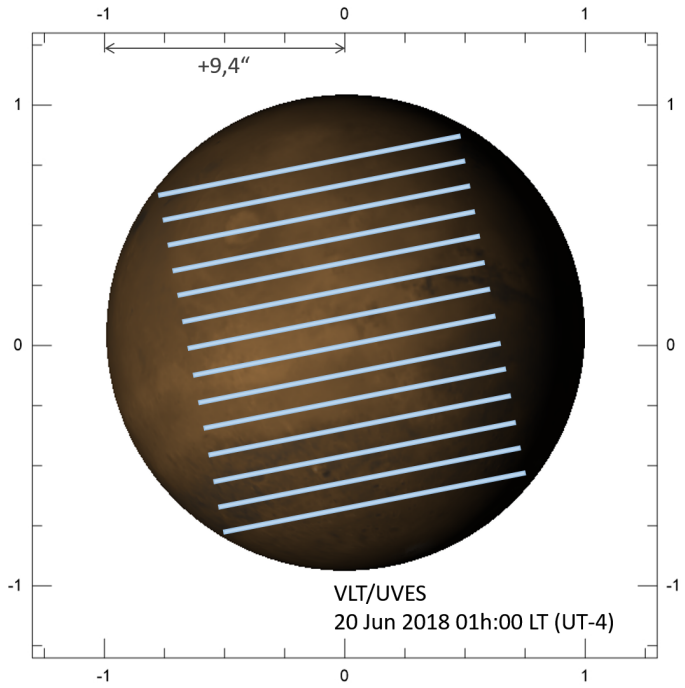

Figure 7.1: Diagram of Mars 2018 observations with UVES at VLT. UVES slit's relative offsets, perpendicular to Mars rotation axis. The slit was placed parallel to the equator at 13 different offsets: 0°, 10° N-S, 20° N-S, 30° N-S, 40° N-S, 50° N-S and 60° N-S .

7.1.2 Jupiter observations with VLT/ESPRESSO

Objectives

In order to study Jupiter's zonal circulation, we have conducted Jupiter observations using ESPRESSO at the VLT, on July 2019. The spectra gathered will be used to retrieve horizontal winds (using DV) as well as to study Jupiter seismology. It was the first time that ESPRESSO, a high-resolution spectrograph designed to study exoplanets, was used to observe a Solar system target.

We explored the high spectral resolution and frequency capabilities of VLT-ESPRESSO observations in order to perform seismology of Jupiter while also applying the Doppler velocimetry method to retrieve zonal wind velocities. In this study we propose to use our Doppler velocimetry technique on the full range of reflected sun ray emissions by using ESPRESSO instrument. The wind velocities retrieved will possess an unprecedented precision (lower than 1 ms^{-1} which will permit, for the first time, to measure and investigate the meridional wind flow on Jupiter, expected to be on the order of 2-3 ms^{-1}, never measured before.

In a first set of observations, the frequency content of Doppler wind estimates will be analysed to: 1) determine the spectral content of observation and noise, 2) search for acoustic and gravity modes of Jupiter and 3) constrain the gravity wave power at cloud top. Local seismology methods (similar to the ones applied to the Sun) will be implemented, allowing to constrain Jupiter structure below the cloud layer. An important by-product will be the determination of zonal winds in Jupiter atmosphere. We will obtain a time series of Doppler wind estimates through sequential fibre exposures. These time series will be long enough to investigate the frequency variations induced by acoustic and gravity waves at cloud top. In addition to vibration modes, this frequency range is covering the transition from gravity waves to acoustic waves. Information on the atmosphere dynamics will also be extracted from these observations (horizontal winds, part of turbulence spectrum).

Additionally, the spectra obtained in this observation was used in a project that aims to retrieve mean spectra of Solar System planets as a template to compare with expolanets. Please see section 7.2.3 for detailed informations.

Observations

We observed Jupiter for a total of 4 hours, at the VLT/ ESPRESSO (380-788 nm) on 22 July 2019. The target had an apparent magnitude of -2.61, angular diameter of 45.92", an illuminated fraction of 99.986 %, which corresponds to a surface brightness SB = 5.44 mag/$arcsec^2$. We performed a series of 60 sec exposures at several positions on Jupiter disk (fig. 7.2), using a UHR mode (Ultra High Resolution, $\sim$ 190 000), which corresponds to a 0.5" instrument FOV.

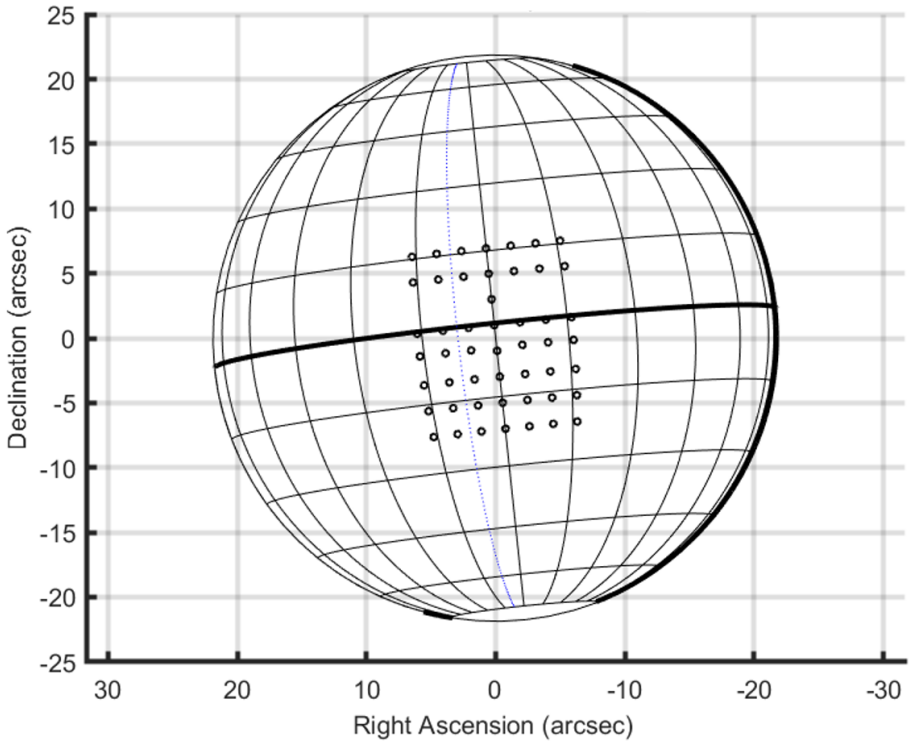

Figure 7.2: Diagram of Jupiter observations at the VLT/ESPRESSO, on 22 July 2019. The solid circles represent the positions of the fibre FOV at Jupiter's disk during observations, on scale (0.5" diameter FOV). The image has a planet's grid of 10°both latitude and longitude. The solid bold line at the right hand side represents the terminator, while the blue dotted line is the location of the 12 h local meridian.

It was the first time ESPRESSO was used to observe Jupiter, or any SS planet. We used a similar technique used to observe Venus in previous observations, based on a transparent template of the planet's disk with all the positions of the instrument FOV we planned to observe (fig. 7.3). Several technical details of the instrument were discovered by both us and the staff astronomers, due to the specifications of our observations when compared to the usual ESPRESSO observations (mainly exoplanet observations).

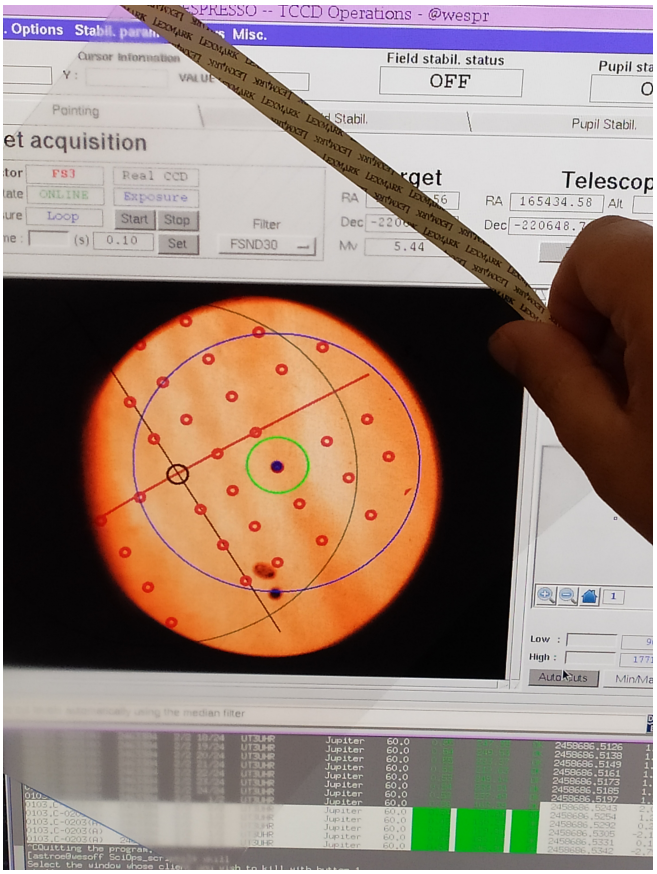

Figure 7.3: Picture of the observation of Jupiter using ESPRESSO (22 July 2019). We used a transparent template of Jupiter disk represented with all the planned fibre relative positions (red circles), to help the on-site real-time navigation of the actual ESPRESSO fibre position (blue solid circles, fibre A on the centre of the image). Note: the Jupiter's disk visible on the screen is just a portion of the actual planet's full disk, as the telescope/instrument FOV were about half the size of the planet's apparent full disk size.

7.1.3 Saturn

Objectives

Our team carried out Saturn observations on the night of 13 June 2017, with the CARMENES (Calar Alto high-Resolution search for M dwarfs with Exoearths with Near-infrared and optical Échelle Spectrographs) instrument, which is installed at the 3.5 m telescope at the Calar Alto Observatory, in southern Spain. It consists of two separated spectrographs covering the wavelength ranges from 0.52 to 0.96 μm and from 0.96 to 1.71 μm with spectral resolutions R = 80 000 - 100 000, each of which performs high-accuracy radial-velocity measurements ($\sim 1 ms^{-1}$).

This project, led by Miguel Silva, aims to retrieve Doppler wind velocities of Saturn's zonal flow at cloud level, in the visible, and also present the preliminary results of the adaptation of DV (Machado et al., 2017; Gonçalves et al., 2020) to the near-infrared wavelengths, based on CARMENES observations. This successful adaptation would be a major milestone in our research, as it would allow DV not only to retrieve wind velocities on Jupiter and Saturn but also to probe new altitudes on Venus' atmosphere (middle cloud deck).

Observations

The observations consisted in 59 exposures of 120 seconds, arranged in 18 distinct positions, with a total of 3 hours of observation time. Figure 7.4 presents all the positions of the fibre FOV, with the respective planetocentric positions described in table 7.1, while 7.5 is an actual image of Saturn' disk taken by CARMENES. We have applied the same technique as in Connes (1985) (Absolute Astronomical Accelerometry or AAA) to the backscattered solar spectrum, to determine the Doppler shift associated with the zonal circulation.

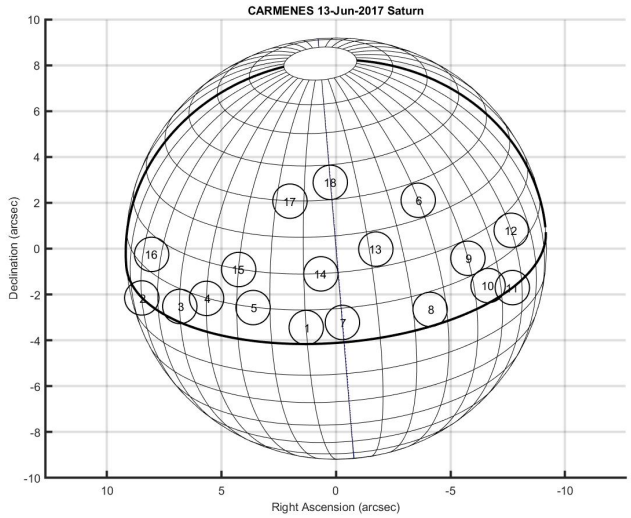

Figure 7.4: Diagram of Saturn's disk as seen during the CARMENES observations on 13 June 2017. The black circles represent the fibre displacement FOV. The planetocentric coordinates of each FOV position is displayed on table 7.1.

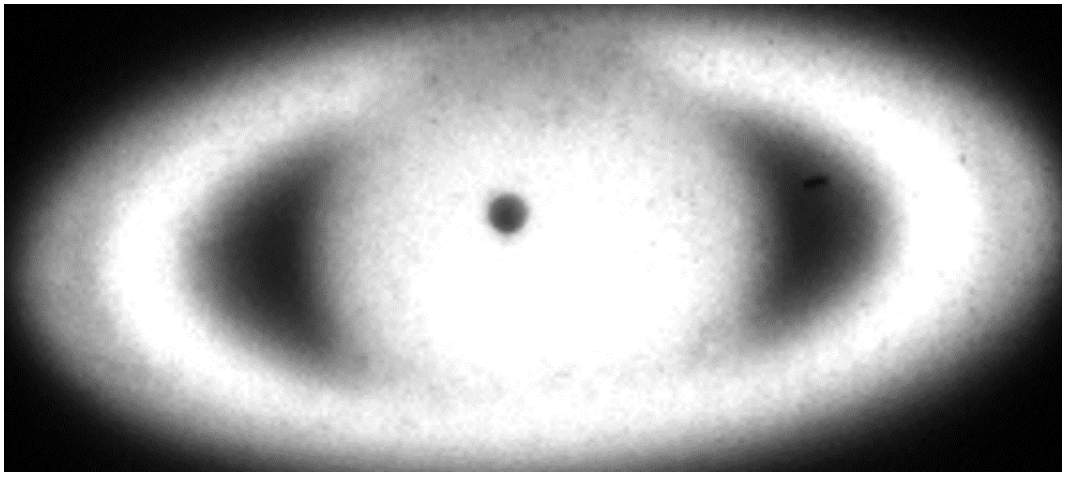

Figure 7.5: Image of Saturn retrieved by CARMENES at 13 June 2017. The solid black circle is the actual position of the spectrograph fibre.

Position #	Latitude	Longitude
1	5	10
2	0	70
4	5	50
5	10	40
6	10	25
7	35	-30
8	6	0
9	5	-25
10	15	-40
11	5	-45
12	0	-55
13	15	-60
14	25	-12
15	20	5
16	20	30
17	15	65
18	40	15
19	45	0

Table 7.1: Planetocentric latitude (2) and longitude (3), in degrees, of each of the FOV positions of the fibre (1) observed in Saturn's disk in 2017 observations (as in figure 7.4).

7.2 Exoplanets

Although several studies had already provided first measurements of exoplanet's wind velocities (Hot-Jupiter), this is still a relatively recent, and certainly challenging, field of research. The advent of new cutting-edge instruments, to be installed in space missions and ground telescopes (30 m diameter), will be a major contribution for the field, massively expanding our capability to characterize exoplanet's atmospheres. Our team's research has been mainly focused on the dynamics of Solar system planets, particularly the detection of wind velocities on Venus, Mars, Jupiter and Saturn. So, the question that arises is, how can we, solar system scientists, contribute to a more comprehensive characterization of exoplanetary atmospheres? Although they are two distinctive fields of researches there are more similarities than differences - both study atmospheres of planets in stellar systems. We can contribute by studying Solar system atmospheres as a field laboratory and a comparable template for a more comprehensive understanding of different types of exoplanetary atmospheres. Our unique skills and knowledge on our own planetary system and how to approach and study are complementary to the exoplanetary science techniques.

The characterization of an exoplanet's atmosphere (composition and dynamics) has been achieved, albeit substantial limitations, by the use of transmission spectroscopy (retrieval of a planet's spectra during its transit). The Solar System provides a variety of complex atmospheres which can, and should, be used as standard templates creating a bridge with the study and modelling of extrasolar atmospheres.

7.2.1 ARIEL collaboration

ARIEL, the Atmospheric Remote-sensing Infrared Exoplanet Large-survey, was selected as the fourth medium-class mission in ESA's Cosmic Vision programme. It will study what exoplanets are made of, how they formed and how they evolve, by surveying a diverse sample of about 1000 extrasolar planets simultaneously in visible and infrared wavelengths (ranging from gas giants to rocky planets and preferentially in the hot to temperate zones of F to M-type stars and compile a catalogue of planetary compositions and properties). It is the first mission dedicated to measuring the chemical composition and thermal structures of hundreds of transiting exoplanets, enabling planetary science far beyond the boundaries of the Solar System. Although the lunch is planned for 2028, our team is already working and involved, as it will continue to do so for the next years, with the scientific consortium.

Our team was invited to be part of the scientific team by leading the working group (WG) "Synergies with Solar System". Our expertise on SS atmospheres

are regarded as highly valuable in the context of building a bridge between SS and exoplanets. The main goal of this WG is to foster the collaboration and share expertise between the scientific community working in the SS planet atmosphere and the new growing community working for the Ariel Science team. We proposed to coordinate the following tasks: (i) use of SS atmospheres as a natural laboratory for the understanding of Extra-solar planet atmospheres; (ii) apply 3D models developed for SS planets to specific cases of known exoplanets; (iii) support and optimise the forthcoming observations and the characterization of terrestrial planets using GCM (General Circulation Models); (iv) take advantage of SS atmospheres' observations, both spectroscopic and photometric, as a proxy in order to develop and test tools and provide science cases; (v) search for chemical compounds in disequilibrium in SS atmospheres in order to fine-tune investigation protocols that could be exported for ARIEL's science framework. The project presented in the previous subsection (Jupiter as an exoplanet) integrates the proposal tasks for the ARIEL WG.

7.2.2 Using Solar System as an exoplanet's laboratory

Our team is currently developing a tool, which will be available to the community, with the goal of a contributing for the exoplanets atmospheres' investigation with ARIEL. On this framework we use Solar System atmospheres as a natural laboratory for the understanding of Extra-solar planet atmospheres. We took advantage of Solar System atmospheres' observations, both spectroscopic and photometric, as a proxy in order to develop and test tools and provide science cases. Although its name is not defined yet, I will address it as the PlanetWarp, to ease the reading. This tool provides spectra templates of Solar System planets reflected light and IR emission spectra. The main goal is to yield an average spectra (point source) using comprehensive coverage data of different Solar System targets, both, at the optical and infrared wavelength range. The chosen targets that could be beneficial in the context of ARIEL research are Venus, Jupiter and Saturn, although our datasets also covers Mars' and Titan's atmospheres.

At a first stage, we remove the spurious Doppler shifts due to planetary rotation. When using Solar System planets' ground-based observations of solar reflected light, the spectra obtained at half phase angle is not affected by the planetary rotation since the retrieved spectra is a consequence of the solar radiation scattering on the atmosphere aerosols, and in the single scattering approximation we may consider that there is an absorption at the solar radiation incidence angle, followed by an emission towards the observer (echo Doppler). Due to the Doppler shift compensation at the half phase angle (HPA) meridian the spectra obtained along this meridian are not affected by a Doppler shift due to planetary rotation. All the spectra obtained at positions on the planetary disk, not on the

HPA, are corrected from the spurious Doppler shift contribution imposed by planetary rotation motion. After this, all the obtained spectra show their set of lines at coincident wavelengths. Then, we produce an averaged spectra based on the totality of observations that covered each target in our datasets.

The next step consists in correcting the telluric absorption lines, which are lines formed due to the interactions between the light of astronomical objects and the components of Earth's atmosphere. For this purpose we use MOLECFIT (Smette et al., 2015), a tool based on synthetic modelling of the Earth's atmospheric transmission. Molecfit can be used with data obtained with various ground-based telescopes and instruments over a broad range of wavelengths and spectral resolutions. The Molecfit package allows the user to simulate and fit tropospheric and stratospheric emission or absorption telluric lines affecting several user-selected regions of an observed spectrum. Additionally, the Molecfit then can take the best information of temperature, pressure, and humidity into account in the atmosphere above the observatory at the time of observing the science target and derive a transmission spectrum (for the selected regions) and corrects for it.

The spectra at this point is still Doppler shifted regarding the relative motion between target position and Earth position at the time of the observation. We remove the Doppler shift due to this relative motion and, finally, we obtain the spectra at the Solar System's barycentric referential. At this point we produce high-resolution template spectra, both in visible and infrared, for the considered target Solar System planets.

On a second stage (ongoing work) we take advantage of our manipulation and synthetic spectra tools in order to add noise as desired by the user. So, we can reproduce on the template spectra the signal-to-noise ratio (SNR) we want, allowing to produce spectra as if the target was a certain number of light years away from the observer. Besides adapting typical intensity and signal to noise ratio, we also consider the spectra "reddening" due to interaction with the averaged interstellar medium along the galaxy arm, however this effect is negligible for the distance range considered in ARIEL target list (< 300 light years).

The PlanetWarp also allows the user to change the spectral resolution of the template spectra and selected the desired wavelength range. Since the basic spectra were obtained at extremely high spectral resolution, our tool could interpolate it in order to mimic the user's chosen spectral resolution. Naturally, one of the most important options is to convolve the template spectra with ARIEL detector's characteristics, both spectral resolution and relevant wavelength ranges.

The main goal of the PlanetWarp is to yield a proxy of how we would see Venus, Jupiter, and Saturn, if those known planets were exoplanets seen by ARIEL, at a chosen distance from Earth.

In a future work, we also will provide a proxy for Earth itself as seen by ARIEL at a certain chosen distance. The initial spectra is, in this case, of Earth

observed by Venus Express (ESA) space probe with its VIRTIS' instrument, from Venus orbit (at a much lower spectral resolution then the other template's cases). Naturally that also in this case the basic spectra is convolved with ARIEL's instruments characteristics. Finally, we will take advantage of transmission spectroscopic and photometric data obtained during the last transit of Venus in order to also provide a proxy template for this planet.

7.2.3 Jupiter as an exoplanet

The Jupiter observations carried out with the ESPRESSO at the VLT, on July 2012 (7.1.2), apart from the original main goal to study the planet's seismology, provided spectra that will be used for two purposes: a) adapt DV ad retrieve horizontal winds on the cloud top atmosphere; b) producing a template of the mean Jupiter's atmosphere spectra. The high-resolution median spectrum can then be downgraded to lower resolutions as if Jupiter had been observed at lower resolution spectrographs and at higher distances, simulating an observation of a Jupiter (like planet) at exoplanetary-like distances. This would be useful as template to compare with observations of Jupiter-like planets and also in exoplanet modelling.

While PlanetWarp is still in a preliminary state, we present Jupiter spectra retrieved by our observation at the VLT in fig. 7.6.

The idea of observing solar system planets as if they were exoplanets, creating useful templates of median spectra, can also be applied to Venus and Saturn. Venus is the closest and the most studied Earth-like planet known. Saturn is a giant gas planet with distinctive features (such as the hexagon polar structure or the white variable storm-like clouds) and a prominent ring system. The proposed goal could also be achieved by using spectra we obtained in previous Venus' (with VLT/UVES 2012, CFHT/ESPaDOnS 2014 and 2015, TNG/HARPS-N 2017) and Saturn's (with CARMENES 2017) observations.

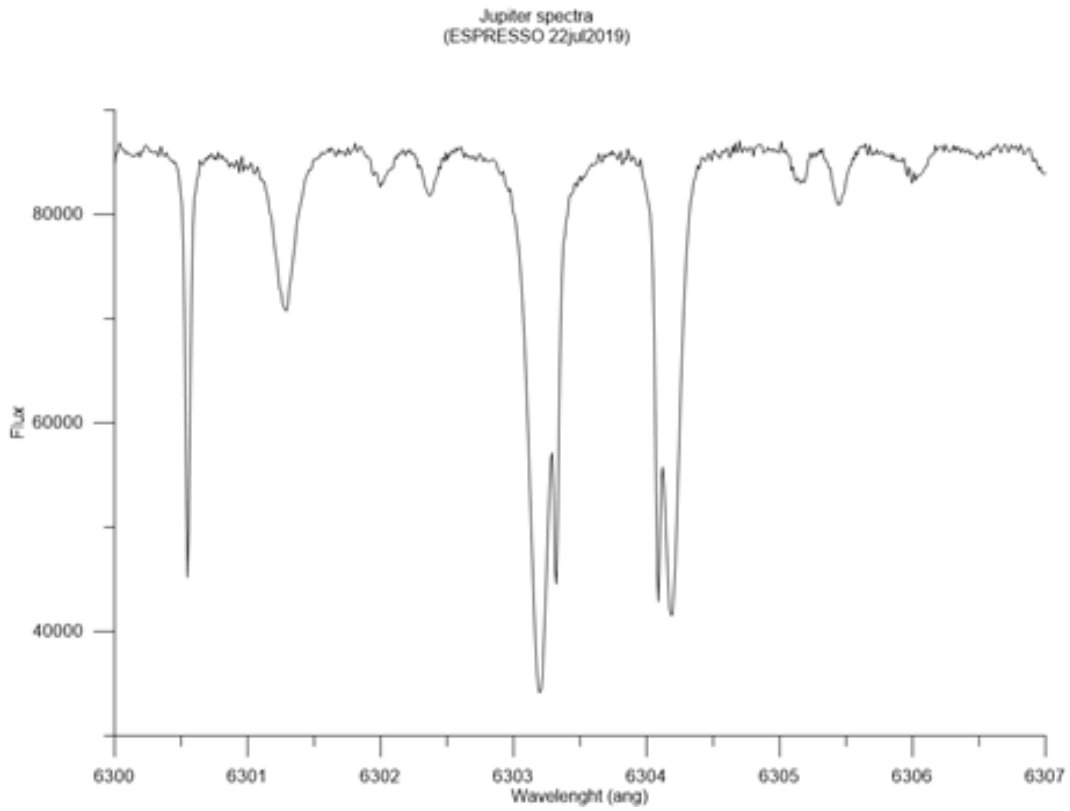

Figure 7.6: Detail of Jupiter very high-resolution spectra (R 225 000) obtained with ESPRESSO using the ultra high resolution calibration at the VLT, on July 2019.

Chapter 8

Conclusions

8.1 Venus: atmospheric dynamics

The study of Venus' atmospheric dynamics was the main focus of this thesis. Venus' is a key player in the study of planetary atmospheres.

Both Venus and Earth and their respective atmospheres were developed in the same proto-planetary disk, formed at the same time, with the same ingredients, at almost the same location in the solar system. Yet, their atmospheres present very distinct masses and compositions, leading to very distinct surfaces conditions. The study of Venus' atmospheric dynamics, composition and evolution is of utmost importance in our understanding of possible scenarios of Earth' atmosphere.

In the Solar System there are a total of 4 terrestrial bodys with an equilibrium atmosphere- Earth, Venus, Mars and Titan. Both Venus and Titan are have atmospheres in a superrotation state, where the atmosphere rotates much faster than the solid body (up to 60 times faster on Venus). This means 50 % of the terrestrial atmospheres in SS are in this, still not fully studied, superrotational state. What factors, mechanisms and interactions originate and drive the superrotation, are questions we need to address before we can start to fully characterize exoplanetary atmospheres. Therefore, the precision of models and characterization of exoplanets, current and future, will be supported by our capability to distinguish an Earth-like from a Venus-like exoplanet, and the subsequent implications on determining the habitable zone of a Star/planet.

The constrain of Venus' wind circulation and evolution is one of the key factors that will contribute to our understanding of a superrotation atmosphere. Doppler Velocimetry (ground-based) and Cloud-Tracking (space-based) are two powerful techniques in the retrieval of Venus' horizontal winds (zonal and meridional) at dayside cloud-top ($\sim$ 70 km), where the retrograde zonal wind velocity peaks due to the atmospheric superrotation.

Constraining the meridional wind component at cloud top has long-time been an open issue for diagnosing the maintenance of the super-rotation of the Venus atmosphere by determining the global mean and eddy circulations, as well as the accompanying meridional transports of angular momentum and energy (Limaye and Rengel, 2013). The role of thermal tides that transport angular momentum vertically in the low latitudes was confirmed by re- cent works (Lebonnois et al., 2010; Takagi and Matsuda, 2007). We also note that the latitudinal distribution of zonal wind at cloud tops may result from an equilibrium between the impact of ther- mal tides, and the angular momentum transport by the meridional circulation (Lebonnois et al., 2010), providing grounds for future systematic, simultaneous observations of both dynamical regimes

We have retrieved horizontal winds at different altitudes of Venus' atmosphere using two different techniques.

8.1.1 Cloud-top Doppler results

We have retrieved zonal and meridional winds from Venus' cloud-top using the Doppler velocimetry technique. The technique was initially developed by Widemann et al. (2008) and fine tuned by Machado et al. (2012, 2014, 2017). It was successfully adapted to be used on three distinct high-resolution spectrographs: UVES (long-slit) at VLT (Machado et al., 2012); ESPaDOnS (fibre-fed) at CFHT (Machado et al., 2014, 2017; Gonçalves et al., 2020b submitted); and HARPS-N (fibre-fed) at TNG (Gonçalves et al., 2020).

Zonal wind

The zonal wind results presented in this work are highly consistent within all observation campaigns, using multiple instruments and datasets over a 6 years period 3.23. With the exception of HARPS results (Gonçalves et al., 2020), all results present a similar latitudinal zonal profile: (i) an uniform velocity between 115-120 ms^{-1} at lower latitudes ($< 10°$); (ii) high speed jets, with velocities up to 130 ms^{-1}, around $40-50°$ on both hemispheres; (iii) a steep decrease at latitudes higher than $50-55°$. No significant asymmetry between the two hemispheres can be inferred in the daytime mean zonal wind field

When comparing all the Doppler results, with the exception of the 2017 data from Gonçalves et al. (2020) there's an absence of unambiguous temporal variability (figures 3.23 and 3.24). This suggest a long-term stability of the Venus dynamics for the period of time under study, 2011-2015.

Regarding spatial variability, all our results show evidence of an higher velocity of up to 15 ms^{-1} near the terminator, across all latitudes (figures 3.7,3.15,3.21. The increase of zonal wind velocities close to the terminator(s) could be explained by wind structures associated with the existence of a thermal tide, as discussed by several authors, such as Sánchez-Lavega et al. (2008); Hueso et al. (2015); Horinouchi et al. (2018); Takagi et al. (2018). Thermal tides are global-scale atmospheric waves excited by the solar heating, which move with the Sun.

The HARPS-N zonal wind results acquired in the equatorial region between 10°N and 10°S (fig. 3.17) show slightly higher velocities, when compared to the results of Machado et al. (2012, 2014, 2017) and (Gonçalves et al., 2020b submitted). The profile suggests the presence of a high speed jet near the equator, however, considering that these results are based on a limited temporal and spatial observation (one day of observations and reduced amount of points on Venus disk), additional observations are required to confirm the intrinsic nature of this jet-like feature.

HARPS-N is a high resolution spectrograph observing the northern skies and it was especially designed for searching extrasolar planets. The work presented

in Gonçalves et al. (2020) was the first use of HARPS-N to observe a solar system planetary atmosphere. HARPS-N spectrograph provided unprecedented high quality spectra of Venus atmosphere, allowing the retrieval of wind velocities with and unmatched precision of the order of 3-4 ms^{-1}. This opens a new window of opportunity for future solar system observations using HARPS-N.

Meridional wind

The DV has proven to be a powerfull and precise technique in the retrieval of meridional wind circulation at cloud-top Venus' atmosphere. Despite the low magnitude of the wind (peak velocities around 25-30 ms^{-1}, compared to the 120 ms^{-1} of zonal wind), DV successfully retrieved consistent meridional wind profiles with precision similar to those achieved by space-based CT.

Machado et al. (2017), using ESPaDOnS at CFHT, obtained, for the first time, a complete latitudinal profile of the meridional wind along both hemispheres (fig.3.9, which shows the evidence of a Hadley-type cell of meridional wind flow on Venus, corroborated by simultaneous southern hemisphere VIRTIS-M cloud-tracked measurements.

Gonçalves et al. (2020), using HARPS-N at TNG, retrieved the most complete and precise meridional wind latitudinal profile ever retrieved (fig. 3.16), with precision unmatched even by space-based measurements. This emphasizes the uniqueness and importance of ground-based Doppler velocimetry technique in the constrain of Venus cloud-top meridional wind circulation, which is of utmost importance to understand and constrain the mechanisms of Venus' super-rotational atmosphere. The Hadley cell circulation, extending from the equator to the poles, is a key mechanism on the generation and/or maintenance of the super-rotation state, as shown by recent GCM studies (Yamamoto and Takahasi, 2006; Lebonnois et al., 2010, 2016).

We have retrieved meridional wind velocities from several observation campaigns, using different telescopes and instruments. The results presented are highly consistent throughout each dataset (fig.3.24).

Our meridional wind model is assumed to vary sinusoidally with latitude, having zero velocity at equator and the poles, and a maximum value at 45° latitude. It can be noted that our measurements are consistent with the model between mid-latitudes region (between 50° S and N), however they differ significantly from this model poleward of 50°, meaning lower winds than predicted at high latitudes near the cold collar.

The mean latitudinal meridional profile presents (i) sinusoidal and symmetrical shape with null velocities (~ 0 ms^{-1}) at latitudes lower than 10°; (ii) peak velocities of up to 30 ms^{-1} at around 30-35° on both hemispheres; (iii) gradual decrease in wind speed from 40° poleward, approaching 0 ms^{-1} at 60°N. The

meridional wind profiles obtained throughout multiple observations campaigns show variations along time in the order of 5 ms^{-1}. However, the associated uncertainties do not allow an unambiguous conclusion on meridional wind variability.

8.1.2 Cloud-top CT results

We have conducted two coordinated ground and space observations, using DV and CT respectively, to retrieve zonal and meridional winds from Venus' cloud-top. From space, clouds features were tracked on images obtained by the VenusExpress using VIRTIS-M imaging at 0.38 μm acquired during orbits from 2918 and 2923, on the 16 and 21 April 2014, respectively (Machado et al., 2017). The second coordinated ground and space observation consisted on applying CT technique to images taken by Akatsuki instrument (UVI) operating in the ultraviolet range (365 nm filter), acquired in orbit #39, between 26 and 31 of January 2017.

Zonal wind

Mean latitudinal distribution of the zonal wind profile by VEx/VIRTIS-M (fig.4.9)is in agreement with general VIRTIS-M (Peralta et al., 2007; Hueso et al., 2012, 2015; Machado et al., 2014) and VEx/VMC cloud-tracked results (Khatuntsev et al., 2013): zonal circulation is characterized by almost uniform velocity up to the middle latitudes (near 50°N-S), where the wind speed tends to show a weak maximum.

Akatsuki UVI's high-resolution images of Venus' atmosphere, gathered during a coordinated ground and space observations on January 2017 (Gonçalves et al., 2020) allowed us to retrieve high precision cloud-top zonal and meridional wind velocities, from both hemispheres simultaneously, with a high consistency with previous cloud-tracking space observations (Hueso et al., 2015; Horinouchi et al., 2018). We were able to study spatial variability of both wind circulations due to the high illuminated fraction of Venus' disk visible on UVI images, ranging from 80° S to 70° N latitude and from 7:30 to 18:00 local time.

The Akatsuki/UVI results presented in this work show evidence of an asymmetry on zonal wind speed between northern and southern hemisphere, particulary on the first day (26 January) - velocities on the southern hemisphere are generally higher, in the order of $\sim 10\ ms^{-1}$ (fig. 4.12). This N-S asymmetry was previously detected by Horinouchi et al. (2018) based on Akatsuki UVI observations from October 2016 - March 2017 (therefore encompassing this work's Akatsuki/UVI observations). Yet, previous data sets extending from December 2015 to August 2016 did not show any evidence of N-S asymmetry. This may suggest the existence of a time-variable phenomena or episodic event. Additionally, our analysis also evidences a N-S asymmetry of the meridional wind component (fig. 4.14),

with higher velocities in the northern hemisphere. This asymmetrical behaviour (zonal and meridional, North & South hemisphere) appears to be anti-correlated. It may be the result of a persistent vertical shear and hemispheric asymmetry of the altitude of the upper cloud features, as discussed by Horinouchi et al. (2018). It might also be the result of 3-dimensional structures of wind and temperature associated with the thermal tides (Takagi et al., 2018). However, we cannot properly disentangle the contributions from atmospheric waves (such as the Y-feature wave) and solar tides, thus, additional zonal wind measurements acquired simultaneously on both hemispheres, based on ground-based observations on longer periods, will be required to constrain and study the amplitude and time dependency of this asymmetry.

The latitudinal variation of the zonal wind obtained shows an almost uniform velocity up to 50° N-S, where a maximum is reached, and a steep decrease at higher latitudes. A North-South asymmetry is noticeable, particularly on the results of the 26^{th} January, with a zonal wind magnitude difference of about 10-15 ms^{-1}, being higher at the southern hemisphere. This N-S asymmetry was also measured by Horinouchi et al. (2018), also using Akatsuki/UVI.

We find evidence of an increases in the magnitude of the zonal wind velocity near the evening terminator (fig. 4.12). We also find evidence of a decrease (about 5 ms^{-1}) in the magnitude of meridional wind with local time, at some latitudes. The decrease of meridional wind velocities and the increase of zonal wind velocities close to the evening terminator may reflect a combination of a vertical wind shear and local-time dependence of temperature and wind structures associated with the thermal tide. The existence of a thermal tide near the evening terminator has been discussed in previous studies and models (Sánchez-Lavega et al., 2008; Moissl et al., 2009; Hueso et al., 2015; Machado et al., 2014, 2017; Lebonnois et al., 2016; Horinouchi et al., 2018; Takagi et al., 2018).

Meridional wind

We retrieved meridional wind profile using CT technique with images provided by VEx/VIRTIS-M (April 2014) and Akatsuki/UVI 385 nm (January 2017). The latitudinal profile of meridional wind obtained is highly consistent with previous space observations - wind velocity peaks at around 40°-50° with a magnitude of about 15 ms^{-1}, with a steep decrease at 60°. However, the associated errors are of the same order of the magnitude of the meridional wind velocities.

Regarding our Akatsuki/UVI results, a day-to-day variability of about 4-8 m^{-1} is noticeable on the meridional wind. There is evidence of a N-S assymmetry with velocities higher up to 8 ms^{-1} on the northern hemisphere, particularly on the first day, 26^{th} January (fig. 4.14. This assymmetry is opposite of the one detected for zonal wind velocities, suggesting they should be anti-correlated.

8.1.3 Cloud-top DV and CT comparison

We have retrieved zonal and meridional winds from cloud-top Venus' atmosphere using both DV (Machado et al., 2017; Gonçalves et al., 2020,b) and CT techniques (Machado et al., 2017; Gonçalves et al., 2020). The CT observations were in coordination with ground DV observations. The results presented show evidence of a systematic difference in zonal wind velocity, of up to 15 ms^{-1} higher for DV ground results when compared with CT space results, noticeable across multiple observation campaigns along several years (fig. 5.5). A difference in wind velocities is also noted on the meridional circulation, where the Doppler results present velocities higher up to about 10 ms^{-1}, at 30° N and S, when compared with cloud-tracking results (fig. 5.6. It has been long discussed (e.g. Gierasch et al. (1997), Kawabata et al. (1980), Widemann et al. (2007), Ignatiev (2009), Machado et al. (2014), Machado et al. (2017), Peralta et al. (2017)) whether this is caused by a difference in the averaged altitude probed by the cloud-tracking technique, examined for instance with both VEx/VIRTIS (Sánchez-Lavega et al., 2008; Hueso et al., 2012, 2015) and Akatsuki/UVI (Horinouchi et al., 2018), and the Doppler velocimetry method.

CT measurements do not reflect instantaneous wind velocity neither its variability at time scales shorter than the time interval between images A and B ($\approx$ 120 minutes, in the case of this work). Its results may reflect the phase speed of an atmospheric condensation wave, the speed of iso-pressure regions, possibly with contributions from atmospheric, thermal and gravity waves, eddy, the combination of horizontal flow with vertical mixing, or just chemical processes associated with the temporal variation of cloud features. The unknown nature of the UV absorber may lead to an uncertainty in the altitude of the cloud features of several kilometres. In addition, tracked UV features may be positioned at a variety of altitude within the upper cloud top layers. Therefore, the unknown nature of the UV absorber may lead to an uncertainty in the altitude of the cloud features of several kilometres.

On the other hand, the DV technique provides instantaneous velocities using visible Fraunhofer lines scattered by Venus' cloud tops, obtained through a bolometric measure along the FOV at the altitude where optical depth reaches unity, around 70 km Ignatiev (2009); Fedorova et al. (2016). Thus, our technique constitutes a complementary way of probing the Venus' atmosphere, and a unique approach from the ground, seen that this method measures directly the aerosol particles motion, and the retrieved wind velocities are instantaneous measurements.

We have retrieved zonal winds using the CT technique based on images from both UVI filters (385 nm and 283 nm), from Akatsuki observations on 26-31 January 2017. While the results from the 385 nm filter were published by Gonçalves et al. (2020), the 283 nm filter results are part of an ongoing work to be submit-

ted later this year, as Machado et al. (2020b in preparation). When comparing zonal wind retrieved by CT using images from both UVI filters, it is clear that the 283 nm filter results present consistently higher wind velocities than the results retrieved by the 365 nm filter, in the order of $10 ms^{-1}$ (fig. 5.7). This presents an evidence that the 283-nm images likely reflect cloud features at higher altitude than the 365-nm images, as also previous stated by Horinouchi et al. (2018). The SO_2 vertical is still not fully constrain, while it's know it has horizontal variability along local time and latitude Horinouchi et al. (2018); Encrenaz et al. (2013, 2020). Our results suggest that the altitude probed by UVI 283 nm filter, during the Janurary 2017 observations, is consistent with the altitude probed by several DV observations. Machado et al. (2020b in preparation) will further address this subject, providing additional observation data and an comprehensive comparison with several GCMs. Machado et al. (2020b in preparation) will further address this subject, providing additional observation data and an comprehensive comparison between DV results, CT results and GCMs predictions for could-top zonal wind speed.

The results and comparisons presented, despite not constituting a unambiguous proof by themselves, do show evidence that (1) the altitude of zonal wind probed by DV technique is highly consistent with both the UVI 283 nm filter and the prediction of the Venus' LMD GCM for 70-72 km (Gilli et al., 2017); (2) the altitude of CT results, from both VenusExpress/VIRTIS-M (Hueso et al., 2015; Machado et al., 2017) and Akatsuki/UVI 385 nm filter (Horinouchi et al., 2018; Gonçalves et al., 2020), are highly consistent with Venus' LMD GCM prediction for altitudes around 68 km (Gilli et al., 2017). Therefore, a difference in altitude of up to 2-3 km could be enough to explain the difference in the measurements of zonal wind from DV and CT. We presented evidence that both ground-based DV results, as well as CT results using UVI 283-nm filter images, probe cloud-top winds at altitude around 70-72 km, while CT results using VIRTIS-M and UVI 365-nm images probe UV cloud features (originated by an unknown UV absorber) at an altitude of around 68 km.

8.1.4 Lower cloud deck - ground based CT

We retrieved zonal wind velocities from Venus' lower cloud deck ($\sim$48 km) from the night-side, using CT on ground-based observations at the TNG/NICS. The 2.28 μm window allowed us to probe the lower cloud deck, where the bright thermal background from lower layers contrasts with thicker clouds at around 48 km altitude, which can be visible at the night hemisphere of Venus with IR cameras, such as NICS (k filter) at TNG.

We used a semi-automatic CT tehcnique based on a phase correlation between two images Peralta et al. (2012). Our zonal wind results are consistent with previ-

ous measurements at the same altitude, from VenusExpress using VIRTIS-M 1.74 μm filter (Sánchez-Lavega et al., 2008; Hueso et al., 2012). The mean latitudinal profile of zonal wind is symmetric (N-S) and presents an almost constant velocity of 60-65 ms^{-1}, with higher jets at around 60° in the order of $5ms^{-1}$, followed by a steep decrease poleward.

We also detected a meridional circulation (ongoing work) although the magnitude of the wind speed is of the same order of the uncertainty of the measurements, therefore, we could not derive any unambiguous conclusions.

Our results have proven the usefulness and viability of the CT method on ground-based observations, yielding results with precision comparable to the results provided by space observations. This opens new opportunities for coordinated ground and space observations of Venus' lower deck on the night side.

8.1.5 Summary

We present, in summary, the highlights of the results on Venus atmosphere achieved by this thesis.

- DV observations: we have retrieved zonal and meridional winds with DV technique, using muliple ground telescopes and instruments (TNG/HARPS-N, CFHT/ESPaDOnS).
- CT observations: we have retrieved zonal and meridional winds with CT technique, using multiple space telescopes and instruments (VEx/VIRTIS, Akatsuki/UVI);
- Coordinated ground and space observations: we have conducted simultaneous ground and space observations campaigns, using two telescopes (CFHT and TNG) in coordination with both VenusExpress and Akatsuki missions;
- Unambiguous detection of meridional circulation: we have retrieved, for the first time, a complete latitudinal profile of the meridional wind along both North and South hemispheres, using DV at the CFHT/ESPaDOnS (fig. 3.9, as in Machado et al. (2017));
- Meridional profile: we have retrieved the most precise and complete meridional wind latitudinal profile ever retrieved, using DV at the TNG/HARPS-N (see fig. 3.16, as in Gonçalves et al. (2020);
- Wind variability along spatial coordinates: we have retrieved horizontal winds in a wide spatial coverage of Venus' disk, compassing both hemispheres and from morning to evening terminator, allowing the study of spatial variability and local time dependence of the wind;

- Wind variability along time: we have retrieved horizontal winds in a temporal coverage of 4 years span, allowing an analysis of both short and long term variability;

- Altitude probed by DV and CT: we provided a comparison between several DV and CT results, along with Venus' LMD GCM, allowing a new insight on the altitude probed by each of the techniques and suggesting a difference in altitude of about 2-3 km.

- Venus' lower cloud: we have retrieved horizontal winds at Venus' nigh-side using ground-based CT observations at the TNG/NICS, probing the lower cloud-deck around 48 km altitude.

8.2 Solar System

Venus atmosphere has been the perfect field laboratory for our team to develop and fine tuned two powerful and precise techniques in the study of wind circulation and atmospheric dynamics: the DV and the CT techniques. CT technique has been used retrieve zonal winds from Jupiter (García-Melendo et al., 2011) and Saturn Hueso et al. (2020) atmospheres using images from orbiting space missions (HST, Juno and Cassini-Huygens). Our team is currently adapting the DV technique used in Venus to study and retrieve horizontal winds from Mars, Jupiter and Saturn's atmospheres.

Mars

We have conducted Mars observation with the UVES high-resolution spectrograph at the VLT, during a rare global dust storm on the red planet, on 20 June 2018 (section 7.1.1).

Observing Mars with VLT/UVES during one of the most intense dust storm ever observed on the Red Planet, represented a unique moment to study its atmospheres dynamics. These successful observations will allow the retrieval of horizontal winds by using an adaptation of the DV method detailed by Machado et al. (2012), where the same instrument was used to retrieve Doppler winds from Venus atmosphere.

Jupiter

We have successfully performed Jupiter observations using the high-resolution ESPRESSO at the VLT, on July 2019. We explored the high spectral resolution

of VLT-ESPRESSO observations in order to perform seismology of Jupiter while also applying the Doppler velocimetry method to retrieve zonal wind velocities.

In a first set of observations, the frequency content of Doppler wind estimates will be analysed to: 1) determine the spectral content of observation noise, 2) search for acoustic and gravity modes of Jupiter and 3) constrain the gravity wave power at cloud top. Local seismology methods (similar to the ones applied to the Sun) will be implemented, allowing to constrain Jupiter structure below the cloud layer. In addition to vibration modes, this frequency range is covering the transition from gravity waves to acoustic waves. Information on the atmosphere dynamics will also be extracted from these observations, retrieving horizontal winds using the DV method.

It was the first time ESPRESSO, a high-resolution spectrograph specially designed to detect and study exoplanets, was used to observe Jupiter, or any other SS planet. We used a similar technique used to observe Venus in previous observations, based on a transparent template of the planet's disk with all the positions of the instrument FOV we planned to observe (fig. 7.3).

Saturn

Our team carried out Saturn observations on the night of 13 June 2017, with the CARMENES (Calar Alto high-Resolution search for M dwarfs with Exoearths with Near-infrared and optical Échelle Spectrographs) instrument, which is installed at the 3.5 m telescope at the Calar Alto Observatory, in southern Spain.

This project, led by Miguel Silva, aims to retrieve Doppler wind velocities of Saturn's zonal flow at cloud level, in the visible, and also present the preliminary results of the adaptation of DV (Machado et al., 2017; Gonçalves et al., 2020) to the near-infrared wavelengths. This successful adaptation would be a major milestone in our research, as it would allow DV to not only to retrieve wind velocities on Jupiter and Saturn but also to probe new lower altitudes on Venus' atmosphere (middle cloud deck).

8.3 Exoplanets

ARIEL, the Atmospheric Remote-sensing Infrared Exoplanet Large-survey, was selected as the fourth medium-class mission in ESA's Cosmic Vision programme. It is the first mission dedicated to measuring the chemical composition and thermal structures of hundreds of transiting exoplanets, enabling planetary science far beyond the boundaries of the Solar System. Although the lunch is planned for 2028, our team is already working and involved, as it will continue to do so for the next years, with the scientific consortium.

Our team is leading the Ariel's space mission working group (WG) "Synergies with Solar System". Our expertise on SS atmospheres are regarded as highly valuable in the context of building a bridge between SS and exoplanets. The main goal of this WG is to foster the collaboration and share expertise between the scientific community working in the SS planet atmosphere and the new growing community working for the Ariel Science team. We proposed to coordinate the following tasks: (i) use of SS atmospheres as a natural laboratory for the understanding of Extra-solar planet atmospheres; (ii) apply 3D models developed for SS planets to specific cases of known exoplanets; (iii) support and optimise the forthcoming observations and the characterization of terrestrial planets using GCM (General Circulation Models); (iv) take advantage of SS atmospheres' observations, both spectroscopic and photometric, as a proxy in order to develop and test tools and provide science cases; (v) search for chemical compounds in disequilibrium in SS atmospheres in order to fine-tune investigation protocols that could be exported for ARIEL's science framework. The project presented in the section previous subsection 7.1.2 integrates the proposed tasks for the ARIEL WG. On this framework we use Solar System atmospheres as a natural laboratory for the understanding of Extra-solar planet atmospheres. We took advantage of Solar System atmospheres' observations, both spectroscopic and photometric, as a proxy in order to develop and test tools and provide science cases.

We are developing the PlanetWarp (temporary name), a tool that provides spectra templates of Solar System planets reflected light in visible and IR. The main goal of PlanetWarp is to yield an average spectra (point source) using comprehensive coverage data of different Solar System targets, both, at the optical wavelength range and at the infrared domain, yielding a proxy of how we would see Venus, Jupiter, and Saturn, if those were exoplanets, at a chosen distance from Earth. The chosen targets that could be beneficial in the context of ARIEL research are Venus, Jupiter and Saturn, although our datasets also covers Mars' and Titan's atmospheres.

Our team, using PlanetWarp, will retrieve a median spectra of Jupiter's atmosphere that could serve as a template to compare with exoplanet's spectra, while also improving the modelling of Jupiter-like planets. The high-resolution median spectrum obtained with ESPRESSO (VLT) can then be downgraded to lower resolutions as if Jupiter had been observed at lower resolution spectrographs and at higher distances, simulating an observation of a Jupiter (like planet) at exoplanetary-like distances. This would be useful as template to compare with observations of Jupiter-like planets and also in exoplanet modelling.

The idea of observing solar system planets as if they were exoplanets, creating useful templates of median spectra, can also be applied to Venus and Saturn. The proposed goal could also be achieved by using spectra we obtained in previous Venus' (with VLT/UVES 2012, CFHT/ESPaDOnS 2014 and 2015,

TNG/HARPS-N 2017) and Saturn's (with CARMENES 2017) observations. We intend to complete the "Jupiter as an exoplanet" project and possibly starting to work on another Solar system planet's median spectra within next year.

In a future work, we also will provide a proxy for Earth itself as seen by ARIEL at a certain chosen distance. The initial spectra is, in this case, of Earth observed by Venus Express (ESA) space probe with its VIRTIS' instrument, from Venus orbit (at a much lower spectral resolution then the other template's cases). Naturally that also in this case the basic spectra is convolved with ARIEL's instruments characteristics. Finally, we will take advantage of transmission spectroscopic and photometric data obtained during the last transit of Venus in order to also provide a proxy template for this planet.

Bibliography

Acton, Ch.H. Ancillary data services of NASA's navigation and ancillary information facility. Planet. Space Sci. 44, 65-70, 1995.

Allen, C. W., Astrophysical Quantities, University of London, Athlone Press, 1973.

Ahrens, D., Meteorology Today, Brooks/Cole-Thomson Learning, 2003.

Barstow, J., Taylor, F.W., Tsang, C.C.C., Wilson, C.F., Irwin, P.G.J., McGouldrick, K., Drossart, P., Piccioni, G. Tellman, S., New models of the cloud structure on Venus derived from Venus Express observations. Icarus 217 (2), 542-560, 2012.

J. Kelly Beatty, Carolyn Collins Petersen, Andrew Chaikin: *The New Solar System*, 4th Edition, Cambridge University Press, 1999.

Belton, M.J.S. et al., Images from Galileo of the Venus cloud deck. Science, volume 253, p. 1531-1536, 1991.

Bengtsson, L., and Grinspoon, D., Towards understanding the climate of Venus, (Vol. 11). Springer, 2013.

Bertaux JL, Khatuntsev IV, Hauchecorne A, Markiewicz WJ, Marcq E, Lebonnois S, Patsaeva M, Turin A, Fedorova A; Influence of Venus topography on the zonal wind and UV albedo at cloud top level: The role of stationary gravity waves. J Geophys Res Planets 121(6):1087-1101, 2016

Bevington P.R. and Robinson D.K., 1992: Data reduction and error analysis for the physical sciences. New York: McGraw-Hill, 2nd edition, 1992.

Bougher, S., Hunten, D. and Philips, R., Upper Atmosphere Dynamics, Global Circulation and Gravity Waves, Venus II: Geology, Geophysics, Atmosphere, and Solar Wind Environment, University of Arizona Press, Tucson, AZ, Bougher S.W, Hunten D.M. and Phillips R.J., Eds., p. 259-291, 1997.

Boyer, Ch. and Carmichel, H., Observations photographiques de la planéte Vénus, Annales d'Astrophysique, volume 24, p. 531, 1961

Bullock, A., Grinspoon, D.H., The recent evolution of climate on Venus. Icarus 150, 19-37, 2001.

Cardesín, Study and Implementation of the End-to-End data pipeline for the VIRTIS imaging spectrometer on board Venus Express : From Science operation Planning to Data Archiving and Higher Level Processing", PhD thesis, Centro Interdipartimentale di Studi e Attività Spaziali (CISAS), Universita degli Studi di Padova, 2010.

Civeit, T. et al., On measuring planetary winds using high-resolution spectroscopy in visible wavelengths, Astronomy and Astrophysics, volume 431, p. 1157-1166, 2005.

Connes, P., Absolute astronomical accelerometry, Astrophysics and Space Science (ISSN 0004-640X), volume 110, no. 2, p.211-255, 1985.

Cosentino R., Lovis C., Pepe F., et al., Harps-N: the new planet hunter at TNG. Proc. SPIE 8446, Ground-based and Airborne Instrumentation for Astronomy IV, 84461V (24 September 2012); doi:10.1117/12.925738, 2012.

Cottini, V., Ignatiev, N., Piccioni, G., Drossart, P., Grassi, D., Markiewicz, W., Water vapour near the cloud tops of Venus from Venus Express/VIRTIS dayside data, Icarus, Volume 217, Issue 2, p. 561-569, 2012.

Dartnell L. R., Nordheim T. A., Patel M. R., Mason J. P., Coates A. J., Jones G. H; Constraints on a potential aerial biosphere on Venus: I. Cosmic rays.; Icarus 257, 396-405, 2015

Del Genio A.D. and Rossow W.B., Planetary-scale waves and the cyclic nature of cloud top dynamics on Venus, Journal of the Atmospheric Sciences, volume 47, p. 293-318, 1990.

Dollfus, A., Venus - evolution of upper atmospheric clouds. J. Atmos. Sci. 32, 1060-1070, 1975b.

Drossart, P., Piccioni, G., Gerard, J.C., et al. A dynamic upper atmosphere of Venus as revealed by VIRTIS on Venus Express. Nature, vol. 450, no 7170, p. 64-645, 2007.

Encrenaz, T. K. Greathouse, M. J. Richter, J. Lacy, T. Widemann, B. Bezard, T. Fouchet, C. deWitt, and S. K. Atreya 2013, HDO and SO2 thermal mapping

on Venus. II. The SO2 spatial distribution above and within the clouds, Astron. Astrophys. 2013

Encrenaz, T.; Greathouse, T. K.; Marcq, E.; Sagawa, H.; Widemann, T.; BÃ©zard, B.; Fouchet, T.; LefÃ¨vre, F.; Lebonnois, S.; Atreya, S. K.; Lee, Y. J.; Giles, R.; Watanabe, S.; Shao, W.; Zhang, X.; Bierson, C. J.; HDO and SO_2 thermal mapping on Venus. V. Evidence for a long-term anti-correlation; Astronomy and Astrophysics 639; 2020

Esposito, L. W., Knollenberg, R., Marov, M., Toon, O. and Turco, R., The clouds and hazes of Venus, in Venus, edited by D.M. Hunten, L. Colin, T.M. Donahue, and V.I. Moroz, pp. 484-564, University of Arizona Press, Tucson, 1983.

Esposito, L. W., Bertaux, J. L., Krasnopolsky, V., Moroz, V. I., Zasova, L. V. (1997). Chemistry of lower atmosphere and clouds. Venus II, 415-458, 1997.

Fedorova A., Marcq E., Luginin M., Korablev O., Bertaux J.L., Montmessin F., Variations of water vapor and cloud top altitude in the Venus' mesosphere from SPICAV/VEx observations. Icarus, vol. 275, p. 143-162, 2016.

Fukuhara T., Futaguchi M., Hashimoto G. L., Horinouchi T., Imamura T., Iwagaimi N., Kouyama T., et al.; Large stationary gravity wave in the atmosphere of Venus.; Nature Geoscience 10, 85-88, 2017

Garate-Lopez, I., Hueso, R., Sanchez-Lavega, A., Peralta, J., Piccioni, G., Drossart, P., A chaotic long-lived vortex at the southern pole of Venus, Nature Geoscience 6, 254-25, 2013.

García-Melendo E., Arregi J., Rojas J., Hueso R., Barrado-Izagirre N., Gómez-Forrellad J. M., érez-Hoyos S., Sanz-Requena J. F., Sánchez-Lavega A., Dynamics of Jupiter's equatorial region at cloud top level from Cassini and HST images, Icarus, Volume 211, Issue 2, Pages 1242-1257,2011 https://doi.org/10.1016/j.icarus.2010.11.020.

Gaulme P., Schmider F.-X., GonÃ§alves I., Measuring planetary atmospheric dynamics with Doppler spectroscopy. Astronomy & Astrophysics, Volume 617, A41, 2018.

Ghail R.; Wilson C.; Widemann T.; Bruzzone L; Dumoulin C.; Helbert J.; Herrick R.; Marcq E. et al.; EnVision: understanding why our most Earth-like neighbour is so different.(ES M5 mission proposal) 2017

Gierasch, P., Meridional circulation and Venus atmospheric rotation, Journal of the Atmospheric Sciences, volume 32, p. 1038-1044, 1975.

Gierasch, P. et al., The general circulation of the Venus atmosphere: an assessment, Venus II: Geology, Geophysics, Atmosphere, and Solar Wind Environment, University of Arizona Press, Tucson, AZ, Bougher S.W, Hunten D.M. and Phillips R.J., Eds., p. 459-500, 1997.

Gilli, G.; Lebonnois, S.; González-Galindo, F.; López-Valverde, M. A.; Stolzenbach, A.; Lefèvre, F.; Chaufray, J. Y.; Lott, F, Thermal structure of the upper atmosphere of Venus simulated by a ground-to-thermosphere GCM. Icarus 281, 55-72, 2017

Goldstein, J., Absolute Wind Velocities in the Lower Thermosphere of Venus using Infrared Heterodyne Spectroscopy, PhD thesis, Univ. of Pennsylvania, Philadelphia. 1989

Gonçalves, R.; Machado, P.; Widemann, T.; Peralta, J.; Watanabe, S.; Yamazaki, A.; Satoh, S.; Takagi, M.; et al., Venus' cloud top wind study: Coordinated Akatsuki/UVI with cloud tracking and TNG/HARPS-N with Doppler velocimetry observations. Icarus, volume 335, 113418, 2020.

Gonçalves, R.; Machado, P.; Widemann, T.; Venus' cloud top wind study: new Doppler velocimetry observations with ESPaDOnS at CFHT. 2020, submitted to 'Atmosphere - Observations of Venus Atmosphere, Special Issue'.

Goody, R.; Walker, J. Atmosferas Planetárias, Editora Edgard, 1975.

Greaves J. S., Richards A. M. S., Bains W., Rimmer P. B., Sagawa H., Clements D. L., Seager S., et al.; Phosphine gas in the cloud decks of Venus.; Nature Astronomy, 2020

Grinspoon, D.H., Venus Revealed: A New Look Below the Clouds of Our Mysterious Twin Planet (Helix Books, Perseus Publishing, Cambridge, Massachusetts, 1997.

Grinspoon, D.H., Bullock, M., in Astrobiology and Venus Exploration, ed. by L.W. Esposito, E.R. Stofan, T.E. Cravens. Exploring Venus as a Terrestrial Planet (American Geophysical Union, Washington DC, 2007.

Hansen, J.E., Hovenier, J.W., 1974. Interpretation of the polarization of Venus. J. Atmos. Sci. 31, 1137-1160.

Holland, H.D., The Chemistry of the Atmospheres and Oceans, Wiley, New York, 1978.

Horinouchi T., Kouyama T., Lee Y.J., Murakami S., Ogohara K., Takagi M., Imamura T., Nakajima K., Peralta J., Yamazaki A., Mean winds at the cloud top of Venus obtained from two-wavelength UV imaging by Akatsuk. Earth, Planets and Space, 70:10, 2018.

Hueso R., Legarreta J., Rojas J.F., Peralta J., Pérez-Hoyos S., Del Río-Gaztelurrutia T. and Sánchez-Lavega A.: The Planetary Laboratory for Image Analysis (PLIA). Advances in Space Research, 46, 1120-1138, 2010.

Hueso, R., Peralta, J., Sánchez-Lavega, A., Assessing the long-term variability of Venus winds at cloud level from VIRTIS-Venus Express, Icarus, volume 217, p. 585-598, 2012.

Hueso R., Peralta J., Garate-Lopez I., Bandos T.V., Sánchez-Lavega, A., Six years of Venus winds at the upper cloud level from UV, visible and near infrared observations from VIRTIS on Venus Express, 2015

Hueso R, Sánchez-Lavega A., Rojas J.F., Simon A., Barry T., Río-Gaztelurrutia T., Antuñano A., Sayanagi K.M., Delcroix M., Fletcher L.N., García-Melendo E., Pérez-Hoyos S., et al. Saturn atmospheric dynamics one year after Cassini: Long-lived features and time variations in the drift of the Hexagon, Icarus, Volume 336, 2020 https://doi.org/10.1016/j.icarus.2019.113429.

Ignatiev, N.I. et al., Altimetry of the Venus cloud tops from the Venus Express observations, Journal of Geophysical Research, vol. 114, E00B43, 2009.

Imamura, T. (2006), Meridional propagation of planetary-scale waves in vertical shear: Implication for the Venus atmosphere, J. Atmos. Sci., 63, 1623-1636, 2006

Iwagami N, Seiko Takagi S, Ohtsuki M, Ueno K, Uemizu T, Satoh T Sakanoi, Hashimoto GL, Science requirements and description of the 1 μm camera onboard the Akatsuki Venus Orbiter. Earth Planets Space 63:487-492, 2011 https://doi.org/10.5047/eps.2011.03.007

Kasting, J.F., Runaway and moist greenhouse atmospheres and the evolution of Earth and Venus, Icarus, 74, 472-494, 1988.

Kawabata, K., Coffeen, D.L., Hansen, J.E., Lane, W.A., Sato, M., Travis, L.D., Cloud and haze properties from pioneer Venus polarimetry. J. Geophys. Res. 85, 8129-8140, 1980.

Khatuntsev, I., Patsaeva, M., Titov, D., Ignatiev, N., Turin, A., Limaye, S., Markiewicz, W., Almeida, M., Roatsch, Th., Moissl, R., Cloud level winds

from the Venus Express Monitoring Camera imaging, Icarus, Volume 226, p. 140-158, 2013.

Knollenberg, R. G.; Hunten, D. M., The microphysics of the clouds of Venus - Results of the Pioneer Venus particle size spectrometer experiment, Journal of Geophysical Research, vol. 85, p. 8039-8058, 12/1980.

Kopparapu, R-K, Wolf E. and Victoria M., "Characterizing Exoplanet Habitability." Earth and Planetary Astrophysics, 2019

Kouyama T., Imamura T., Nakamura M., Satoh T. and Futaana Y.,: Long-term variation in the cloud-tracked zonal velocities at the cloud top of Venus deduced from Venus Express VMC images. Journal of Geophysical Research: Planets, 118, 37-46, 2013.

Kouyama, T., T. Imamura, M. Nakamura, T. Satoh, and Y. Futaana; Vertical propagation of planetary-scale waves in variable background winds in the upper cloud region of Venus, Icarus, 248, 560-568, 2015.

Lebonnois, S., Hourdin, F., Eymet, V., Crespin, A., Fournier, R., and Forget, F., Superrotation of Venus' atmosphere analyzed with a full general circulation model, Journal of Geophysical Research (Planets), 115 , 2010.

Lebonnois, S., et al., Models of Venus Atmosphere, Towards Understanding the Climate of Venus, ISSI Scientific Report Series, Volume 11. ISBN 978-1-4614-5063-4. Springer Science+Business Media New York, 2013, p. 129, Springer, 2013.

Lebonnois, S. , Sugimoto, N. , Gilli, G.; Wave analysis in the atmosphere of venus below 100-km altitude, simulated by the LMD venus GCM. Icarus 278, 38-51, 2016

Lee Y-J., Titov D., Tellmann S., Piccialli A., Ignatiev N., Vertical structure of the Venus cloud top from the VeRa and VIRTIS observations onboard Venus Express. Icarus, vol. 217, p. 599-609, 2012.

Lee Y. J., Jessup K.-L., Perez-Hoyos S., Titov D. V., Lebonnois S., Peralta J., Horinouchi T., et al.; Long-term Variations of Venus's 365 nm Albedo Observed by Venus Express, Akatsuki, MESSENGER, and the Hubble Space Telescope. The Astronomical Journal 158. 2019

Lellouch, E. et al., Global circulation, thermal structure, and carbon monoxide distribution in Venus' mesosphere in 1991, Icarus, volume 110, no. 2, p. 315-339, 1994.

Lewis, J. Physics and Chemistry of the Solar System, Elsevier Academic Press, 2004.

Limaye, S., Grund, C., Burre, S., Zonal mean circulation at the cloud level on Venus - Spring and fall 1979 OCPP observations, Icarus, vol. 51, p. 416-439, 1982.

Limaye, S.S. et al., Venus Atmospheric Circulation: Known and unknown, volume 112, E04S09, 2007.

Limaye, S.S. et al., Vortex circulation on Venus: Dynamical similarities with terrestrial hurricanes, Geophysical Research Letters, volume 36, L04204, doi:10.1029/2008GL036093, 2009.

Limaye S.S. and Rengel M.; Atmospheric Circulation and Dynamics. In: Bengtsson L., Bonnet RM., Grinspoon D., Koumoutsaris S., Lebonnois S., Titov D. (eds) Towards Understanding the Climate of Venus. ISSI Scientific Report Series, vol 11. Springer, New York, NY, 2013

Limaye S. S., Mogul R., Smith D. J., Ansari A. H., Słowik G. P., Vaishampayan P.; Venus' Spectral Signatures and the Potential for Life in the Clouds.; Astrobiology 18, 1181-1198, 2018

Luz, D. et al. Characterization of zonal winds in the stratosphere of Titan with UVES, Icarus, volume 179, p. 497-510, 2005a.

Luz, D. et al. Characterization of zonal winds in the stratosphere of Titan with UVES: 2. Observations coordinated with the Huygens Probe entry, Journal of Geophysical Research, volume 111, CiteID E08S90, 2006.

Luz, D. et al. Venus's Southern Polar Vortex Reveals Precessing Circulation, Science, volume 332, p. 577-580, 2011.

Machado, P., Luz, D. Widemann, T., Lellouch, E., Witasse, O, Characterizing the atmospheric dynamics of Venus from ground-based Doppler velocimetry, Icarus, Volume 221, p. 248-261, 2012.

Machado, P., Widemann, T., Luz, D., Peralta, J., Wind circulation regimes at Venus' cloud tops: Ground-based Doppler velocimetry using CFHT/ESPaDOnS and comparison with simultaneous cloud tracking measurements using VEx/VIRTIS in February 2011, Icarus, 2014.

Machado P., Widemann T., Peralta J., Gonçalves R., Donati J., Luz D., Venus cloud-tracked and Doppler velocimetry winds from CFHT/ESPaDOnS and Venus Express/VIRTIS in April 2014. Icarus, vol. 285, p. 8-26, 2017.

Machado P., Gonçalves R., et al., Cloud tracked winds at the lower cloud level using Venus' night side observations at 2.28 μm with TNG/NICS and coordinated VIRTIS/VEx observations. 2020, submitted to Icarus.

Machado P., Gonçalves R., et al., Venus' atmosphere cloud tracked winds (283 and 385 nm): comparison with Doppler winds and GCM simulations. 2020, submitted to 'Atmosphere - Observations of Venus Atmosphere, Special Issue'.

Markiewicz, W. et al., Morphology and dynamics of the upper cloud layer of Venus, *Nature*, volume 450, p. 633-636, 2007.

Meadows V.S., Barnes R.K., Factors Affecting Exoplanet Habitability. In: Deeg H., Belmonte J. (eds) Handbook of Exoplanets. Springer, Cham. 2018, https://doi.org/10.1007/978-3-319-30648-3_57-1

Moissl, R. et al., Venus cloud top winds from tracking UV features in Venus Monitoring Camera, Jornal of Geophysical Research, volume 114, E00B31, 2009.

Morowitz H. and Sagan C.; Life in the Clouds of Venus?; Nature 215, 1259-1260, 1967.

Nakamura, M. et al., Planet-C: Venus Climate Orbiter mission of Japan, Planetary and Space Science, Volume 55, p. 1831-1842, 2007.

Nakamura, M., Imamura, T., Ishii, N. et al. Overview of Venus orbiter, Akatsuki. Earth Planet Sp 63, 443-457, 2011. https://doi.org/10.5047/eps.2011.02.009

Nakamura M. et al., AKATSUKI returns to Venus. Earth, Planets and Space, 68:75, doi: 10.1186/s40623-016-0457-6, 2016.

Ogohara, K., Tagaki, M., Murakami, S., Horinouchi, T., et al., . Overview of Akatsuki data products: definition of data levels, method and accuracy of geometric correction. Earth Planets Space 69 (1), 167, 2017.

Peralta, J., Hueso, R., Sánchez-Lavega, A., A reanalysis of Venus winds at two cloud levels from Galileo SSI images, *Icarus*, volume 190, p. 469-477, 2007.

Peralta, J. et al., Solar Migrating Atmospheric Tides in the Winds of the Polar Region of Venus, *Icarus, in press*, 2012.

Peralta, J., Imamura T., Read P., Luz D., Piccialli A., López-Valverde M. A., Analytical Solution for Waves in Planets with Atmospheric Superrotation. I. Acoustic and Inertia-Gravity Waves. Astrophys. J. Suppl. Ser. 213(1), 2014

Peralta, J; Lee, Y. J.; Hueso, R.; Clancy, R. T.; Sandor, B. J.; Sánchez-Lavega, A.; Lellouch, E.; Rengel, M.; Machado, P.; Omino, M.; Piccialli, A.; Imamura, T.; Horinouchi, T.; Murakami, S.; Ogohara, K.; Luz, D.; Peach, D. Venus's winds and temperatures during the MESSENGER's flyby: An approximation to a three-dimensional instantaneous state of the atmosphere. Geophysical Research Letters 44, 3907-3915. 2017

Peralta J., Muto K., Hueso R., Horinouchi T., Sánchez-Lavega A., Murakami S., Machado P., Young E., Lee Y. J., Kouyama T., Nightside Winds at the Lower Clouds of Venus with Akatsuki/IR2: Longitudinal, Local Time, and Decadal Variations from Comparison with Previous Measurements. The American Astronomical Society. The Astrophysical Journal Supplement Series, Volume 239, Number 2, 2018

Peralta J., Navarro T., Vun C. W., Sánchez-Lavega A., McGouldrick K., Horinouchi T., Imamura T., et al.; A Long-Lived Sharp Disruption on the Lower Clouds of Venus. Geophysical Research Letters 47, 2020.

Piccioni G. et al., South-polar features on Venus similar to those near the north pole, *Nature*, volume 450, p. 637-640, 2007.

Rossow, W., Williams, G., Large-scale motion in the Venus stratosphere, Journal of the Atmospheric Sciences, volume 36, p. 377-389, 1979.

Sánchez-Lavega, A., Hueso, R., Piccioni, G., Drossart, P., Peralta. J., Pérez-Hoyos, J., Wilson, C., Taylor, F., Baines, K., Luz, D., Erard, S., Lebonnois, S.: Variable winds on Venus mapped in three dimensions, *Geophysical Research Letters*, vol. 35, 2008.

Sánchez-Lavega, A., Lebonnois, S., Imamura, T., Read, P., Luz, D.; The Atmospheric Dynamics of Venus. Space Science Reviews 212, 1541-1616, 2017

Schubert, G., Covey, C., del Genio, A., Elson, L. S., Keating, G., Seiff, A., Young, R., Counselman, C., Kliore, A., Limaye, S., Revercomb, H., Sromovsky, L., Suomi, V., Taylor, F., Woo, R., von Zahn, U, Structure and circulation of the Venus atmosphere, Journal of Geophysical Research, vol. 85, p. 8007-8025, 1980.

Smette A., Sana H., Noll S., Horst H., Kausch W., Kimeswenger S., Barden M., et al.; Molecfit: A general tool for telluric absorption correction. I. Method and application to ESO instruments; Astronomy and Astrophysics 576, 2015.

Suomi, V.; Limaye, S., Venus - Further evidence of vortex circulation, Science, volume 201, p. 1009-1011, 1978.

Taguchi, M., T. Fukuhara, T. Imamura, M. Nakamura, N. Iwagami, M.Ueno, M. Suzuki, G. L. Hashimoto, and K. Mitsuyama, Longwave infrared camera onboard the Venus Climate Orbiter, Adv. Space Res., 40, 861-868, 2007.

Takagi, M., Matsuda, Y., Effects of thermal tides on the Venus atmospheric superrotation. J. Geophys. Res.-Atmos. 112, 9112, 2007.

Takagi M., Sugimoto N., Ando H., Matsuda Y., Three-Dimensional Structures of Thermal Tides Simulated by a Venus GCM, Journal of Geophysical Research, vol. 123, Issue 2, p 335-352, 2018.

Tavener, T. et al., Planetary Sp. Sciences, 56, pp. 1435, 2008.

Taylor, F., McCleese, D., Elson, L., Martonchik, J., Diner, D., Houghton, J., Delderfield, J., Schofield, J., Bradley, S., Infrared remote sensing of the atmosphere of Venus from the Pioneer 12 Orbiter, Space research. Volume 20 - Proceedings of the Open Meetings of the Working Groups on Physical Sciences, Bangalore, India, May 29-June 9, 1979. Oxford and Elmsford, N.Y., Pergamon Press, p. 227-230, 1980.

Taylor, F., Hunten, D. and Ksanfomaliti, L., The thermal balance of the middle and upper atmosphere of Venus, pages 650-680. 1983.

Taylor, F., Grinspoon, D., Climate evolution of Venus, Journal of Geophysical Research, Volume 114, 2009.

Tellmann, S., Paetzold, M., Hausler, B., Bird, M. K., and Tyler, G.L., Structure of Venus neutral atmosphere as observed by the Radio Science experiment VeRa on Venus Express, J. Geophys. Res. (Planets), volume 114, E00B36, 2009.

Titov, D., Markiewicz, W., Ignatiev, N., Li, S., Limaye, S., Sanchez-Lavega, A., Hesemann, J., Almeida, M., Roatsch T., Matz T., Scholten, F., Crisp, D., Esposito, L., Hviid, S., Jaumann R., Keller, H., Moissl, R., Morphology of the cloud tops as observed by the venus express monitoring camera. Icarus, 217, 2, 682-701, doi:10.1016/j.icarus.2011.06.020, 2012.

L. Trompet, S. Robert, A. Mahieux, F. Schmidt, J. Erwin and A. C. Vandaele. Phosphine in Venus' atmosphere: Detection attempts and upper limits above the cloud top assessed from the SOIR/VEx spectra. Astronomy & Astrophysics, 645, L4, 2021.

Way M. J., Del Genio A. D., Kiang N. Y., Sohl L. E., Grinspoon D. H., Aleinov I., Kelley M., and Clune T., Was Venus the first habitable world of our solar system?, Geophys. Res. Lett., 43, 8376- 8383, 2016, doi:10.1002/2016GL069790.

Way M. J., and Del Genio A. D., Venusian habitable climate scenarios: Modeling Venus through time and applications to slowly rotating Venus-like exoplanets.Journal of Geophysical Research: Planets, 125, 2020. https://doi.org/10.1029/2019JE006276

Widemann, T. et al., New wind measurements in Venus lower mesosphere from visible spectroscopy, Planetary and Space Science, volume 55, p. 1741-1756, 2007.

Widemann et al., Venus Doppler winds at cloud tops observed with ESPaDOnS at CFHT, Planetary and Space Science, Volume 56, p. 1320-1334, 2008.

Yamamoto, M., and Takahashi, M., Superrotation maintained by meridional circulation and waves in aVenus-like AGCM. J. Atmos. Sci. 63, 296-314, 2006.

Yamazaki A., Yamada M., Joo Lee Y., Watanabe S., Horinouchi T., Murakami S., Kouyama T., Ogohara K., Imamura T., Sato T., Fukuhara T., Ultraviolet imager on Venus orbiter Akatsuki and its initial results. Earth, Planets and Space, 70:23, doi: 10.1186/s40623-017-0772-6, 2018.

Young A., Is the Four-Day "Rotation" of Venus Illusory?, Icarus, volume 24, p. 1-10, 1975.

Young, A.; Schorn, R.; Young, L.; Crisp, D., Spectroscopic observations of winds on Venus, I-technique and data reduction. Icarus, volume 38, p. 435-450, 1979.

Young, E., et al., Bulletin American Astronomical Society, 40, pp. 513, 2008.